# *Artemisia Afra* (*Ariti*) Leaf Extract Mediated Ag/$SiO_2$ Nanocomposites for Antibacterial and Antifungal Activity

Nardos Asefa Mergia

A Thesis Submitted to the Department of Applied Chemistry

School of Applied Natural Science

Office of Post Graduate Studies

Adama Science and Technology University

In partial fulfillment of the Requirements for the Degree of Master of Science in Applied Chemistry (Analytical Chemistry)

June 2023

Adama, Ethiopia

# *Artemisia Afra* (*Ariti*) Leaf Extract Mediated Ag/$SiO_2$ Nanocomposites for Antibacterial and Antifungal Activity

Nardos Asefa Mergia

Advisor: Hizkeal Tsade (PhD)

Co-advisor: Aschalew Tadesse (PhD)

Thesis Submitted to the Department of Applied Chemistry
School of Applied Natural Science
Office of Post Graduate Studies

Adama Science and Technology University
In partial fulfillment of the Requirements for the Degree of Master of Science in Chemistry (Analytical Chemistry)

June 2023
Adama, Ethiopia

# DECLARATION

I hereby declare that this M.Sc. thesis entitled **"*Artemisia Afra* (*Ariti*) Leaf Extract Mediated Ag/$SiO_2$ Nanocomposites for Antibacterial and Antifungal Activity"** is my original work and has not been presented for a degree in any other university and all sources of material used for this thesis has been duly acknowledged through citation

NARDOS ASEFA _____ _____

Name of student Signature Date

## RECOMMENDATION OF ADVISORS

We the advisor of this thesis, hereby certify that we have read the revised version of the thesis entitled **"*Artemisia Afra* (*Ariti*) Leaf Extract Mediated Ag/$SiO_2$ Nanocomposites for Antibacterial and Antifungal Activity"** by Nardos Asefa submitted in partial fulfillment of the requirements for the degree of Masters of Science in applied chemistry (Analytical chemistry). Therefore, we recommend the submission of a revised version of the thesis to the department following the applicable procedures

| | | |
|---|---|---|
| Main Advisor | Signature | Date |
| Co-Advisor | Signature | Date |

# APPROVAL SHEET

We, the advisors of the thesis entitled **"*Artemisia Afra* (*Ariti*) Leaf Extract Mediated Ag/$SiO_2$ Nanocomposites for Antibacterial and Antifungal Activity"** and developed by Nardos Asefa hereby certify that the recommendation and suggestions made by the board of examiners are appropriately incorporated into the final version of the thesis.

| | | |
|---|---|---|
| Major Advisor | Signature | Date |
| Co-Advisor | Signature | Date |

## APPROVAL OF THE EXAMINERS

We, the undersigned, members of the Board of Examiners of the thesis by Nardos Asefa have read and evaluated the thesis entitled **"*Artemisia Afra* (*Ariti*) Leaf Extract Mediated Ag/$SiO_2$ Nanocomposites for Antibacterial and Antifungal Activity"** and examined the candidate during the open defense. This is, therefore, to certify that the thesis is accepted for partial fulfillment of the requirement of the degree of Master of Science in Analytical chemistry.

| | | |
|---|---|---|
| _____ | _____ | _____ |
| Chairperson | Signature | Date |
| _____ | _____ | _____ |
| Internal Examiner | Signature | Date |
| _____ | _____ | _____ |
| External Examiner | Signature | Date |

Final approval and acceptance of the thesis are contingent upon the submission of its final copy to the Office of Postgraduate Studies (OPGS) through the Department Graduate Council (DGC) and School Graduate Committee (SGC)

| | | |
|---|---|---|
| _____ | _____ | _____ |
| Department Head | Signature | Date |
| _____ | _____ | _____ |
| School Dean | Signature | Date |
| _____ | _____ | _____ |
| Office of Postgraduate Studies, Dean | Signature | Date |

# ACKNOWLEDGEMENTS

First and foremost, I would like to thank the Almighty God and his mother St. Marry for giving me the health, strength, wisdom, and patience to complete this thesis. Next, I would like to express my sincere gratitude to my advisor, Hizkeal Tsade (Ph.D.), for his professional, technical, very invaluable, and unreserved advice, guidance, and constructive criticism support during the whole period of this thesis work.

Also I would like to express my genuine heartfelt gratitude to my Co-adviser Aschalew Tadesse (PhD) for his valuable suggestion, comments, corrections, and professional & technical guidance throughout my work for the successful accomplishment of this thesis paper.

Last but not least, I would like to express my sincere gratitude to all academic, technical, and support staff of the Department of Applied Chemistry, Adama Science and Technology University and for providing the necessary knowledge, assistance, and facilities to conduct my research work.

Finally, I must express my very profound gratitude and heartfelt special thanks to my family Asefa Mergia, Askalche Zenbaba, Esayes Asefa, Lily Asefa, Betlehem Asefa, and Keneni Asefa who helped in all directions for my success, for providing me with unfailing support and continuous encouragement throughout my years of study and for their support in everything I need. This accomplishment would not have been possible without them. Thank you!

# TABLE OF CONTENTS

Contents Pages

# LIST OF TABLES

# LIST OF FIGURES

## LIST OF ABBREVIATIONS

| | |
|---|---|
| *A.Afra* | Artemisia Afra |
| APHRRLC | Adama Public Health Research and Referral Laboratory Center |
| ATCC | American Type Culture Collection |
| CFU | Colony Forming Unit |
| DMSO | Dimethyl Sulfoxide |
| DNA | Deoxyribose nucleic acid |
| FCC | Face Centered Cubic |
| FT-IR | Fourier Transmission Infrared |
| FWHM | Full width half maximum |
| JPCDS | The Joint Committee on Powder Diffraction Standard |
| MBC | Minimum Bactericidal Concentration |
| MIC | Minimum Inhibitory Concentration |
| NCs | Nanocomposites |
| NPs | Nanoparticles |
| PDA | Potato Dextrose Agar |
| ROS | Reactive Oxygen Species |
| SEM | Scanning Electron Microscopy |
| SPR | Surface Plasm Resonance |
| UV-Vis | Ultraviolet visible Spectroscopy |
| XRD | X-ray Diffraction |

# ABSTRACT

*Increasing case of drug resistance, unwanted side effects of existing antibiotics, and the reappearance of earlier known infection have demanded the need for new, safe, and effective antimicrobial agent. For this reason, Nanotechnology is the new advanced technology for increasing new antibiotic production. This study aimed to synthesize environmentally friendly Ag/$SiO_2$ NCs for antibacterial and antifungal activity by a green method. Artemisia Afra (Ariti) is used as a reducing and capping agent in the NPs and NCs synthesis method. The synthesized materials were characterized using Uv-Visible spectroscopy, XRD, FTIR, and SEM. UV-Visible study revealed the optical band gap energy of NPs and NCs was estimated with different concentrations. The XRD pattern of Ag and $SiO_2$ showed peaks, confirming the formation of the silver FCC structure and amorphous structure(non-crystalline) of $SiO_2$ NCs.The XRD pattern also confirmed the formation of Ag/$SiO_2$ NCs.The average crystallite size of the Ag NPs and Ag/$SiO_2$ NCs estimated from the XRD diffraction pattern using Debye Scherrer's formula was 16.68 and 8.99nm. The FTIR analysis shows the presence of hydroxyl, carbonyl, alkyl, amide, alcohol, and nitro functional group in NPs and NCs.The porosity of $SiO_2$ NPs, the spherical shape of Ag NPs, and their combination of the morphology structure were confirmed by SEM analysis. The antimicrobial activity of the biosynthesized NPs and NCs was screened against two Gram-positive bacteria (Streptococcus pyogenes and Staphylococcus aureus) and two Gram-negative bacteria (Escherichia coli and Pseudomonas aeruginosa) and fungal strains (Candida albicans) using the Agar disc diffusion method. Ag/$SiO_2$ NCs showed better antibacterial activity, with maximum zone inhibition values of 15 mm and 16 mm at 10 mg/mL dosage towards Gram-negative and Gram-positive bacteria, respectively. The best antifungal activity was displayed by Candida albicans at Ag/$SiO_2$ NCs with a maximum zone inhibition of 14mm at the concentration of 10mg/mL. The MIC and MBC was recorded for both bacterial activities.*



***Keywords**: Antibacterial activity, Artemisia Afra, Nanoparticle, Nanocomposite, Green Synthesis*

# 1. INTRODUCTION

## 1.1 Background of the study

Nanotechnology is the most advanced and emerging field in the present era. It encircles the application and production of nanoscale material in biological, chemical, and physical systems. It involves the synthesis, characterization, and application by controlling shape and size. Nanotechnology has recently sparked tremendous research, with applications in science, engineering, agriculture, biotechnology, food science, environment, energy, electronics, space, industry, medicine, and biology (*Achamo et al., 2022*). Nanomaterials are particles having at least one of its dimensions in a nanometer scale, and they are very small particles with advanced thermal conductivity, catalytic reactivity, nonlinear optical performance, and chemical balance because of their high surface area-to-volume ratio (*Kalpana & Devi Rajeswari, 2018*). Due to their unique chemical and biological reactivity, they may easily interact with cells and microorganisms, inducing or enhancing existing properties. Silver nanoparticles, "a wonder of modern medicine", can fight against a much larger number of microorganisms compared with most antibiotics, which are active against a much smaller number of microorganisms. Metal nanoparticles, especially those of noble metals, show an absorption band in the visible region (at 380–750 nm) due to their localized surface. Localized Surface Plasmon resonance (LSPR), which is due to the distinctive optical properties of metal nanoparticles, arises from the collective oscillation of conduction electrons upon interaction with electromagnetic radiation *(Salem et al., 2023)*.

Silver nanoparticles show a Plasmon resonance in the visible region and find even wider applications (Zhang et al., 2016). This is because Ag is sensitive to the surrounding chemicals, causing oxidization and significant degradation because of its plasmonic properties. Ag nanoparticles aggregate due to van der Waals forces in the aqueous solution. To overcome these problems, Ag nanoparticles require the application-specific combination of other materials to passively or fuse the nanoparticle to the target molecules or surfaces and the formation of nanocomposites. Silica ($SiO_2$) nanoparticles can be efficiently utilized as a stabilizing matrix for preventing the aggregation of Ag NPs. Because of $SiO_2$ NPs are nontoxic, have high porosity, thermal stabilities, and are biocompatible, which makes them excellent carriers for other nanoparticles (Cha et al., 2007).

Ag nanoparticles may be transported using $SiO_2$ nanoparticles, allowing regulated release and long-term antimicrobial action. Additionally, $SiO_2$ nanoparticles can make Ag nanoparticles more stable and biocompatible, lowering the possibility that they will be hazardous to human cells or tissues (Khezerlou et al., 2018).

Various methods based on the synthesis of supported metal nanoparticles, including physical and chemical methods, have been developed. Metal nanoparticles (NPs) are frequently immobilized on solid supports using the wet impregnation approach. In this method, a support material (such as silica, alumina, or carbon) is submerged in a solution of a metal precursor, such as a metal salt (such as silver nitrate for Ag NPs), which is commonly dissolved in a solvent like water or ethanol. Then after, the support is kept in the solution for a while to allow the precursor to impregnate the material. This metal nanoparticle reduced by appropriate reducing agents such as $NaBH_4$ (Jana et al., 2006; Li et al., 2017) and hydrazine (Shi et al., 2015), which are toxic and harmful to the environment. Due to the easy transfer of metal ions, reduced atoms, and nanocrystals in the reaction system, the preparation process possibly leads to the formation of larger-sized metal nanoparticles and their aggregation, which is not desirable for the application of supported metal NPs. So, it is an important research direction to develop new methods for preparing small-sized ( $<$10 nm) and evenly dispersed metal nanoparticles using more environmentally benign reducing agents.

Among the best techniques plant extract in the synthesis of nanomaterials in the biosynthesis route has many advantages compared with the physical, chemical, and microbial synthesis routes because of its generation of less harmful chemicals, wasteful purifications, or high energy requirements. Furthermore, the composition of these extracts usually contains both reducing agents and capping agents, which involve reduction and stabilization in one step (Ahmed et al., 2016). In short, green synthesis is an eco-friendly and cost-effective alternative to classical physical and chemical methods. Plant extracts are the most conventional reducing agents in green synthesis. Moreover, certain extracts exhibit strong biological activity such as antimicrobial, anti-inflammatory, antitumor, etc., potentiating the biological activity of the nanomaterials.

*Artemisia Afra*, the African wormwood (Family: *Asteraceae*; *Ariti:* Amharic), is a common species of the genus *Artemisia* in Africa, with a wide distribution from South Africa to areas reaching to the north and eastern part of Ethiopia. *Artemisia Afra* is the only species in this genus indigenous to the African continent (Nguyen et al., 2016). This perennial species has a height range of 0.5 to

2 meters and is characterized by its soft, fern-like leaves with silver-grey foliage. These leaves are aromatic and effortless to cultivate, making them a popular choice for medicinal purposes. The major phytochemicals screened in *Artemisia Afra* are alkaloids, flavonoids, saponins, phenolic compounds, tannins, and essential oils. The range of uses for this species is extensive, encompassing a variety of illnesses such as coughs, colds, fever, loss of appetite, colic, headaches, earaches, intestinal worms, and even malaria. (Asfaw & Demissew, 2015).

In addition to this, to increase the unique properties of *Artemisia Afra* leaf extract Ag and $SiO_2$ nanoparticle were impregnated to make Ag/$SiO_2$ nanocomposites (NCs). Reactive oxygen species (ROS) are produced by nanocomposites, which prevent electron pair recombination and cause harm to microorganisms and DNA. A mixture of nanoparticles that successfully increase the band gap is used to achieve this purpose (Kessler et al., 2022). Therefore, this study focused on the synthesis of Ag/$SiO_2$ NCs using *Artemisia afra* as a mediator through the green synthesis method for antibacterial and antifungal activity.

## 1.2. Statement of the problem

Nanotechnology is widely used in developed countries, but it is still in its infancy in Ethiopia, so there is a lot of scope for advancement in this area. Today, antibiotic resistance is becoming a serious problem in Ethiopia. While silver nanoparticles have been found to possess excellent bioactivity, which makes them useful for a variety of applications, including in the production of drugs, there are also some potential issues associated with their use. During this process, there is a major problem with using them. The first is the release of silver ions from silver nanoparticles contributes to the microbial efficacy of these nanoparticles, but their releases need to be controlled and the excessive release can lead to toxicity for human cells, especially cancer. Therefore, it is essential to control the release of silver ions from silver nanoparticles to achieve the desired antimicrobial activity without any adverse effects (Assis et al., 2021).

The second one is poor dispersion stability, thereby increasing aggregation and decreasing their antimicrobial properties. When nanoparticles are not equally dispersed throughout a solution or matrix, this is referred to as having poor dispersion. This can happen when nanoparticles clump together or cluster together, generating clusters that are larger than the individual nanoparticles. Aggregated nanoparticles may not be able to penetrate microbial cells or interact with cellular components effectively, reducing their activity (Bélteky et al., 2019). The above problems need to be solved by green synthesizing Ag/$SiO_2$ NCs for antibacterial activity. $SiO_2$ nanoparticles can

also act as carriers or supporter for Ag nanoparticles, allowing for the controlled release of the silver ions. The release rate of Ag ions from the nanocomposite can be controlled by adjusting the size and concentration of the $SiO_2$ nanoparticles. This controlled release of Ag ions can enhance the antibacterial activity of the nanocomposite and reduce the risk of toxicity.$SiO_2$ NPs can contribute by in increase the band gap in NCs and producing a greater generation of ROS species which can damage the DNA and cell membrane of microbes by decreasing electron pair in combination (Khezerlou et al., 2018). Therefore, Ag/$SiO_2$ NCs mediated from plant extracts have indicated better antimicrobial potential against human pathogens and infections caused by bacteria and fungi. *Artemisia Afra* is one of the important and most widely used herbs in traditional medicine. Currently, it has gained significant attention from the scientific community. Several studies have been conducted either to verify or substantiate the traditional use of this herb. Furthermore, its use is also being investigated in modern diseases like diabetes, cardiovascular diseases, cancer, respiratory diseases, etc. It is used to treat various ailments ranging from coughs and colds to malaria and diabetes (Liu et al., 2009).

Although it is one of the most popular local herbal medicines in Ethiopia, only limited scientific research, but in this studies mainly used for reducing and capping agent for nanomaterials. To the best of the author's knowledge, still today, no study has been reported on the green synthesis of Ag/$SiO_2$ NCs using leaf extracts of *Artemisia Afra* and their characterization and antimicrobial activities. In this regard, the current research was focused on the facile synthesis of Ag/$SiO_2$ NCs using an aqueous extract of *Artemisia Afra* leaves and the characterization of synthesised Ag/$SiO_2$ NCs.

## 1.3. Objectives of the Study

### 1.3.1. General objective

The main objective of this research was the synthesis and characterization of $Ag/SiO_2$ nanocomposite using *Artemisia Afra* leaves extract for antibacterial and antifungal activity.

### 1.3.2. Specific objectives

The specific objectives of this study are:

- To synthesize of Ag NPs, $SiO_2$ NPs, and $Ag/SiO_2$ Nanocomposites using *Artemisia Afra* plant leaf extract
- To characterize the synthesized Ag NPs, $SiO_2$ NPs, and $Ag/SiO_2$ NCs using UV-visible, FTIR, XRD and SEM
- To investigate the antibacterial activity of Ag NPs, SiO2 NPs, and $Ag/SiO_2$ NCs against *S. aureus, S. pyogenes, P. aeuruginosa* and *E. coli*
- To investigate the antifungal activity of Ag NPs, SiO2 NPs, and $Ag/SiO_2$ Nanocomposites against *Candida Albicans.*

## 1.4. Significance of the Study

This study provides more information concerning the biological synthesis of the $Ag/SiO_2$ NCs using locally available plant *Artemisia afra* leaves. The use of easily available $Ag/SiO_2$ nanocomposites (NCs) for their antimicrobial properties is expected to have several advantages, particularly in the area of community health. The $Ag/SiO_2$ NCs are relatively easy to prepare and can be synthesized using simple and scalable methods, making them accessible to a wide range of users. The discovery of new and effective antibacterial and antifungal agents is a critical area of research, especially given the increasing prevalence of antibiotic-resistant microbial. Its applications are a very promising, efficient, and cost-effective method for remediating this environmental health concern. It is believed that this work has a positive impact on increasing the number of available research works dealing with $Ag/SiO_2$ NCs biosynthesis and its antimicrobial activities. Furthermore, this study provides how efficient the nanocomposites in general and $Ag/SiO_2$ NCs in particular are in antibacterial and antifungal activity.

## 1.5. Scope of the Study

This research works was limited to the synthesis, characterization of the synthesized nanocomposite using UV-Visible, XRD, FTIR, and SEM technique. Finally, it evaluated the efficiency of antimicrobial properties of NPs and NCs biosynthesized using disc diffusion method against selected bacterial strains: Gram-negative bacteria *E. coli, P. aeruginosa,* and Gram-positive Bacteria *S. aureus, S. pyogenes*, and fungal strain *Candida Albicans.*

# 2. LITERATURE REVIEW

## 2.1 Nanotechnology

Nanotechnology is a fast-evolving field that deals with manufacturing new materials on the nanoscale level. This nanoscale size generally confers larger surface areas to nanoparticles (NPs) compared with macro-sized particles  The goal of nanotechnology is to create, characterize and manipulate matter that is between 1-100nm (Pillai et al., 2020). This technology is capable of providing miscellaneous novel applications that range from innovative fabric compounds, food processing, and agricultural production to sophisticated medicinal techniques. Nanomaterials have extremely small sizes having at least one dimension of 100 nm or less. Nanomaterials can be nanoscale in one dimension (e.g. surface films), two dimensions (e.g. strands or fibers), or three dimensions (e.g. particles) (Arti, 2020). Generally, nanomaterials are referred to as the infrastructure or building blocks element for nanotechnology.

## 2.2. Nanoparticles

Nanoparticles can be defined as objects ranging in size from 1- 100 nm that due to their size may differ from the bulk material. Nanoparticles are being used for diverse purposes, from medical treatments, and use in various branches of industry production such as solar and oxide fuel batteries for energy storage, to wide incorporation into diverse materials of everyday use such as cosmetics or clothes (Rawat, 2016a). Organic nanoparticles and inorganic nanoparticles are two categories of nanoparticles based on ingredients. Organic nanoparticles include carbon nanoparticles (fullerenes), and inorganic nanoparticles include magnetic nanoparticles, noble metal nanoparticles (gold and silver), and semiconductor nanoparticles (such as zinc oxide, Silicon dioxide, and titanium dioxide) (Drug, 2021). A decrease in particle size to Nano-size demonstrates peculiar and improved properties such as particle size distribution and morphology, which is not shown by larger particles of bulk material Nanoparticles have both solute and separate particle phase properties.

## 2.3. Silver Nanoparticles and their Properties

### 2.3.1. Electrical properties

Silver, due to its unique electrical properties can be used in electronic devices. Ag NPs can be used to make electronic devices. The electrical conductivity of Ag NPs ranging in size from 4 to 12 nm

and grown in glass-ceramic was investigated (Mohd Radzuan et al., 2017). Silver has the highest electrical conductivity, thermal conductivity, ductility, and contact resistance of any metal. As for metallic silver form, it is insoluble in water, but its metallic salts such as $AgNO_3$, and AgCl are water-soluble the electrons that cannot move freely at the nano level and their motion became restricted, and this confinement at the nanoscale resulted in the changes in electrical properties, such as the bulk conductor/semiconductor materials behaving as superconductors or conductors at the nanoscale. Similarly, nan silver (of size less than 10 nm) cannot conduct electricity. Other applications include data storage, devices, optoelectronics, Nano electronics, and soon (Syafiuddin et al., 2017).

### 2.3.2. Optical properties

When silver nanoparticles are exposed to the light of a specific wavelength, collective coherent oscillations of free electrons occur, resulting in charge separation for the ion lattice and the formation of dipole oscillations along the direction of the optical electric field. This phenomenon is called surface Plasmon resonance (SPR). The absorption and scattering properties of silver nanoparticles can be modified by controlling the particle size, shape, and refractive index near the particle surface. Smaller nanoparticles mainly absorb light, with a peak around 400 nm, while larger nanoparticles have increased scattering, broadening the peak and shifting it to longer wavelengths. Particle agglomeration also delocalizes conduction electrons near each particle surface, which can also change the optical (Shrivas et al., 2016). The band gap energy of silver nanoparticles was also found to be dependent on the concentration of nanoparticles, with an increase in Ag NPs concentration from 1 to 19% causing a decrease in band gap from 2.98 to 2.63 eV.

### 2.3.3. Morphologies and sizes

Silver nanomaterial fabrication can be tuned to produce colloidal silver nanoparticles with a variety of morphologies, including monodisperse Nano spheres, triangular prisms or nanoplates, cubes, wires, and Nano rods. The morphological change of silver nanoparticles (Ag NPs) is due to a complex interaction of molecular surface and crystalline properties. The antibacterial activity of Ag NPs is enhanced by the large surface-to-volume ratio of that of a spherical shape. Smaller particles that have a large surface area are more effective as antibacterial than larger particles when Ag NPs can interact with bacterial cells (Bélteky et al., 2019). Okaiyeto *et al*. obtained silver

nanoparticles of different sizes and morphologies by using various reducing and capping agents. They analyzed the effects of the reducing agent on Ag NPs sizes at ambient temperature and found that spherical silver particles of 8 and 24 nm diameter were obtained when applying the reducing agent to the silver salt in liquid crystalline pulmonic (Syafiuddin et al., 2017).

### 2.3.4. Crystalline structures

A crystalline structure is a structure that has a repeating pattern throughout its structure. It is characterized by its symmetry, which is determined by the shape and arrangement of its atoms, molecules, or ions. The atoms are arranged in a regular pattern that repeats itself in three dimensions to form a crystal lattice. The lattice can be thought of as a three-dimensional grid of points that represents the positions of the atoms in the crystal. According to *Khan et al.2018* study the XRD was done to determine the crystalline nature of Ag NPs and the resulting peaks were found at 37.90°, 44.05°, 64.25°, and 77.20° representing (111), (200), (220) and (311) face-centered cubic structure of silver which were compared with the standard powder diffraction card of Joint Committee on Powder Diffraction Standards (JCPDS). The average particle size was calculated by the Debye-Scherer equation where full width at half maximum (FWHM) data was used (M. Z. H. Khan et al., 2018).

### 2.3.5. Chemical properties

The chemical symbol of silver is Ag and the atomic number is 47. It has a melting temperature of around 961.78℃ and a boiling temperature of 2162℃. Silver can be present naturally in $Ag^0$, $Ag^+$, $Ag^{2+}$, and $Ag^{3+}$ forms of possible oxidation states. From these $Ag^0$ and $Ag^{2+}$ are the most abundant ones and $Ag^{3+}$ is unstable in the aquatic environment. Metallic silver is insoluble in water, but metallic salts such as silver nitrate and silver chloride are soluble in water-soluble. Although acute toxicity of silver in the environment is dependent on the availability of free silver ions, investigations have shown that these concentrations of $Ag^+$ ions are too low to lead to toxicity (Rawat, 2016b).

## 2.4. Synthesis of Silver Nanoparticles

Currently, there are two main approaches for the synthesis of nanomaterials and fabrication of nanostructure: “top-down” and “bottom-up” approaches. In the top-down (physical) approach, the size of silver metal in its bulk form reduces mechanically to the nano-scale by using sophisticated

methodologies such as laser ablation, thermal decomposition, evaporation-condensation, *etc.* The bottom-up (chemical and biological) approach is also known as the self-assembly technique, silver nanoparticles are obtained from their basic building blocks which react to produce silver nanoparticles of the desired shape and size and includes of dissolution of silver salt into a solvent, reduction of silver ions to their element using the addition of a reducing agent and then stabilization of the forming silver nanoparticles using a stabilizing agent to prevent agglomeration of nanoparticles (Ahmed et al., 2016).

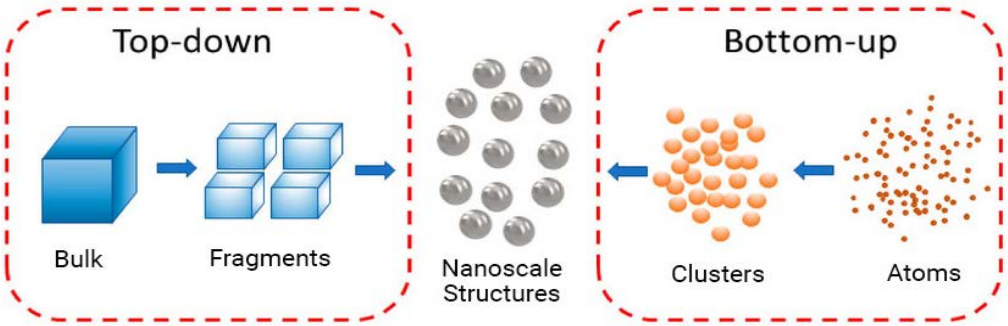


Figure 2.1**:** Top-down and Bottom-up synthesis of nanofabrication

The synthesis of silver nanoparticles is of much interest to the scientific community because of their wide range of applications. Generally, nanoparticles are prepared by a variety of chemical and physical methods which are quite expensive and potentially hazardous to the environment and involve the use of toxic and perilous chemicals that are responsible for various biological risks. The development of biologically-inspired experimental processes for the synthesis of nanoparticles is evolving into an important branch of nanotechnology.Recently, biologically-mediated synthesis of nanoparticles is a simple, cost-effective, dependable, and environmentally friendly approach and much attention has been given to the high-yield production of Ag NPs of defined size using various biological systems including bacteria, fungi, plant extracts, and small biomolecules like vitamins and amino acids as an alternative method to chemical methods not only for Ag NPs but also for the synthesis of several other nanoparticles, such as gold and graphene (J. Singh et al., 2018)

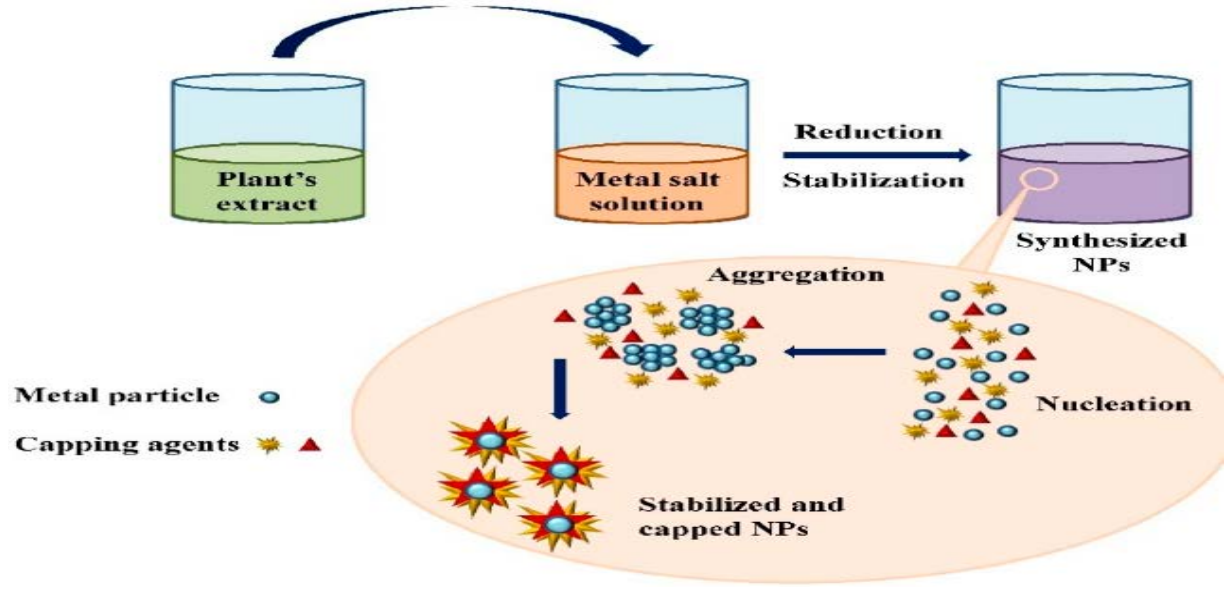


Figure 2.2:Mechanism of nanoparticle synthesis using phytoextracts (F. Khan et al., 2022)

For the synthesis of Ag NPs, plant biodiversity has been broadly considered due to the availability of effective phytochemicals in various plant extracts, especially in leaves such as ketones, aldehydes, flavones, amides, terpenoids, carboxylic acids, phenols, and ascorbic acids. These components are capable of reducing metal salts into metal nanoparticles (Baran, 2019).

## 2.5. $SiO_2$ Nanoparticle and its properties

Silica is another name for the chemical compound composed of silicon and oxygen with the chemical formula $SiO_2$, or silicon dioxide. There are many forms of silica. Silicon dioxide is indeed a very stable compound due to its high bond energy and lack of polarity. It is used as an insulator and semiconductor in electronics due to its high dielectric strength and ability to form a stable oxide layer on its surface. It is also used as a filler in rubber and plastics, as a thickening agent in paints and coatings, and as an abrasive in toothpaste and other cleaning products (Asst et al., 2018). $SiO_2$ NPs are currently one of the new inorganic materials due to their extraordinary characteristics of excellent chemical purity, ultrafine particle size, enhanced surface adsorption and energy, excellent dispersion, and high thermal resistance.(Raturi et al., 2021).All silica forms have the same chemical composition but differ in their atomic arrangements. Silica compounds can be divided into two groups: crystalline (c-silica) and amorphous silica (a-silica or non-crystalline silica). Crystalline silica compounds have structures with repeating patterns of silicon and oxygen. Silica is one of the most complex and abundant families of materials, which can exist as a

compound of several minerals and as a synthetic product. Some examples include fused quartz, fumed-silica, silica-gel, and different kinds of aerogels. Inside the majority of silicates, the Si atom shows tetrahedral coordination, consisting of four oxygen atoms surrounding a central Si atom. (Hardikar & Matijević, 2000).According to *Rodrigues et al.*, the amorphous structure shows a broad peak. There is no diffraction peak observed except for a broad band centered at 22°-$30^0$ which is the characteristic peak for amorphous $SiO_2$ Moreover, no sharp peak was observed in other scanning angles starting from 10° to 80° showing the absence of any ordered crystalline structure This also indicated relatively high disordered particle geometry of silica (Nayak, 2021) Basic silica particles have a hydrophilic surface with terminal Si-OH bonds, which are highly stable in organic solvents and aqueous buffers (Mebert et al., 2017) .The large surface area of $SiO_2$ nanoparticles makes more pore size available on their surface, which can significantly increase their adsorption capacity.

## 2.6. Synthesis of $SiO_2$ Nanoparticle

Several methods have been put forward for the synthesis of these materials, namely chemical vapor condensation, arc discharge, hydrogen plasma-metal reaction, laser pyrolysis in the vapor phase, micro-emulsion, hydrothermal, sol-gel, green method etc. The chemically synthesized silica nanoparticles are widely used as the chemical route is easy to follow and we have options for modification of the different parameters of the silica nanoparticle, in reverse micro emulsion, the spherical micelles are formed by the dissolving surfactants molecules in the presence of water. The major catch of this method is the high cost and difficulties in the removal of surfactants in the final products. But this method was successfully used for the coatings of nanoparticles to attach different functional groups for ample applications (Jeelani et al., 2020).Sol-gel method for the synthesis has been used for decades for the production of silica, glass, and ceramic materials due to its propensity to form pure and homogeneous products at a clement state. In this process, initially, colloidal particles are dispersed in a liquid forming a sol (Saravanan, 2020). Deposition of this sol can produce a thin coating on any substrate utilizing spraying, spinning, or coating. The particles in the sol are left to polymerize by removing the stabilizing components and further produce a complex network gel. The remaining organic and inorganic are components of pyrolysis at the end by heat treatment to form amorphous or crystalline coatings. This method involves hydrolysis and condensation of metal alkoxides such as TEOS, TMOS, or inorganic salts as sodium silicate in the

presence of mineral acid (e.g., HCl) or base (e.g., $NH_3$) as catalyst (Thomas et al., 2008).Sol-gel polymerization of tetra-alkoxysilanes, $Si(OEt)_4$ (TMOS), is a mild and convenient method for the synthesis of amorphous silica gels. The sol-gel process is the name given to any one of several processes in which solution or sol undergoes a sol-gel transition. At this transition, the solution becomes a rigid non-fluid mass. A specific example of a sol-gel process is the polymerization of TEOS in ethanol and water. Following the addition of a catalyst, this homogenous solution undergoes a sol-gel transition to a rigid gel consistent with silica ($SiO_2$) and solvent-filled pores (Nandanwar et al., 2015).

Green synthesis methods of NPs using plant extraction, fungi, algae, and microbes have numerous advantages, especially for biomedical applications (Sasivarnam et al., 2021). Among all green methods, plants have noteworthy quantities due to a huge number of phytochemicals such as flavonoids, polyphenols, glycosides, terpenoids, and proteins. The most significant difference between green synthesis and other techniques for producing NPs is that, first, the NPs are reduced, capped, and stabilized by the phytochemicals present in the plant extractions. One common green synthesis method $SiO_2$ NPs use plant extracts as reducing and stabilizing agent. The precursors such as silicic acid or sodium silicate, TEOS) can help to convert into $SiO_2$ NPs (Prabha et al., 2021).

## 2.7 Nanocomposite

Nanocomposites are materials that are made up of two or more components, with one of them being a nanoscale material. They have unique properties that are not found in their components. Composites are materials made from two or more constituent materials with significantly different physical or chemical properties that, when combined, produce a material with characteristics different from the individual components (Mrsc & Universiy, 2015). The matrix phase is continuous and surrounds the reinforcement material, which is discontinuous. The reinforcement material can be in the form of fibers, particles, or flakes. Composites are generally divided into three basic classes according to the size of the reinforcement in the structures. These are macro composites, micro composites, and nanocomposites (Karthik et al., 2021a; Okpala, 2013).

Nanocomposites are materials that incorporate Nano-sized particles into a matrix of standard materials. Nanocomposites are a special type of material with enhanced properties. When a small number of nanoparticles, such as metal, metal oxides, carbon nanotubes, graphene, graphene

oxide, and layered silicates, are dispersed in a polymer or non-polymer matrix, nanocomposites are formed. In general, nanocomposites are multiphase materials with at least one of the constituents in the Nano dimension in different structures and compositions. The inorganic components can be three-dimensional framework systems such as zeolites, two-dimensional layered materials such as clays, metal oxides, metal phosphates, chalcogenides, or even one- and zero-dimensional materials such as $Mo^{3}Se^{3-n}$ chains and clusters. (Okpala, 2013).Generally, the nanocomposite is used for drug delivery systems, anti-corrosion barrier coatings, UV protection gels, lubricants, scratch-free paints, new fire retardant materials, new scratch- and abrasion-resistant materials, superior-strength fibers, and films.(Karthik et al., 2021b).

## 2.8 Silver/Silicon dioxide ($Ag/SiO_2$) Nanocomposites

Silver/silicon dioxide ($Ag/SiO_2$) nanocomposites have attracted significant attention in recent years due to their unique physical, chemical, and optical properties, which render them suitable for a wide range of applications in various fields such as catalysis, electronics, sensing, and antimicrobial surfaces. The combination of the noble metal nanoparticles, such as silver (Ag) with excellent conductive, plasmonic, and antibacterial characteristics, and the semiconductor silicon dioxide ($SiO_2$) with high thermal stability and good insulating properties, offers tremendous opportunities for the design of advanced materials with tailored functionalities (Taheri, 2018)

As efficient and cost-effective noble metal nanoparticles (NPs), Ag NPs are considered one of the most promising functional materials in the electronic, chemical, biological, and catalytic fields. However, the practical use of Ag NPs is severely hindered by their severe aggregation during the catalytic process, which unavoidably gives rise to a decrease in active surface area and further degradation of performance under long-term operation. One way to improve the stability of the metal NPs is to stabilize them with the protection of $SiO_2$ during the catalytic process, which is very resistant to coagulation, even at high-volume fractions (Allafchian et al., 2017). Furthermore, their diminutive size with an appropriate distribution on appropriate support is the primary requirement for the synthesis of active Ag-supported composites. Various solid supports, such as metal oxides, zeolites, carbon, etc., are employed for the catalytic NPs to prevent their aggregation. $SiO_2$ nanoparticles are generally considered inert or non-reactive because they have a stable and robust structure, which makes them resistant to chemical reactions. The surface of $SiO_2$ nanoparticles is typically covered with a layer of silanol groups (-Si-OH), which are chemically

stable and unreactive. This layer forms a barrier that prevents the interaction of the nanoparticles with other substances. Furthermore, $SiO_2$ is considered one of the promising materials for high-performance drug delivery (Azimi & Lasemi, 2022).

$Ag/SiO_2$ nanocomposites are better for increasing antibacterial activity and avoiding aggregation than Ag nanoparticles. In addition, they have been employed in electronics, biomedicine, and other fields. The significant problem is the poor dispersion stability, thereby increasing the aggregation and decreasing their antibacterial properties. Therefore, much has been done to develop the dispersion stability of nanomaterials by coating the nanoparticles with different chemical compositions. Hence, the silver nanoparticles are rarely used by themselves and are often dispersed in a matrix. (Shi et al., 2015).

### 2.8.1 Synthesis $Ag/SiO_2$ Nanocomposite

The synthesis of uniformly sized nanocomposites is very important because their properties include optical, magnetic, electrical, and biological properties depending on their size and dimensions. Synthetic methods are frequently classified into three classes: solution-based synthesis, vapor-phase synthesis, and gas-phase synthesis. Another approach is to divide these synthetic approaches into two broad categories: a) the top-down approach, which includes physical methods, and b) the bottom-up approach, which encompasses wet methods. The choice of synthetic approach depends on the desired characteristics required in the nanoparticle composites, e.g., size, morphology, crystal structure, etc., but the benefit of physical methods is the production of large amounts of nanocomposites, but the synthesis of equal-sized nanocomposite particles is not easily attainable. (Duhan et al., 2010) .

$Ag/SiO_2$ nanocomposite can be synthesized using various methods, including sol-gel, gamma irradiation, biosynthesis, and chemical reduction. The choice of method depends on the desired properties of the nanocomposite and the specific application. In comparison, wet chemical methods give uniformity in the size of nanocomposites, as controlled particle size can be easily achieved. By varying conditions of reaction, different shapes (nanorods, nanowires, nanotubes, etc.) of nanocomposites can also be synthesised (*AL-Jobory et al., 201*9)

The synthesis of $Ag/SiO_2$ nanocomposites can be achieved through various methods, including chemical reduction, sol-gel, co-precipitation, and electrochemical techniques. Precise control of the size, morphology, and dispersion of the silver nanoparticles embedded in the silica matrix is

crucial for the optimization of the desired properties and performance of the nanocomposites. Additionally, the interaction between the Ag nanoparticles and $SiO_2$ matrix plays a significant role in defining the overall characteristics of the hybrid materials(Tri et al., 2021).

Ag/$SiO_2$ nanocomposites with catalyst are synthesized by three steps (*$SiO_2$ Nanocomposites.Pdf*, n.d.)The first step is deprotonation of hydroxyl ligand in SiOH. Adding base catalyst into SiOH generates the $SiO^-$ group: Si-O-H

$$Si\text{-}O\text{-}H + B: \rightarrow SiO^- + BH \qquad (1)$$

The second step is electrophilic attack. Electrophilic metal ($Ag^+$) is easily bonded with the nucleophilic part (SiO-):

$$SiO^- + Ag^+ \rightarrow SiO\text{-}Ag \qquad (2)$$

The third step is growth of the Ag nanoparticles by attaching more $Ag^+$ on the surface of the $SiO_2$ nanoparticle. The Ag forming process we employed is considered to be sensitive to the configuration of terminal groups on the $SiO_2$ surface, since such surface groups obviously provide the capability required for the reduction of Ag ions via reactions such as

$$Si\text{-}O\text{-}H + Ag^+ \rightarrow Si\text{-}O\text{-}Ag + H^+ \qquad (3)$$

Terminal OH groups usually form on the oxide surface by dissociative adsorption of water molecules, depending on their coordination symmetry. Accordingly, nanocomposite may form by auto reduction of noble metal ions with oxide surfaces. The efficiency of the surface-mediated reduction process can be decreased with consumption of hydroxyl groups and generation of surface charging (*$SiO_2$ Nanocomposites.Pdf*, n.d.).

### 2.8.2. Biological Synthesis Ag/$SiO_2$ Nanocomposites

Biological nanoparticles are stable, yet despite this, they are not monodispersed, and the rate of synthesis is slow. The poly disparity of nanoparticles and an ensuing slowdown in the rate of synthesis are caused by the fluctuating concentration of synthesised macromolecules or components involved in the nucleation of particles over time. Ag/$SiO_2$ is attracting a lot of attention among the many metal/semiconductor composites because of its exceptional qualities. $SiO_2$ is thermally stable and highly bioactive, and it can not only prevent particle agglomeration and improve surface hydrophilicity but also further improve stability (Assis et al., 2021).Ag/$SiO_2$ nanocomposites are a type of nanocomposite that is made up of silver nanoparticles and silicon

dioxide. They were synthesized using a green synthesis method that involves using plant extract as both the reducing agent and capping agent. The plant extract is used to reduce silver ions to silver nanoparticles and also to cap the surface of the nanoparticles with organic molecules from the plant extract. Silicon dioxide is then added to the mixture to form the final nanocomposite. The green synthesis method is an eco-friendly approach that avoids the use of toxic chemicals and solvents, making it a safer and more sustainable alternative to traditional methods of synthesis (Taheri, 2018). Biological synthesis of $Ag/SiO_2$ nanocomposites typically involves the use of microorganisms, such as bacteria, fungi, algae, or plant extracts. These organisms can act as reducing agents, which can reduce silver ions to form Ag nanoparticles and can also provide a template for the formation and stabilization of the $SiO_2$ matrix.(Khattab et al., 2022).

## 2.9. *Artemisia Afra (Ariti)* Plants

### 2.9.1. Botanical Description and Phytochemistry

*Artemisia afra* (African wormwood, family Asteraceae) is widely distributed along the eastern parts of Africa. *A. afra* is a common species in South Africa with a wide distribution from the Cedarburg Mountains in the Cape, northwards to tropical East Africa and stretching as far north as Ethiopia especially, In Ethiopia, this plant is found in Bale, Sidamo, Arba Minch, and Keffa. It usually grows in rocky mountainous areas along forest margins and stream sides and its natural distribution extends from Bale Mountains National Park (Dinsho) southeastern. Worldwide there are about 500 species of *Artemisia*, mainly from the northern hemisphere. Many of the other *Artemisia* species are aromatic perennials and are used medicinally (G. V. Patil et al., 2011). There are many different common or local names describing this plant in English “African wormwood” and in Afrikaans “Wilde als” in Ethiopia Ariti (Amharic), Kapani (Afan Oromo), Kodo (Guragna). In Ethiopia, the genus is represented by four species, namely *A. schimperi Sch. Bip. ex Engl*., *A. abyssinica Sch. Bip. ex A. Rich., A. afra Jacq. ex Willd*., and *A. absinthium L* (Asfaw & Demissew, 2015).

It is used to treat coughs, colds, diabetes, malaria, sore throat, asthma, headache, dental care, gout, and intestinal worms. In vitro, studies have revealed that *Artemisia Afra* is a potential antidepressant, with cardiovascular, spasmolytic effects, antioxidant, and antimicrobial activity (Graven et al., 1992). Traditional in Ethiopia people used *Artemisia Afra* the roots stem and leaves in many different ways and are taken as enemas, poultices, infusions, body washes, lotions,

smoked, snuffed, or drunk as a tea. Most of the time for holidays coffee ceremonies they used for decoration (Toit & Kooy, 2019).

*Artemisia Afra* grows in tufts with ribbed woody stems and reaches 0.5 to 2 meters in height. The leaves are dark green, soft to the touch, and shaped like fern leaves. The underside of the leaves is light green and covered with white bristles. *Artemisia Afra* flowers in late summer with profuse butter-colored flower bracts about 3 to 5 mm in diameter. *Artemisia Afra* gives off a pungent, sweet scent when part of the plant is damaged (G. V. Patil et al., 2011).

Figure 2.3: Different parts of *Artemisia Afra* leaf plant in Wondo Genet

## 2.10. Characterization of Ag/$SiO_2$ Nanocomposite

Characterization of nanoparticles is important to understand and control nanoparticle synthesis and applications. The typical characteristic parameters pursued include size, shape, chemical composition, crystal structure, morphology, surface charge, and stability. After synthesis of the Ag/$SiO_2$ Nanocomposite, various analytical techniques, such as Scanning electron microscope (SEM), Ultraviolet-Visible (UV-Vis) spectroscopy, X-ray diffraction (XRD), Fourier transform infrared spectroscopy (FT-IR)

### 2.10.1. X-ray Diffraction Spectroscopy (XRD)

X-ray diffraction is a versatile non-destructive analytical method for identifying and quantifying various crystalline forms, known as 'phases' of compounds, present in powders and solid samples It can be used to determine the crystal structure of solids, including lattice constants and geometry, identification of unknown materials, orientation of single crystals, defects, etc. The composition

of the nanoparticles can be then evaluated by comparing the peak intensity and position with the reference patterns available from the Joint Committee powder Diffraction Data Standard (JCPDS) database (Science et al., n.d.). The average size of the nanoparticles can be estimated using the Debye–Scherer equation:

$$D = k\lambda/\beta \cos\theta \qquad (4)$$

Where,

D = Crystalline size diameter

k = Scherer constant (usually 0.9),

λ = Wavelength of the X-Ray source, Cu Kα radiation (1.5406Å),

β = Full width at half-maximum (FWHM) of the diffraction peak

Θ = Bragg's diffraction angle (Science et al., n.d.)

### 2.10.2. Scanning Electron Microscopy (SEM)

A scanning electron microscope is a kind of electron microscope that images a sample by scanning it using a high-energy electron beam. It is a high-resolution surface imaging technique used to obtain information about the structure of nanoscale and microscale samples using an electron beam. Due to the large depth of field and high magnification, depending on the electron density on the surface, SEM images are useful for evaluating the surface topology of $Ag/SiO_2$ Nanocomposite. Information about the morphology, orientation, and crystal structure of $Ag/SiO_2$ Nanocomposite can be obtained from the recorded signals (Akintelu & Folorunso, 2020).

SEM uses backscattered electrons and secondary electrons emitted from the sample to construct a three-dimensional image of the analyzed sample. The image is created by directing an electron beam onto a thin probe. The probe uses scanning coils to scan the sample surface and provide a series of high-resolution images at various magnifications.

### 2.10.3. Fourier Transform Infrared (FTIR) Spectroscopy

FTIR spectroscopy is used to identify the functional groups of the active component based on the peak value in the region of infra-red region. FTIR was used to characterize the nanoparticles using the powdered nanoparticles samples by the KBr pellet method. The absorbance maxima were scanned by FTIR at the wavelength of 400- 4000 $cm^{-1}$. This method is particularly useful for identifying organic and inorganic compounds. It can be used to quantify some components of an unknown combination (I. Khan et al., 2019).

### 2.10.4. UV-Visible Spectroscopy

The electronic structures of atoms, ions, molecules, or crystals through exciting electrons from the ground to excited states (absorption) and relaxing from the excited to ground states (emission) are used for determination in UV-Vis spectroscopy It deals with the study of electronic transitions between orbitals or bands of atoms, ions or molecules in gaseous, liquid and solid state (The et al., 2021). UV-Vis spectroscopy can be utilized to study the unique optical properties of nanoparticles. This characterization method can be used to analyze the absorbance range of the $Ag/SiO_2$ NCs. The absorbance range will be monitored within the wavelength range of 200-800 nm (Demissie et al., 2020). The optical band gap of the entire sample was determined from the absorption coefficient value. The Tauc relations are used to calculate the energy bandgap for the samples

$$(\alpha hv)^2 = k(hv - Eg) \qquad (5)$$

Where α absorbance co-efficient, h is Plank constant, ν is incidental UV radiation frequency, k is Constant, *hv* is Energy, and Eg is Band gap energy

$$Eg = \frac{1240}{\lambda max}\,(\text{e.v}) \qquad (6)$$

Absorbance co-efficient α is calculated as

$$\alpha = 2.303 * \frac{A}{t} \qquad (7)$$

Where $A$ is absorbance and $t$ is the thickness of the cuvette. As a result, its value is 1 cm. The absorption coefficient measures the amount of light that might be absorbed by a given sample thickness; it tells us how much light at a specific wavelength will be absorbed by materials (Jubu et al., 2020)

## 2.11. Applications of $Ag/SiO_2$ Nanocomposite

These $Ag/SiO_2$ nanocomposites are used in various applications, including: Antimicrobial coatings: These nanocomposites can be incorporated into coatings for medical devices, textiles, food packaging, and water treatment systems due to their strong antimicrobial properties. Biosensors: The combination of silver and silica particles enables the development of effective biosensors, which can be used to detect biological molecules such as proteins or DNA.Drug delivery systems: $Ag/SiO_2$ nanocomposites can be used as carriers for drugs, enabling targeted

delivery to specific sites in the body, which can improve efficacy and reduce the side effects of certain medications Catalysis: The nanocomposites can be used as catalysts to improve the rate and selectivity of chemical reactions, particularly in environmental applications such as water purification and air purification.

### 2.11.1 Antibacterial Activity

Antibacterial activity is defined as the action by which bacterial growth is inhibited or destroyed. Bacteria are classified into Gram-positive and Gram-negative depending on whether they give positive or negative results on Gram's stain test. That is, while those which retain the initial pink color of crystal violet stain, under their thick peptidoglycan layer in their cell walls are named Gram-positive, those that are decolorized and are stained red with carbo fuchsine or safranin owing to their relatively thinner peptidoglycan layer in their cell walls are Gram-negative. Metal-based nanoparticles establish a strong bond with membranes, resulting in the disruption of cell walls and, consequently, increasing their permeability(Cotton et al., 2019).

Nanoparticles can also release metal ions from the extracellular space, capable of entering the cell and disrupting biological processes. Inside the cell, either metal ions or nanoparticles can induce the production of reactive oxygen species ROS, which generate oxidative stress leading to the oxidation of glutathione and suppression of the antioxidant defense mechanism of bacteria against ROS. Metal ions can form strong coordination bonds with N, O, or S atoms which are abundant in organic compounds and biomolecules. Since the bond between metal ions and biomolecules is generally non-specific, metal-based nanoparticles generally exhibit a broad spectrum activity (Slavin et al., 2017).

The outer membrane of gram-negative bacteria acts as a barrier that can prevent the entry of certain molecules, including some antimicrobial agents. This barrier function is due to the presence of LPS, which can repel or exclude hydrophobic or large molecules. This can make gram-negative bacteria more resistant to some types of antimicrobial agents, such as certain antibiotics. Gram-positive bacteria generally lack an outer membrane, which can make them more susceptible to certain antimicrobial agents that target the cell membrane, such as polymyxins (Cotton et al., 2019). The absence of an outer membrane can also make gram-positive bacteria more susceptible to the action of lytic enzymes, such as lysozyme, which can break down the peptidoglycan layer.

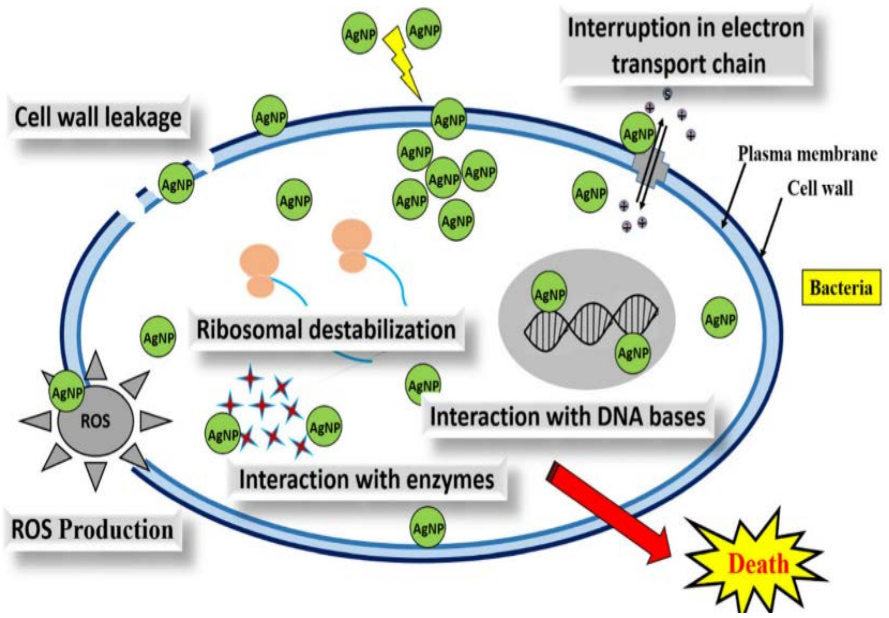


Figure 2.4 :Mechanism of Antibacterial activity for Ag NPs *(M. P. Patil & Kim, 2017)*

In Figure 2.4 showed the interaction between the positive charge of Ag+ and the negative charge on the bacterial cell wall affects the structure of the cell wall and increases cell permeability, which ultimately causes cell death. Phosphorus- and sulfur-containing biomolecules are found in both external (membrane protein) and intracellular (DNA bases, protein) components; these biomolecules influence cell division, respiration, and ultimately the survival of the cell. AgNPs have a higher affinity for interacting with these biomolecules (M. P. Patil & Kim, 2017).

Antibacterial activity can be measured by activity index (AI) which is obtained by dividing the inhibition zone of the sample by that of the positive control, both measured in millimeters. The zone of inhibition or clearance zone is the area where there is no growth of any bacteria observed due to the antibacterial action of the applied test nanocrystals suspended in an appropriate solvent such as dimethyl sulfoxide, which doesn't kill bacteria itself Standard antibiotics such as ampicillin, chloramphenicol is used as a positive control against which the inhibition zone of test solutions are compared (Dong et al., 2019)**.**

Ag nanoparticles synthesized by using different methods are easily aggregated and then cause deterioration of their chemical properties and decrease antibacterial properties. To improve these problems, we synthesized Ag nanoparticles formed on the surface of $SiO_2$ nanoparticles. Also, to increase antibacterial properties, more Ag nanoparticles were formed on the surface of $SiO_2$

nanoparticles. If Ag is formed on supporting materials, the release time of Ag can be delayed for a long time so that Ag-supported materials will be of great potential for antibacterial application.

The antibacterial activity that strong adsorption ability cause both bacteria and part of the dispersed Ag nanoparticles to be adsorbed on the surface of $SiO_2$ nanoparticles, where the bacteria have more opportunities to contact Ag nanoparticles. From this point of view, to avoid the aggregation of Ag nanoparticles, an optimum level of Ag nanoparticle loading is recommended for the synthesis of Ag formed on the surface of $SiO_2$ nanoparticles for antibacterial activity. Antibacterial activities of $Ag/SiO_2$ nanocomposites against microorganisms considered in the present study were qualitatively and quantitatively assessed by determining the presence of inhibition zones respectively. Antibacterial effects in the form of inhibition zones, evaluated by the disk diffusion assay of the $Ag/SiO_2$ nanocomposites, The values of inhibition zones against gram-positive and gram-negative bacteria(Mohammed, 2019).According to Kessler et al.,( 2022) they mostly consist of radicals (a species with one or more unpaired electrons) such as the hydroxyl radical (HO), superoxide ($O2^-$) and singlet oxygen ($O_2$),in addition to non-radicals such as hydrogen peroxide ($H_2O_2$). Finally, Silver nanoparticles (Ag NPs), and silica nanoparticles ($SiO_2$ NPs) liberated from $Ag/SiO_2$ nanocomposite penetrate inside the bacteria and interact with cellular organelles, thereby influencing individual cellular machinery and modulating the cellular signal design and inducing cell death. $Ag/SiO_2$ nanocomposite may serve as a vehicle to effectively deliver Ag+, and $Si^{+2}$ ions to the bacterial cytoplasm and membrane (Abduraimova et al., 2021).

### 2.11.2 Antifungal Activity

Pathogenic fungi are those fungi that cause disease in animals and humans. Those are considered to play a vital role in causing fungal infections, especially in hospitals. Although fungi are eukaryotic organisms, on the other hand, many pathogenic fungi are also microorganisms(Huang et al., 2023). Moreover, compared with bacteria, fungi have higher tolerances too, and uptake competencies for, metals, particularly in terms of the high wall-binding capability of metal salts with fungal biomass for the high-yield production of nanoparticles. In various studies, Ag/SiO2 nanocomposites have shown promising results in inhibiting the growth of different types of fungi, such as *Candida albicans*, *Aspergillus niger*, and *Fusarium solani*. Therefore, $Ag/SiO_2$ NCs have potential applications in areas such as food packaging, medical coatings, and water purification systems, where preventing fungal contamination is crucial.

$Ag/SiO_2$ nanocomposites (silver-silica nanocomposites) have been shown to exhibit effective antifungal properties due to the presence of silver nanoparticles. Silver nanoparticles have been widely recognized as antifungal agents because they can disrupt fungal cell membranes, produce reactive oxygen species (ROS), and interfere with DNA replication, thus inhibiting fungal growth and replication. $SiO_2$ NPs have been widely researched for potential drug delivery applications, due in large part to the facile synthesis routes available to create $SiO_2$ NPs with high porosity, tunable pore sizes in the micro to mesoporous range, and large specific surface areas. Although the antifungal efficacy of $SiO_2$ NPs themselves is low, using them as carriers of antifungal drugs has achieved very good results.(Huang et al., 2023).

The antifungal activity of the nanocomposite may be due to a synergistic effect between the silver nanoparticles and the silica matrix. The silica matrix may enhance the stability and activity of the silver nanoparticles, leading to a more potent antifungal agent (Nguyen et al., 2016). Nanosilver is a more effective and fast-acting fungicide against a broad spectrum of common fungi including genera such as *Candida Albicans*. Because of the high antimicrobial activity of Ag NPs, they have also been used as coatings for other, larger particles to optimize them for potential antifungal applications. One study reported that 7 nm Ag NPs coated on 350 nm $SiO_2$ NPs ($Ag/SiO_2$ NPs) showed 99.9% growth inhibition against Botrytis cinereal at 50 μg/mL (Tutaj et al., 2016). Generally, the antifungal activity of $Ag/SiO_2$ nanoparticles is due to the release of $Ag^+$ ions from the surface of the nanoparticles, which can disrupt the cell membrane of the fungal cells and inhibit their growth. The small size and high surface area of the nanoparticles also contributes to their effectiveness, as they can penetrate the cell walls of the fungi and interact with their cellular components.

# 3. MATERIALS AND METHODS

## 3.1 Chemicals and Reagents

Chemicals and reagents including silver nitrates ($AgNO_3$ 99.9%, AR analytical reagent Trust Chemicals, India), Tetraethylorthosilicate (TEOS 98%,AR analytical reagent Trust Chemicals, India ), distilled water, Sodium hydroxide (NaOH 99%, Sigma Aldrich,India), Ethanol ($C_2H_5OH$ 99.8%,Wasse PHARMA PLC,Ethiopia), Methanol ($CH_3OH$ 99.8%,Sigma Aldrich,India ), Ammonium Hydroxide ($NH_4OH$ 99% Sigma Aldrich, Germany,), Hydrochloric acid (HCl, Riedel dehaen, Germany, 37% HCl), Iodine (I,98.5%, Loba Chemie,Japan),Potassium iodide (KI,99.8%, Showa,Japan), Benedict's solution, Ascorbic acid (98%, Sigma Aldrich, Germany) Dimethyl sulfoxide (DMSO 99.5%, SRL,Japan), Mueller Hinton Agar (Sigma Aldrich,India), Potato Dextrose Agar (Sigma Aldrich, Germany), Sabouraud Dextrose Agar (Sigma Aldrich,India)

### 3.1.2 Apparatus and Instruments

The apparatus and equipment that were used during this research work were a UV-Vis spectrometer (T80+- PG instrument), XRD (Shimadzu, XRD-7000S South Korea), FTIR (FTIR Perkin Elmer's spectrophotometer), SEM (Scanning Electron Microscopy) (SEM, JEOL, JCM-6000Plus, Japan), electronic balance, oven, beaker, test tube, magnetic stirrer, thermometer, Whatman No.41, filter paper, measuring cylinder, pH-meter, spatula, Erlenmeyer flask, volumetric flask, ceramic crucible, Buchner funnel, bare magnet, Pipette, aluminum foil, spatula, brown bottle, electronic beam balance, electrical grinding machine, vials, magnetic stirrer with hot plate, petri-dish, refrigerator, mortar and pestle, dropper and centrifuge.

## 3.2. *Artemisia Afra (Ariti)* Plant Leaves Collection and Preparation

### 3.2.1. Collection of *Artemisia Afra (Ariti)* Plant Leaves

The leaf of *Artemisia afra* was collected on February 4,2023 from the Southern part of Ethiopia, Sidama regional state, Wondo Genet zone located 211.9 km far from Adama city. The fresh leaf of the plant *Artemisia Afra* was collected from the farm land which is shown in Figure 3.1.

Figure 3.1: *Artemisia Afra (Ariti)* plant collection place at Wondo Genet

The collected plant was packed in a plastic bag and immediately brought to the Chemistry research laboratory ASTU. The leaf samples were thoroughly washed several times with tap water. Followed by distilled water to remove extraneous matter. The cleaned *A. Afra* (*Ariti)* leaves were completely dried at room temperature in open air and under shadow for about two weeks (15 days) to remove any remaining moisture content from the leaves (Hagos et al., 2018). The dried leaves of the *A. Afra* plants were crushed by using an electrical grinding machine to produce a fine powder. Finally, the dried and ground sample was stored for further processing (Figure 3.2).


Figure 3.2: Steps involved in the Pre-extraction *Artemisia Afra* plant Leaf extract

### 3.2.2. Extraction of *Artemisia Afra* leaf extract

The extraction was carried out by taking 25 g of the powdered leaf of *Artemisia Afra* in 800 mL of glass beaker containing 500 mL of distilled water. The beaker was covered with aluminum foil, to prevent the effect of light. After that, the mixture was stirred using a magnetic stirrer for 15 min and allowed to be heated at 50 °C for 1 hour on a hot plate with a magnetic stirrer. Then the heater was turned off after 1 hour and the mixture was allowed to cool down to room temperature and settle as shown in Figure 3.3. After settlement, the prepared extract was filtered twice with Whatman No.41 filter paper to get a clear solution for further experiments. Finally, the filtrate was stored in a refrigerator at 4 °C (Balciunaitiene et al., 2021).

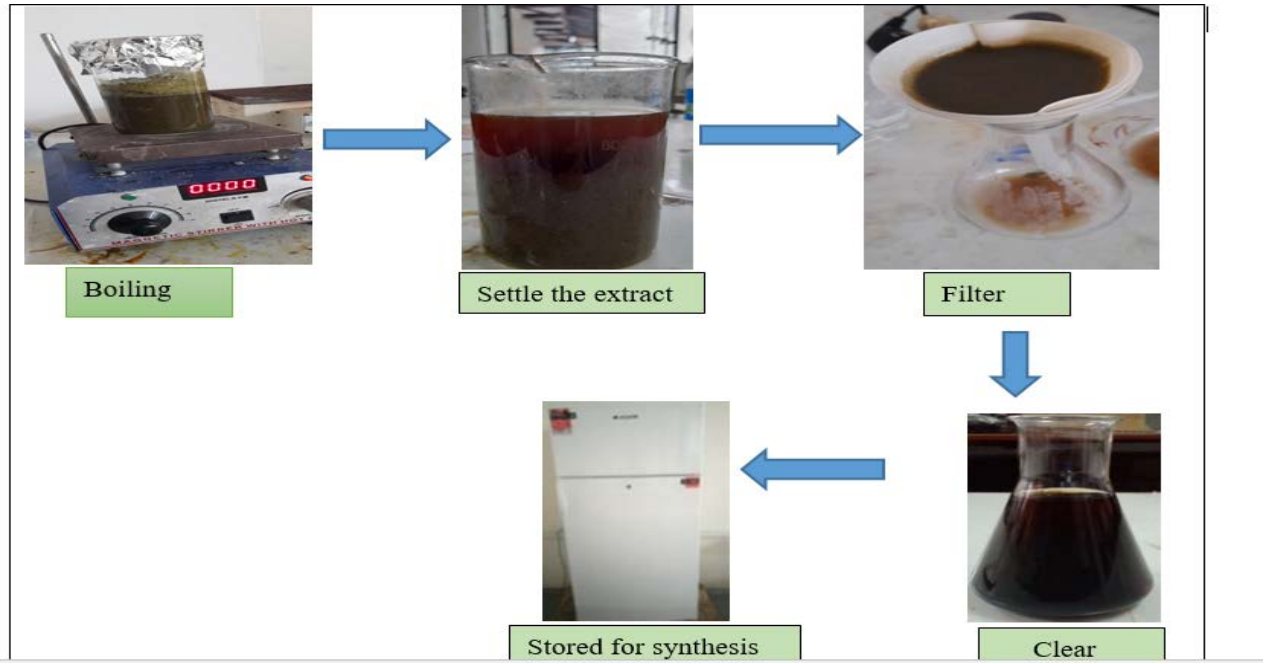


Figure 3.3: Extraction of *Artemisia Afra* leaf extract

## 3.3. Phytochemical Tests of *Artemisia Afra Leaf* Extracts

*Artemisia Afra leaf* extract was used as a reducing agent and capping agent, it was necessary to assess whether the phytochemicals, such as flavonoids, phenols, alkaloids, etc. do naturally exist in the extract or not. A phytochemical test was used to detect the presence of alkaloids, flavonoids, saponins, steroids, phenol, glycoside, and reducing sugar and were carried out using standard methods.

**Detection of Flavonoids**

The presence of flavonoid in leaf extract was checked through Ferric chloride test 5 mL of extract aqueous solution was dissolved into 7 drops of 5% ferric chloride solution (Garg et al., 2019).If flavonoid present in sample extract, it formed a green precipitate.

**Detection of Glycoside**

The presence of glycoside in leaf extract was checked through Salkowski test by using 2 mL of concentrated $H_2SO_4$ added to the aqueous plant extract. If glycoside is present in the extract reddish-brow/red color was formed (Shaikh & Patil, 2020).

**Detection of Steroids**

The presence of steroids in leaf extract was checked through Salkowski test by using 2 mL of chloroform and concentrated $H_2SO_4$ was added with 5 mL aqueous plant crude extract. If steroid present in the solution red color was appeared at the bottom. (Yaseen et al., 2017).

**Detection of Alkaloids**

The presence of alkaloids in leaf extract was checked through Wagner's test by dissolving 2mL the aqueous leaf extracts in Wagner's reagent (Iodine in Potassium Iodide) in a test tube. If alkaloids present in sample extracts, it formed brown/red precipitate (Shaikh & Patil, 2020).

**Detection of Phenols**

The presence of the phenolic functional group in leaf extract was checked by taking 5 mL of aqueous extract into a test tube and adding 5 drop of 3% of $FeCl_3$ into an extract drop by drop wisely. If phenol present in extracts, it generate to dark green/bluish/black color (Yaseen et al., 2017).

**Detection of Reducing sugar**

The presence of reducing sugar in the leaf extract was checked through the Benedicts test by taking 3 mL of aqueous leaf extract into a test tube and adding Benedicts reagent drop by drop and heated for 2 min. If carbohydrates/reducing sugar present in the sample, it formed red/blue-green precipitate (Shaikh & Patil, 2020).

**Detection of Saponins**

The presence of saponins in leaf extract was checked through a frothing test by shaking a mixture of 3 mL of aqueous plant extract and 5 mL of distilled water. If saponins present in the extracts, it generate foam layer of 1cm (Bano & Deora, 2019).

## 3.4 Synthesis of Silver Nanoparticles (Ag NPs)

The biosynthesis of Ag NPs has been performed by adapting the reported procedure of Elemike et al., (2018) with a minor modification. Silver nitrate was used as a precursor for the biosynthesis of silver nanoparticles using *Artemisia Afra* leaf extracts (Elemike et al., 2018),. To synthesize Ag NPs, 100 mL of 0.1 M aqueous $AgNO_3$ stock solution was prepared and stored in brown bottle. This solution was mixed with 100 mL of plant leaf extract (1:1). To this mixture a small-sized magnetic bar was put inside the beaker containing the leaf extract and the precursor solution to enhance the reaction kinetics. Then the mixture was heated at 30 $^{o}$C for 1 hour on the hot plate with stirring and after 1 hour, the heater was turned off and the mixture was stirred for 3 h without heating. The color was changed from light yellow to brown which indicates the formation of its silver nanoparticles. Then, after the stirring reaction time was completed the formed silver nanoparticles were allowed to stay within a refrigerator overnight to cool down and settled. Then the mixture was decanted and the formed precipitate was washed with ethanol and distilled water 3 times followed by centrifugation for 15 min at 15000 rpm. After the end of the centrifugation, the formed silver nanoparticles were collected using a crucible ceramic dish and placed into a drying oven at 100 °C. After drying, it was allowed to cool and the obtained product was ground into small fine powder by a mortar and pestle. Finally, the gray powder of silver nanoparticles was obtained. The whole procedure is summarized in Figure 3.4.

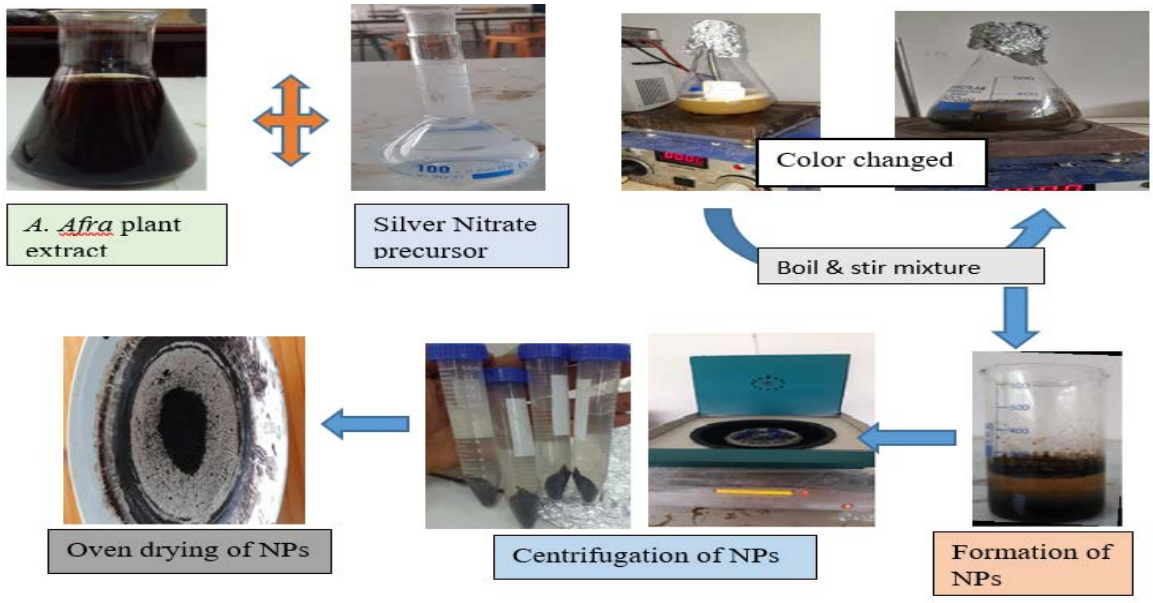


Figure 3.4: Biosynthesis process of silver nanoparticles

## 3.5. Synthesis of $SiO_2$ Nanoparticles

For the synthesis of $SiO_2$ NPs (TEOS), a previously reported method was used (Otari et al., 2019) with minor modifications. 4 mL of TEOS was added dropwise to 40 mL *A. Afra* plant extract. Then stirred on a hot plate for 30 min. 1.5 mL of $NH_4OH$ was added to the above solution to form a precipitate and for adjusting pH value, which was further stirred for 3 hours. After stirring the solution was removed from the hot plate and left for settling down of $SiO_2$ NPs precipitates. White precipitates of $SiO_2$ NPs were washed three times with distilled water and ethanol on the Whatman No. 41 filter paper. It was dried in the hot oven for 3 hours at 100 °C. After drying, it was allowed to cool and the obtained product was ground into small fine powder by a mortar and pestle. Finally, the powder was stored for further study. Figure 3.5 showed the whole procedure $SiO_2$ NPs.

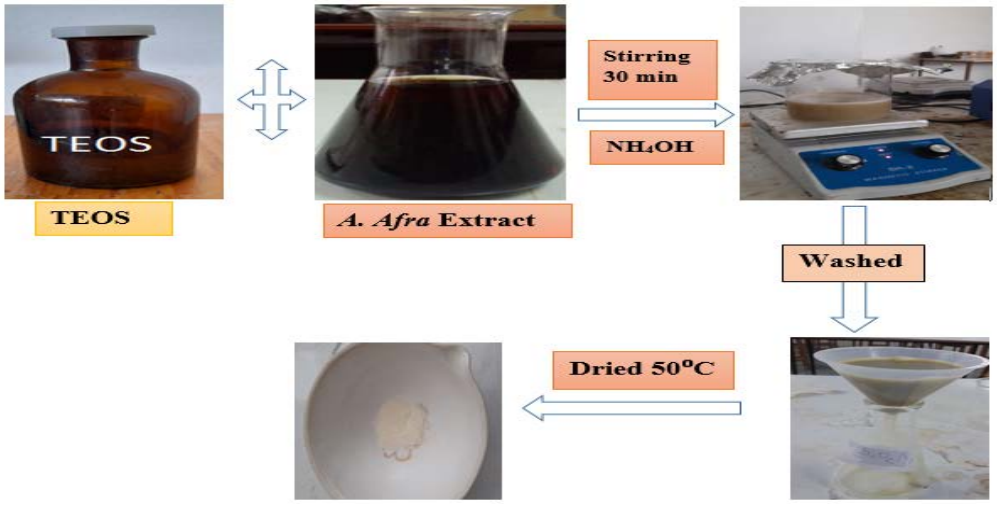


Figure 3.5: Biosynthesis process of $SiO_2$ nanoparticles

## 3.6. Synthesis of Ag/$SiO_2$ Nanocomposite

The synthesis of Ag/$SiO_2$ nanocomposite was performed by mixing 100 mL of 0.1 M silver nitrate solution and 100 mL of plant leaf extract (1:1) through constant stirring while maintaining the temperature at 50 °C. Then, 4 mL of TEOS was diluted with ethanol and added to the mixture silver nitrate and plant extract. After 3 hours stirring, the deep-brown-colored mixture was formed and allowed to settled down overnight. The settled nanocomposites were collected and then centrifuged with deionized water and ethanol three times to remove the residues. Furthermore, the washed material was dried in a hot air oven at 80 °C for 3 hours to obtain the powdered Ag/$SiO_2$

NCs material. Finally, the powder was characterized and stored until it was required for application (*Asst et al., 2018; Otari et al., 2019*). The whole procedure is summarized in Figure 3.6.

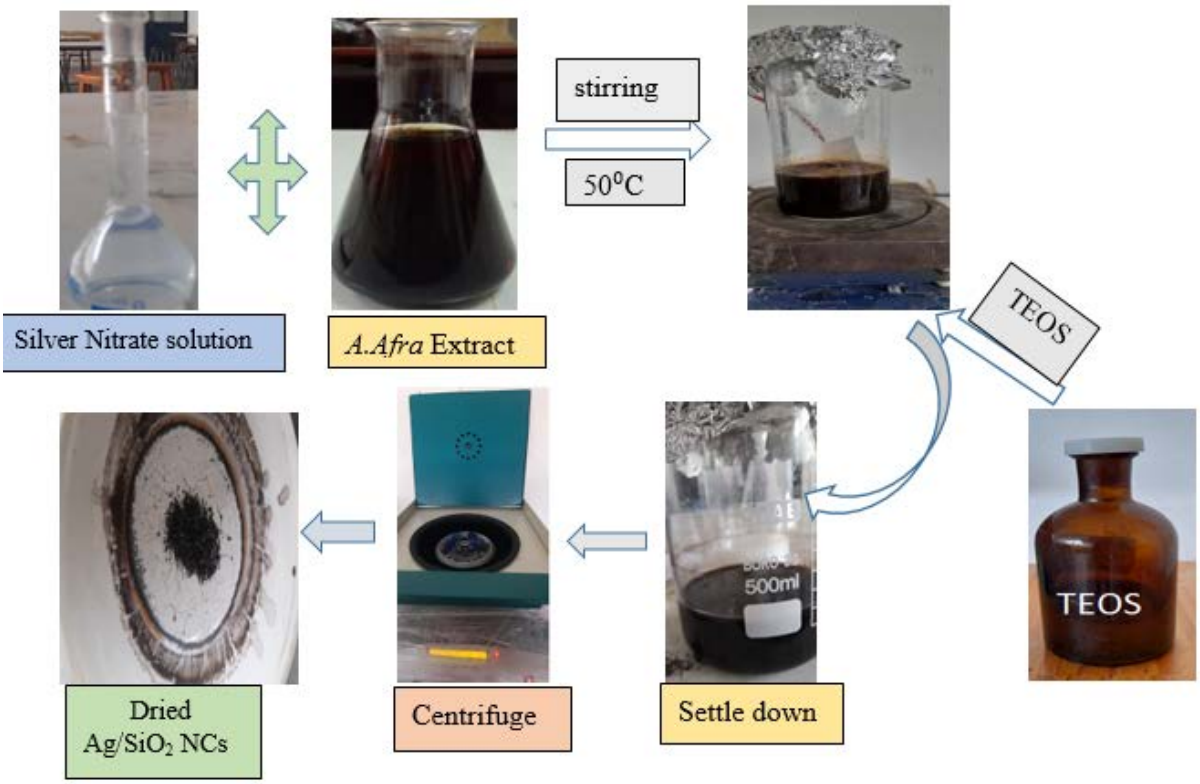


Figure 3.6: Biosynthesis process of $Ag/SiO_2$ Nanocomposite

## 3.7. Characterization Techniques of the Biosynthesized Nanoparticles

The biosynthesized nanoparticles were characterized for the crystallite size, optical properties, surface morphology, and functional group by using analytical tools such as X-Ray diffraction (XRD), Ultra-violate visible spectrophotometry (UV-Vis), Scanning Electron Microscopy (SEM), and Fourier Transform Infrared spectroscopy (FTIR) Analysis, respectively

### 3.7.1. Structural Analysis

The crystalline structure/amorphous nature, the average crystallite size, and the lattice structure of a crystalline substance of the biosynthesized Ag and $SiO_2$ NPs and $Ag/SiO_2$ NCs were characterized by using the XRD diffractometer (radiation operates at a voltage of 40 kV and applied current of 30 mA with Cu K radiation, $\lambda$=1.541 Å) and data were collected and recorded by scanning in the range of 10 to 80° at 2θ value (Gudimalla et al., 2020).XRD analysis of synthesized nanomaterial were performed at Adama Science and Technology University, Material

Engineering Department. The sample was prepared by taking 1.5-2.5 grams of dried NPs and NCs and ground by mortar and pestle. Then it was filled into the sample holder and placed to an X-ray diffractometer. The average crystallite sizes and lattice strain values for Ag NPs and Ag/$SiO_2$ NCs in the form of powder are determined by using Debye Scherrer's formula, which can be given in Equation 8:

$$D = \frac{k\lambda}{\beta \cos\theta} \qquad (8)$$

Where D= Crystalline size diameter = Scherer constant (usually 0.9), λ = Wavelength of the X-Ray source, Cu Kα radiation (1.5406Å),β = Full width at half-maximum (FWHM) of the diffraction peak Θ = Bragg's diffraction angle (Science et al., n.d.).

### 3.7.2 Analysis of Functional Group

Fourier transform infrared (FT-IR) spectroscopy helps to ascertain the identity of various phytochemical constituents involved in the reduction and stabilization of the nanoparticles and nanocomposites. FT-IR spectrum for dry powders of NPs and NCs was obtained using Perkin Elmer FT-IR Spectrophotometer Frontier using the technique of Attenuated Total Reflectance (ATR) in the range of 4000–400 $cm^{-1}$ (Jamkhande et al., 2019). FTIR analysis of the synthesized nanomaterial were done at Bahirdar University Chemistry Department. The biosynthesized AgNPs, $SiO_2$ NPs, and Ag/$SiO_2$ NCs powders of the nanomaterial were mixed with potassium bromide (KBr) and diluted to form a very fine powder. Then powder was then compressed into a thin transparent pellet which was used for recording the FTIR spectra.

### 3.7.3. Analysis of Surface morphology

SEM analysis was used to study morphology, structural features, micrograph images, and size of the biosynthesized NPs and NCs. SEM analysis of the synthesized nanomaterial was done at Chungnam National University, South Korea. A small amount of powder sample was dispersed in acetone and sonicated for a few minutes. Some samples need to be coated to make them conductive.

### 3.7.4. Study of Optical Properties

UV-Visible spectra were carried out using spectrophotometry for monitoring the biosynthesis of Ag NPs, $SiO_2$ NPs, and Ag/$SiO_2$ NCs. UV-Vis absorption spectral analysis was used to evaluate the optical properties of the biosynthesized Ag NPs (measured by using a UV-visible spectrophotometer). UV-Visible analysis was done at Adama Science and Technology Material

Engineering Department. Absorbance were recorded with wavelength of 200 nm to 800 nm with a resolution of 1 nm. The sample were prepared by using the finely ground powder of Ag NPs, $SiO_2$ NPs and Ag/$SiO_2$ NCs dissolved by DMSO then packed into a UV-Vis sample holder then the holder was placed in a UV-Vis spectrophotometer, and absorbance was recorded.

## 3.8. Method of Antimicrobial Evaluation

Bacteria and fungi were used for inhibitory zone tests to investigate the antimicrobial properties of Ag NPs, $SiO_2$ NPs, and Ag/$SiO_2$ NCS using the agar well method. The antimicrobial studies were evaluated and carried out on four bacterial strains*;* two Gram-negative *(Escherichia coli,* and *Pseudomonas aeruginous),* and two Gram-positive *(Staphylococcus aureus, and Streptococcus pyogenes)* and fungal (*Candida albicans)* strain. The tests were performed in Adama Public Health Research and Referral Laboratory Center (APHRRLC).

### 3.8.1. Method of antibacterial activity test

#### A) Media Preparation

Muller Hinton Agar and Sheep Blood Agar Media were prepared by dissolving, 38 g of Muller Hinton powder and 50 mL of Sheep Blood in1L of distilled water separately and then sterilized by autoclave at 121 $^0$C and 15-pound pressure for 20 min. After cooling, about 20 mL of the medium is added aseptically to sterilized Petri dishes. Then the Petri dishes were labeled and incubated until they solidify. The pH of the medium is generally maintained around the physiological pH of 7.4.

#### B). Bacterial cultures, Serial Dilution, and inhibition zone testing of Synthesized Materials

Bacterial cultures were maintained on Blood agar at 37 $^0$C. Bacterial strains were taken from ATCC (American Type Culture Collection) and grown aerobically on Blood Agar for 24 h at 37 $^0$C and 0% $CO_2$. The bacterial suspension was prepared by taking it from blood agar and dissolving it in sterile normal saline until the concentration of bacterial suspensions was achieved to1× $10^8$ colony forming units (CFU) $mL^{-1}$ by comparison with the 0.5 McFarland Standard. 100 µL of 24 hr standardized culture of test bacteria was first evenly spread onto the surface of the Muller-Hinton agar plates using sterile cotton swabs. A sterile swab is used to inoculate the surface of the media in Petri dishes with making three rotations with an angle of 60° to ensure a homogeneous growth (Elemike et al., 2018). The plates were then turned upside down. 6 mm diameter of filter paper was prepared and placed in different areas of the disc. The antibiotic Gentamicin was used as the positive control, and the DMSO solvent was used as the negative control (Gonelimali et al.,

2018).The stock solution of NPs and NCs was prepared in 1 mL of DMSO (20 mg $mL^{-1}$). From 20 mg $mL^{-1}$ concentration of each sample, 10 mg $mL^{-1}$, 5 mg $mL^{-1,}$ and 2.5 mg $mL^{-1}$ were diluted serially for Ag NPS, $SiO_2$ NPs, and Ag/$SiO_2$ NCs. 6 mm diameter disc were saturated with 10µL of each concentration and 25µg of Gentamicin (positive control) and placed on a plate covered with lids and incubated at 37 °C and 0% $CO_2$ for 24 hour (Azimi & Lasemi, 2022). The diameter was measured from the area around the disc where no bacterial growth has been observed, called the inhibition zone. All antibacterial tests were carried out in triplicate and the averages were reported. This diameter can be compared to the critical diameters of antibiotics Gentamicin and digital images were captured.

**C. Determination of the Minimum Inhibitory Concentration (MIC) and Minimum Bactericidal Concentration (MBC)**

Both of the microbiological cultures chosen for the investigation were used to assess the bactericidal effects of Ag/$SiO_2$ nanocomposites. The minimum inhibitory concentration (MIC) is the lowest concentration of a substance that prevents an organism from growing.

The serial dilution method was employed to determine the MIC of the Ag/$SiO_2$ nanocomposite. Each of the 10 test tubes was filled with 2 mL of the liquid Muller-Hinton agar medium. In test tube, number 1,2 mL solution containing 20 mg/mL of nanocomposite that had been sonicated at room temperature was added and thoroughly mixed with the culture medium. The concentration of nanocomposites in test tube 1 becomes 10 mg/mL. Then, 2 ml of the content of test tube number 1 was added to test tube number 2 and mixed completely. Consequently, the 2 mL content of test tube number 11. Then concentration serially putted in to test tube with starting from 10,5,2.5,1.25,0.625,0.312,0.156,0.078,0.039, and 0.019mg/mL. Finally, 0.2 mL of standard microbial suspensions of *Escherichia coli*, *Pseudomonas aeruginous*, *Staphylococcus aureus*, and *Streptococcus pyogenes* containing 1x10 $^{8}$ $CFUmL^{-1}$ microorganisms were added to test tubes numbers 1 to 10, and the test tubes were incubated at 35 °C for 24 hr (Chikezie, 2017). Then, the microbial growth was studied by turbidity observation.

The experiments also included a positive control (a test tube containing nanoparticles and Muller Hinton Agar medium, devoid of inoculum) and a negative control (a test tube containing inoculum and Muller Hinton Agar medium, devoid of nanocomposites). The negative controls indicated a microbial growth profile in the absence of nanocomposites. All the experiments were carried out

in triplicate. From the batch culture investigations, the minimum bactericidal concentration (MBC), or the lowest concentration of nanoparticles that kills 99.9% of the bacteria, was also established. The presence of live microorganisms was evaluated for growth inhibitory concentration (MIC), and the lowest concentration that had a bactericidal effect was reported as MBC (Y. H. Kim et al., 2007).For experiments for bactericidal effect, from each test tube (Specially, negative and positive test tubes) was inoculated on Muller Hinton Agar and incubated at 35 °C for 24 hr. The nanoparticles concentration illustrating bactericidal effect was picked out based on absence of colonies on the agar plate

### 3.8.2. Method of antifungal activity test

The solutions of Ag NPs, $SiO_2$ NPs, and Ag/$SiO_2$ NCs were prepared by reconstituting (10, 5, and 2.5 mg/mL) of each of the powders in 10 mL of DMSO. For preparing the 10 mg/mL, 5 mg/mL, and 2.5 mg/mL solutions of the NPs and NCs were transferred to separate 10 mL capacity volumetric flasks (Hawar et al., 2022).

Antifungal activities against *Candida albicans* were similarly determined using the disc diffusion method. First PDA and SDA of agar were prepared by dissolving distilled water. Then the mixture was heated on the hot plate and autoclaved to get a boiled and uniform solution. The resulting autoclaved medium was transferred into separate petri plates and allowed to solidify. Within 15 min of adjusting the turbidity of the suspension of inoculums, a sterile cotton swab was dipped into the adjusted suspension and rotated several times by pressing firmly on the inside wall of the tube above the fluid level. This removes excess fluid from the swab.

Then, the dried surface of the PDA and SDA plates was inoculated by streaking using the swab three times over the entire surface by rotating plates at approximately 60° each time to ensure an even distribution of the inoculums. Then, plates were left open in the hood for three to five minutes to allow for any excess surface moisture to be absorbed .6 mm diameter discs were prepared from sterile filter paper and cut into small, circular pieces of equal size by a perforator and then they were impregnated each with 0.01 mL of the prepared test of a sample.

The Ag NPs, $SiO_2$, and Ag/$SiO_2$ NCs impregnated discs were placed onto the surface of the inoculated agar plates using sterile forceps. Each disc was pressed down to ensure complete contact with the agar surface. The discs were distributed evenly so that they were no closer than 24 mm from center to center (Cantón et al., 2009). Discs of commercial Ketoconazole/Tilt (10 units/disc) were used as positive controls while DMSO-impregnated discs were used as negative controls.

Then the plates were sealed with Para film and incubated at 27 °C for days 24 hr for fungal pathogens. After incubation, the diameters of the zone of inhibition around each disc were measured to the nearest millimeter along two axes (i.e. 90° to each other) using a transparent ruler, and the means of the two readings were recorded. For each selected pathogen the experiment was carried out with three replications. The zone of inhibition was measured and represented as Mean ± SD (Balakumaran et al., 2016).

### **3.9**. **Statistical Data Analysis**

Data in the current study (antibacterial and antifungal activity data) were analyzed by Microsoft Excel 2010 software. The means of three replications and standard error (± SE) were also calculated for all the results obtained.

# 4. RESULTS AND DISCUSSION

## 4.1. Phytochemical Analysis of the Leaf Extract

The Phytochemical test details are given in Table 4.1. Polyphenols are highly versatile ligands that can bind to a wide range of metal ions, including gold, silver, and copper. During the synthesis process, the polyphenols reduce the metal ions to form nanoparticles with a high degree of stability and biocompatibility. This makes them highly attractive for a wide range of applications, including catalysis, sensing, and biomedicine.

Table 4.1**:** Phytochemicals result of the *Artemisia Afra* plant leaves aqueous extracts

| **No.** | **Phytoconstituents** | **Chemical test/reagent** | **Results** | **Colors observed** |
|---|---|---|---|---|
| **1** | Flavonoids | Ferric chloride test | + | Green |
| **2** | Glycosides | Salkowski test | + | reddish-brown |
| **3** | Steroid | Salkowski test | - | Red |
| **4** | Alkaloid | Wagner's test | + | brown/reddish precipitate |
| **5** | Phenol | Ferric Chloride test | + | Black |
| **6** | Reducing sugar | Benedict test | + | Blue-green |
| **7** | Saponins | Frothing test | + | Stable persistent froth |

+presence -absent

The change formed during phytochemicals investigation is an indicator of the formation of different complexes as a result of oxidation and reduction reactions. Alkaloids, Glycoside, flavonoids, phenols, reducing sugar, and saponins are the extract's main ingredients. The hydroxyl and carboxylic groups found in phenolic compounds have a strong propensity to attract metal ions. Metal ions interact with polyphenolic chemicals in solution to support nanoparticle nucleation and production. The interaction of bioactive chemicals in *A. Afra* plant extract is thought to be what causes nanoparticle production. Phenolic compounds contain hydroxyl and carboxylic groups which have a very high tendency to bind metal ions. (Desalegn Murthy et al., 2021)

## 4.2. Nanomaterials Characterization

### 4.2.1. Study of Optical Properties

UV-Visible absorbance spectroscopy is broadly being utilized as a technique to determine the optical properties of Nano sized particles.

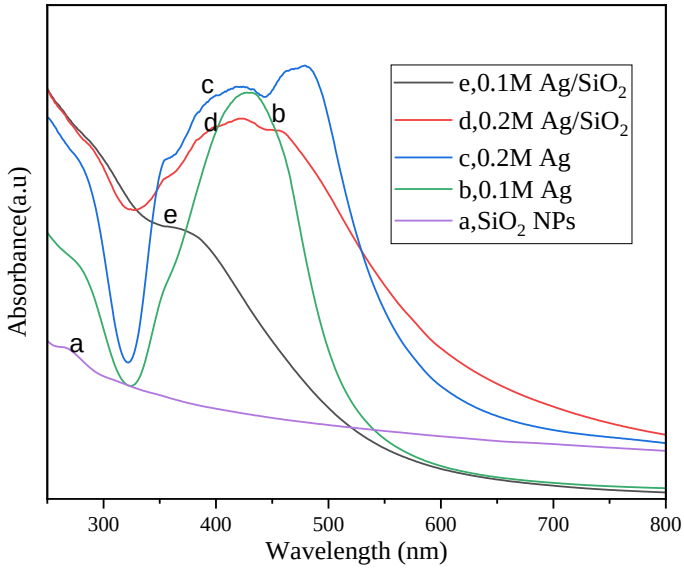


Figure 4.1: Absorbance spectra of $SiO_2$ NPs, Ag NPS, and Ag/$SiO_2$ NCs: a $SiO_2$ b.0.1M Ag, c.0.2M Ag d.0.1M Ag/$SiO_2$ e..0.2M Ag/$SiO_2$

The result obtained from the analysis of UV-Visible spectroscopy of the sample is presented in Figure 4.1a indicated the UV-visible absorption spectrum of prepared $SiO_2$ NPs shows, sharp absorption peak at 260 nm attributed to the aromatic ring's ($\pi$ to $\pi^*$) transition which is in agreement with research (Sasivarnam et al., 2021).The synthesized Ag NPs showed a maximum absorption spectrum at around 416 nm and 420nm (Figure 4.1b, c) suggesting the bio reduction of silver nitrate into silver nanoparticles. The maximum absorption spectra of silver nanoparticles formed in the reaction mixture has increasingly sharp absorbance maximum peak which was due to the availability of more reducing biomolecules for the reduction of silver ions and this absorption band is in the range of other reports (Moreno-Trejo & Sánchez-Domínguez, 2016). The formation of Ag/$SiO_2$ nanocomposite structures display absorption peaks at wavelengths of 390 nm and 411nm as indicated in Figure 4.1(d,e) increased absorbance intensity at 390 nm and 411nm is an indication of the presence of silver content in the nanocomposites (Khedkar et al., 2021).Those absorption peaks were due to the strong surface plasma resonance (SPR) band, these

peaks depend on different concentrations. Due to the increasing number of precursor ions present in the reaction medium, unfavorable particles are produced, and agglomeration and large-size particles were formed. Moreover, the feasible concentration of parent salt among the two for the biosynthesis of NPs and NCs was revealed to be 0.1 M. To achieve surface stability, the reduced nanostructures were agglomerated on the unreacted salt molecules present in the reaction media. To control growth and particle size, 0.1M of silver nitrate solution was used for further study

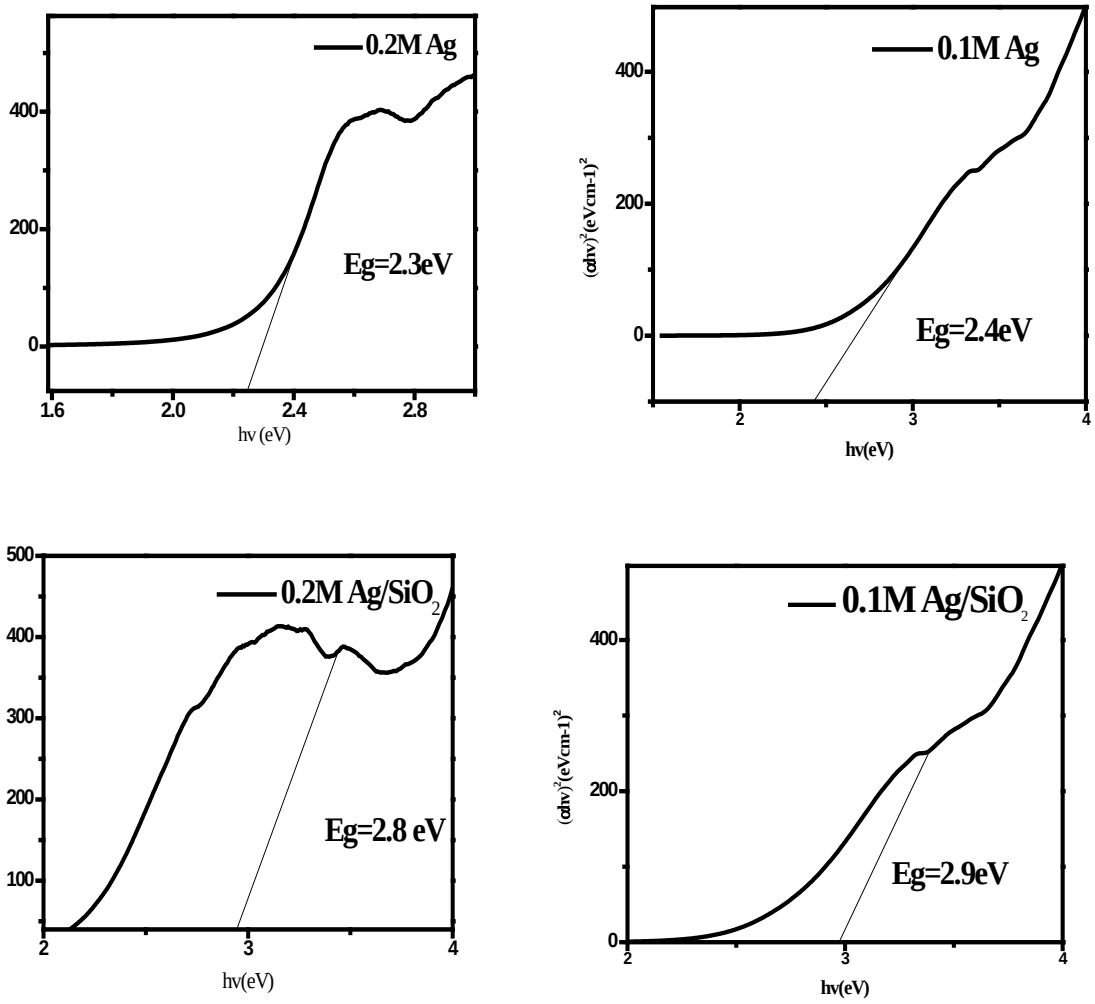

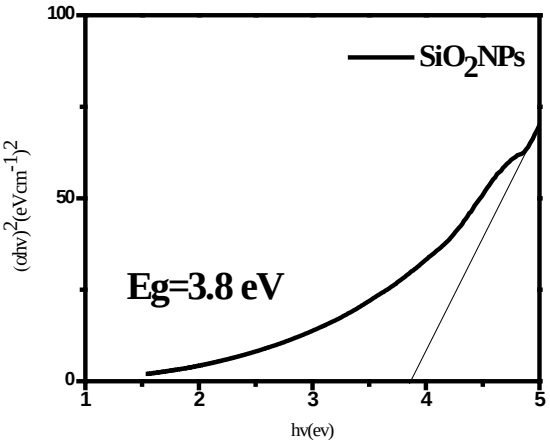


Figure 4.2: Energy bandgap of Ag NPs, $SiO_2$ NPs, and Ag/$SiO_2$NC*s*

The corresponding optical bandgap energy was calculated using Tauc's plot method, which is discussed in Equation (5). The results showed in Figure 4.2 that $SiO_2$, 0.1 M Ag, 0.2 M Ag, 0.1 M Ag/$SiO_2$, and 0.2 M Ag/$SiO_2$ were found at 3.8, 2.4, 2.3, 2.9, and 2.8 eV, respectively. The nanocomposites have a larger band gap energy than the corresponding bulk material due to the presence of $SiO_2$, which can stabilize these nanoparticles and enhance their SPR properties. The band gap energy of semiconductors is affected by many factors, including concentration. When the concentration of impurities is high, the band gap energy decreases. This is because the impurities introduce new energy levels in the band gap that electrons can occupy (Sembiring et al., 2022).0.1M Ag/$SiO_2$ NCs have a large band gap than 0.2M Ag/$SiO_2$ NCs.A larger bandgap means that more energy is required to excite an electron from the valance band to the conduction band and hence light of a higher frequency and lower wavelength would be absorbed (Kayed et al., 2023).Generally, as the band gap increases the size of the nanoparticle decreases, leading to modified electronic and optical properties due to the spacing of the electronic level and the bandgap increases with decreasing particle size (Deng et al., 2007). The band gap increases as a nanoparticle's size decreases. This occurs because the valence and conduction bands' electronic wave functions begin to overlap as the nanoparticle's energy levels become closer together. The electronic wave functions of the valence and conduction bands cannot be considered independent entities when the size of the nanoparticle is small enough, and the energy levels of the nanoparticle become quantized (M. Singh & Singhal, 2018).

### 4.2.2. Structural Analysis of Nanoparticles and Nanocomposites

The X-ray diffraction (XRD) analysis was used to evaluate comprehensively the phase purity, average crystal size and details of the crystal structure of the produced NPs and NCs.

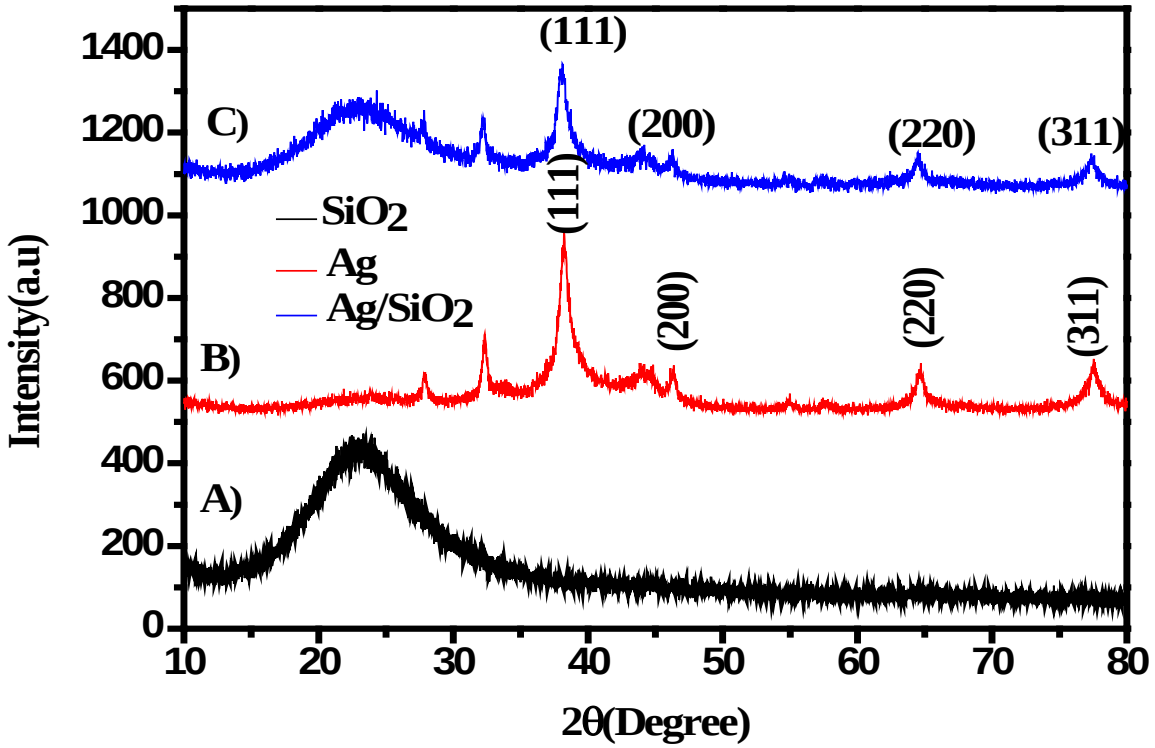


Figure 4.3**:** XRD patterns of materials A) $SiO_2$ NPs B) Ag NPs and C) Ag/$SiO_2$ NCs

As shown in Figure 4.3 (A) $SiO_2$ NPs a broad hump at 2Θ angle of 23° (101) with JCPD file 00-045-1374 was observed which illustrates the amorphous nature of the sample. No sharp peak was observed in other scanning angles starting from 10° to 80° showing absence of any ordered crystalline structure. This also indicated relatively high disordered particle geometry of silica. A similar result was obtained by Nayak, 2021. Unlike crystalline materials, which have a well-defined periodic arrangement of atoms, amorphous $SiO_2$ nanoparticles have a disordered atomic structure that is characterized by a high degree of randomness. Generally, the absence of sharp peaks in the XRD pattern of a material indicates that it is amorphous or disordered (Babu et al., 2018).The diffraction pattern of the Ag NPs showed sharp peaks at 2Θ = $38.56^0$ (111), $44.57^0$ (200), $64.4^0$ (220), and $77.42^0$ (311). The analyzed diffraction peaks were matched well with the standard Ag NPs XRD patterns (JCPDS card file no 00-004-7383), which identifies the

crystallographic systems of face center cubic structure ( Figure 4.3 (B)) this result agreed with (Desalegn Murthy, et al., 2021).Again as shown in Figure 4.3(C) diffraction peaks at 2θ values of 38.2°, 44.26°, 64.57° and 77.4°are assigned to (111), (200), (220), and (311) of lattice plane of face-centered cubic (fcc) for Ag nanoparticle which are also observed for Ag/ $SiO_2$ nanoparticles. In addition, the XRD pattern of Ag/$SiO_2$ nanoparticles shows a strong broad peak at 23°, which is characteristic of amorphous nano-silica corresponds to the silica embedded in nanocomposite structure (Azimi & Lasemi, 2022). Moreover, the unassigned crystalline peaks (27.2°and 34.6°) are also observed in the XRD patterns of Ag-NPs and Ag/$SiO_2$ nanoparticles, due to resemble or correlate with the structure of Ag NPs within the NCs; which indicates the possibility of their crystallization on the surface of the silver nanoparticles.

Table 4.2: crystallite sizes of Biosynthesized Ag NPs and Ag/$SiO_2$ NCs

| **Sample Name** | **Peak position (2Ɵ)** | **Theta(θ)** | **d (Å)** | **FWMH (β)** | **hkl value** | **β(rad)** | **Crystal size D(nm)** | **Average D (nm)** |
|---|---|---|---|---|---|---|---|---|
| Ag NPs | 38.1619 | 19.08 | 2.35 | 0.62000 | 111 | 0.0105 | 10.28 | 16.68 |
| | 44.5710 | 22.28 | 2.032 | 0.37340 | 200 | 0.006 | 23.73 | |
| | 64.4645 | 32.213 | 1.445 | 0.53670 | 220 | 0.0091 | 16.26 | |
| | 77.4292 | 38.71 | 1.232 | 0.52660 | 311 | 0.0089 | 16.45 | |
| Ag/$SiO_2$ NCs | 38.2601 | 19.13 | 2.309 | 0.97000 | 111 | 0.0164 | 9.04 | 8.998 |
| | 44.2612 | 22.13 | 2.04 | 1.58000 | 200 | 0.026 | 5.543 | |
| | 64.5762 | 32.28 | 1.442 | 0.82670 | 220 | 0.014 | 11.13 | |
| | 77.4592 | 38.725 | 1.232 | 0.92000 | 311 | 0.0156 | 10.28 | |

Furthermore, the XRD pattern shows sharp and intense peaks, indicating that the prepared samples were finely ground, homogenized with high crystalline quality, and average bulk composition is

determined (Hagos et al., 2018).The average crystallite sizes and lattice strain value was calculated by using Debye Scherrer's formula.According to Scherer's equation, the calculated average crystallite size of biosynthesized Ag NPs and Ag/$SiO_2$ NCs was found to be 16.68 and 8.99 nm, respectively result is presented in Table 4.2. The D values in NCs decreased due to the intercalation of Ag NPs into $SiO_2$. The remarkable properties of Ag/$SiO_2$ nanocomposites arise from the unique intercalation of Ag nanoparticles (NPs) within the $SiO_2$ matrix. The intercalation process involves the insertion of the Ag NPs into the porous structure of $SiO_2$, resulting in a highly dispersed and well-stabilized nanocomposite material. The intercalation process causes structural changes in $SiO_2$ samples due to the strong electrostatic attraction and hydrogen bonding forces between $SiO_2$ and intercalated NPs. When the crystalline domain size of nanoparticles decreases, the peak in their XRD pattern becomes broader and less intense. This is because smaller crystalline domains have fewer atoms, which makes it more difficult for them to diffract X-rays and produce a sharp peak. As a result, the peak becomes broader and less intense, which can be observed in the XRD pattern. In addition, when peak broadening increases, it can also contribute to a decrease in signal intensity. This is because broader peaks have a lower integrated intensity than sharper peaks, which means that the total amount of XRD is reduced (Holder & Schaak, 2019).Generally, the smaller crystalline size of Ag/$SiO_2$ nanocomposites compared to Ag NPs leads to better antimicrobial activity because smaller particles have a larger surface area to volume ratio, which increases their reactivity and enhances their antimicrobial activity.

### 4.2.3. Analysis of Surface Functional Group

FT-IR measurements were carried out to identify the major functional groups in the Plant leaf extract, Green synthesized Ag NPs, $SiO_2$ NPs, and Ag/$SiO_2$ NCs using plant leaf extract. That was to identify the possible involvement of plant leaf extract in the synthesis and stabilization of NPs and NCs.

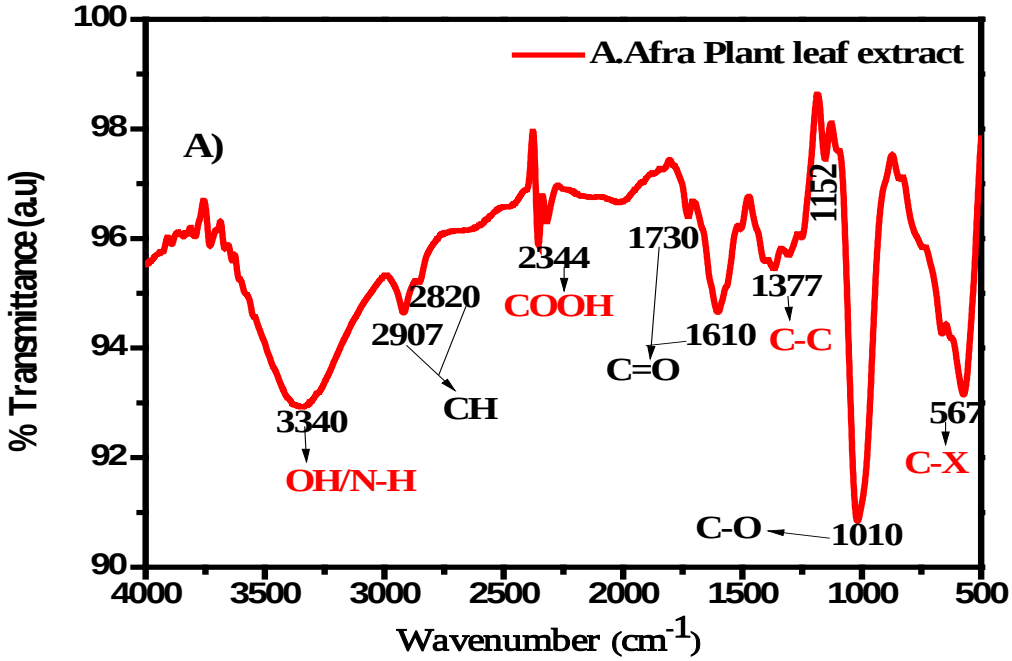


Figure 4.4: FTIR spectrum of *Artemisia Afra* plant leaf extract

The peak observed at 3340 $cm^{-1}$ is typical of OH/N-H amine, while 2907 and 2820 assigned for C-H stretching band for alkanes. The peak at 2344 $cm^{-1}$ indicates the presence of a COOH group. The bands around 1730 and 1610 $cm^{-1}$ were assigned to C=O and C-O vibrations, which are characteristic of carboxylic esters or strained cyclic ketones which appeared as flavones. The signal at 1377 $cm^{-1}$ belongs to C-C stretching band. The peak 1152 and 1010 $cm^{-1}$ C-O stretch is typical of alcohols (Elemike et al., 2018) Figure 4.4.Tannins and flavonoids are simple phenolic compounds that serve as defenses against pathogens and herbivores. A peak at 567 $cm^{-1}$ correlates to alkyl halide vibrations of the C-X bond.

Figure 4.5 (A) showed that region between 3369 and 2345 $cm^{-1}$ on the surface of nanomaterial indicate typical stretching vibration of the hydroxyl functional group (OH) and stretching vibration of (C-H), The band at 1549 $cm^{-1}$ corresponds to N-H bending, indicating the presence of secondary amines (Prakash et al., 2013). The band at 1364 $cm^{-1}$ was due to the presence of the $CH_2$ and $CH_3$ bend stretch, which showed the presence of the alkanes. The C-O-C stretching appears at 1017 $cm^{-1}$(Balaji et al., 2009). These results demonstrate that many organic constituents of plant powders were adsorbed on the surface of biosynthesized Ag NPs. In addition to this, the FTIR spectrum of Ag NPs shows peaks corresponding to the band at 771 and 539 $cm^{-1}$, which is possibly due to the

interaction of Ag with protein molecules in the extract (Thangamani & Bhuvaneshwari, 2022). Silver nanoparticles indicate the presence of bioactive molecules around the nanoparticles, such as alkaloids, phenols, flavonoids, glycosides, and saponins, which are responsible for the biotransformation of silver ions to silver nanoparticles and their stabilization in an aqueous medium (Desalegn, Ravikumar, et al., 2021). These bioactive molecules had been confirmed to have performed a sizable function in the nucleation and growth of silver nanoparticles. In contrast, these peaks were absent and displayed drastically reduced intensities in corresponding Ag NPs. The functional group in this region that is involved in the reduction and stabilization of AgNPs. Additionally, OH, C-O, and C=O or other chemicals are present in *A. Afra* plant. This reducing agent can donate electron pair to the metal when the reduction occurs on the particle surface. Also, the polyphenols act as a capping agent as they introduced a charge on the reduced metal surface (Kumar et al., 2018).

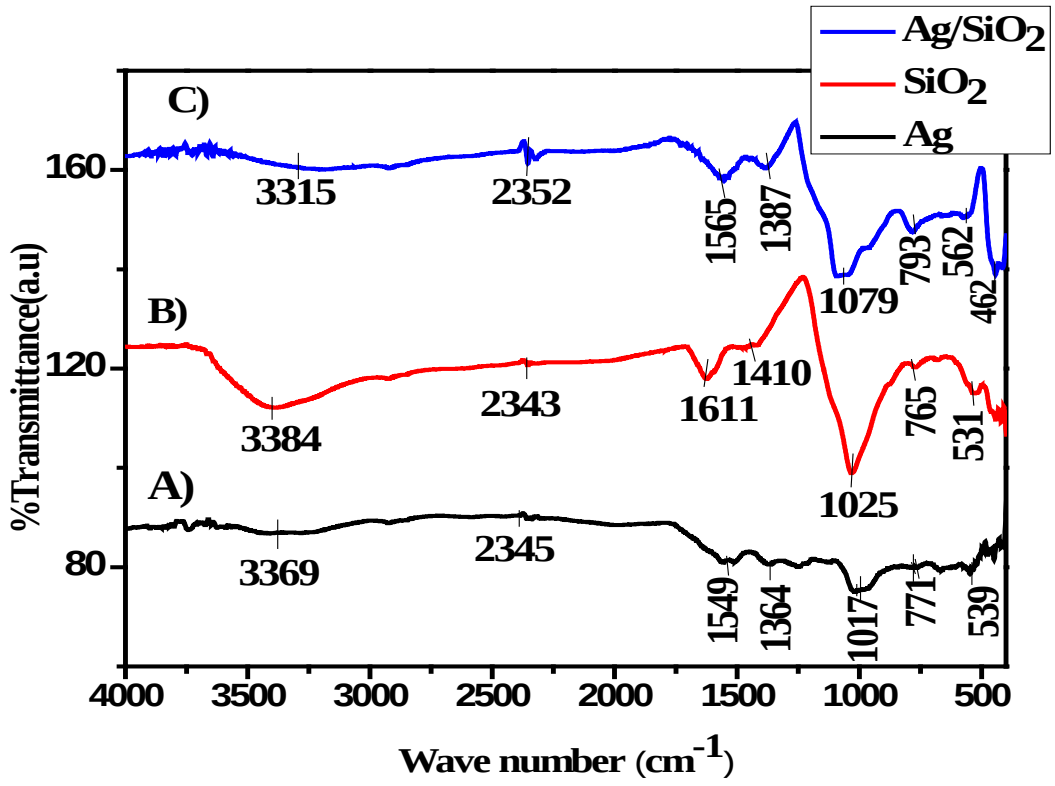


Figure 4.5**:** FT-IR spectra of biosynthesis of A) Ag NPs, B) $SiO_2$ NPs and C) Ag/$SiO_2$ NCs

As shown in Figure 4.5 (B) the FT-IR absorption bands of the biosynthesized $SiO_2$ NPs showed sharp absorption peaks located at about 3384, 2343, 1611, 1410, 1025,756, and 531 $cm^{-1}$. The broad, intense absorption peaks at 3369 $cm^{-1}$, corresponding to phenolic-OH stretching and the

vibration of the silanol group on the silica surfaces. C-H stretching was identified by the presence of a peak at 2343 $cm^{-1}$ (Periakaruppan et al., 2022).The absorption peak indicated at 1611 $cm^{-1}$ represents C=C group of aromatic. The band 1410 $cm^{-1}$ was attributed C-H bending. Moreover, the strong bands at 1025, and 756 $cm^{-1}$ were associated symmetric Si-O-Si stretching and Si-H vibration bonding (Asst et al., 2018). The Si-O bending vibration was observed at 531 $cm^{-1}$ which was typically considered as evidence for amorphous phase (Saravanan, 2020).

Figure 4.5 (C) displays FT-IR spectrum of the nanocomposite. The absorption peaks at 3315 $cm^{-1}$ attributed to the phenol of O-H and 2352 $cm^{-1}$ to the presence of C-H symmetrical stretching of hydrocarbons such as alkanes and aldehydes. The intense peaks around 1565 and 1387 $cm^{-1}$ are attributed to the primary and secondary amine vibration bands, respectively.

These signals confirmed the presence of plants in the $Ag/SiO_2$ NC synthesis. Si-O-Si and Si-OH absorption bands have been observed at 1,079, 793, and 562 $cm^{-1}$. The Si-O-Ag linkages stretching were also seen at around 793 and 562 $cm^{-1}$. The band appears how the *A. afra* plant succefully reducing and stabilizing the $Ag/SiO_2$NCs and leads to the formation of $Ag/SiO_2$ NCs. These results were similar to the previous report on the synthesis of $Ag/SiO_2$ NCs (Rodrigues et al., 2020; Zaki et al., 2022)

Generally, FT-IR spectroscopic studies confirmed that carbonyl groups in amino acid residues and proteins have the stronger ability to bind the metal and could form a layer covering the metal nanoparticles (i.e., capping silver nanoparticles) to prevent agglomeration and stabilize the medium. (M. Z. H. Khan et al., 2018).

### 4.2.4 Analysis of Surface morphology

The surface morphology of the green-synthesized $SiO_2$NPs, AgNPs, and $Ag/SiO_2$ NCs was characterized using a scanning electron microscope (SEM).

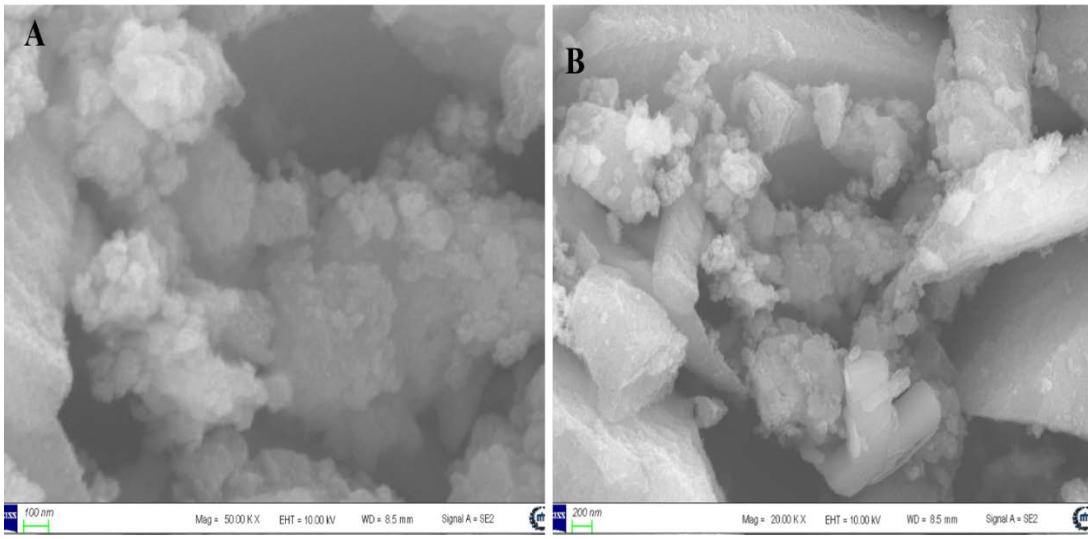


Figure 4.6: SEM Images of $SiO_2$ NPs

In Figure 4.6 (A and B), the image of $SiO_2$ NPs at different magnifications of 100nm and 200nm in shown. It is observed that silica is a high porous material with a large internal surface area (Deshmukh et al., 2012). Amorphous materials appear to be more porous than crystalline materials, hence there is a link between amorphous materials and porous structures. This is due to the fact that in amorphous materials' disorderly atomic arrangements allow for a greater quantity of gaps or empty space, which can result in pores or channels that increase the substance's outer region**.** Furthermore, the $SiO_2$ nanoparticles are somewhat agglomerated, which is characteristic of the green synthesis method. The large porous structure is used for coating Ag NPs and prevents the aggregation of the material. This is attributed to the fact that nanoparticles have a larger surface area and a long-lasting affinity throughout the dehydrating process, which causes agglomeration of the particles. $SiO_2$ NPs have no defined morphology, have an irregular shape, and flat sheets together were observed (Assis et al., 2021).

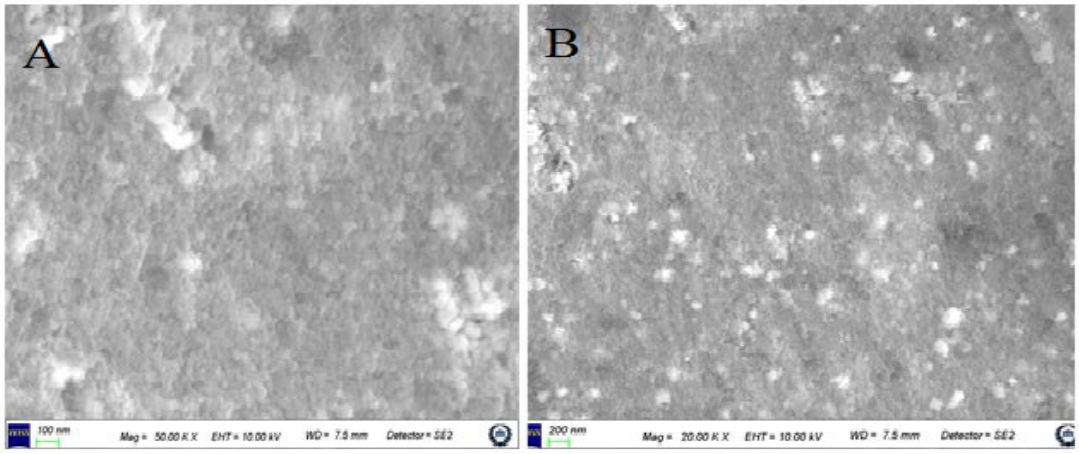


Figure 4.7: SEM images of Ag NPs

The morphology of green synthesizes Ag NPs was evaluated by SEM.Based on SEM image in Figure 4.7 (A and B) metal particle were with small particle, spherical shape (Hagos et al., 2018).In the case of spherical nanoparticle the high surface area to volume ratio with large number of surface atom which can affect the nanoparticle reactivity and ability to interact with other molecule and formed aggregation. Ag Nanoparticle only one side or the active site by one direction can attack the bacterial and fungal strain. With equal ratio of the plant extract and the precursor of Ag was combined but still some agglomeration was indicted (Pavani et al., 2013).

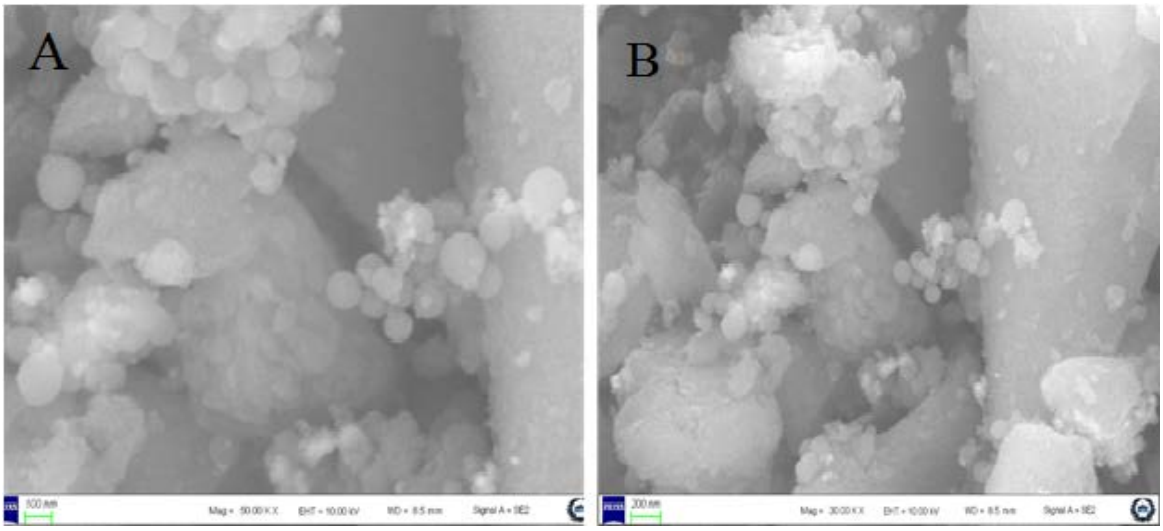


Figure 4.8: SEM image of Ag/$SiO_2$ NCs

Figure 4.8 (A and B) shows Ag/$SiO_2$ NCs that confirm a good combination of nanomaterial obtained from the Ag NPs and $SiO_2$ NPs during the synthesis process, and the presence of the $SiO_2$ coats the surface of the Ag NPs, thus preventing aggregation. The AgNPs are formed by the

reduction of silver ions on the surface of $SiO_2$ NPs (*Karthik et al., 2021)*. The nanocomposite exhibits a spherical shape, and the micrograph shows that the AgNPs formed by reduction appear as bright spots over the surface of $SiO_2$ NPs. The Ag NPs spherical shape is attached to the pore of amorphous $SiO_2$ NPs and prevents the aggregation and Ag stability *(Mohammed, 2019).* Generally, the SEM images also revealed that the nanoparticles are well dispersed and do not aggregate, indicating that the plant extract or natural compound used in the synthesis process effectively stabilized the nanoparticles. Additionally, the images may have shown evidence of the presence of Ag nanoparticles on the $SiO_2$ surface, indicating the successful synthesis of the nanocomposite.

## 4.3. Study of Antibacterial Activity of Nanoparticles and Nanocomposites

The antibacterial activity of the biosynthesized nanomaterials (Ag NPs, $SiO_2$ NPs, and Ag/$SiO_2$ NCs) was investigated against both the two gram-positive bacteria (*Staphylococcus aureus* ATCC25923 and *Streptococcus pyogenes* ATCC19615) and two gram-negative bacteria *(Pseudomonas aeuruginosa* ATCC27853 and *Escherichia coli* ATCC25922*)* through the disc diffusion method. Gentamicin was used as a positive control, Because of its broad-spectrum action against both Gram-positive and Gram-negative bacteria, the aminoglycoside antibiotic gentamicin is frequently utilized in antibacterial activity. Gentamicin prevents protein synthesis by attaching to the bacterial ribosome, which can cause the bacterial cells to die and DMSO was used as a negative control in antibiotics assays, it's important to distinguish between the effects of the test substance and any effects that might be brought on by the solvent or other assay components (Prasetya et al., 2019). Since DMSO is frequently employed in antibacterial assays as a solvent for test compounds, using it as a negative control can help ensure that any antibacterial activity seen is brought on by the test drug and not the solvent respectively. Figures 4.9-4.12 illustrate photographs of the antibacterial test results of at 10mg/mL (denoted by A),5mg/mL (denoted by B) and 2.5mg/mL (denoted by C) of synthesized nanomaterial, and the details are summarized in Table 4.3. The presence of an inhibition zone indicates the antibacterial effect of the Nanomaterial. While the plant powder has an effect as shown by the inhibition zone, the results were more pronounced on gram-positive bacteria *(S. aureus and S. pyogenes)* than on gram-negative bacteria (Gonelimali et al., 2018) .

*Artemisia afra* plant leaf powder showed against both tested bacterial strains. The maximum inhibition zone of plant powder towards *S. aureus* was 9 mm at 10 mg/mL and a minimum of 7 mm at 2.5 mg/mL. where 7 mm at 10 mg/mL and 6 mm at 2.5 mg/mL while the maximum and minimum values, respectively, for *S. pyogenes.* Moreover, *in E. coli* and *P. aeruginosa,* at A (10 mg/mL), the maximum inhibition zone is 8mm and the minimum is 7.3 and 7mm, so in table 4.3 showed detail result. The result shows higher activity in S. aureus than other strains, but at C (2.5 mg/mL) it showed 7 mm, which means the zone was dependent on the dose. Solvent extracts displayed a higher zone of inhibition against gram-positive bacteria compared to gram-negative ones, similar results were reported (Martini et al., 2020).Before testing the extract of *A. afra, the* detection of different phytochemicals in this plant leaf was undertaken, and it was confirmed that the extract of this plant leaf had several secondary metabolites. This means the studied plant leaf extract contains different compounds that have contributed to its antibacterial activity against the tested multi-antibiotic-resistant clinical pathogenic bacteria. Therefore, the study suggested the extract of *A.Afra* exhibited broad-spectrum antibacterial activities against the above-mentioned multi-antibiotic-resistant pathogenic bacteria. Furthermore, the presence of these phytochemicals is an indicator that the plant can be a potential source of precursors in the development of synthetic drugs (Bora & Sharma, 2010)**.** Figure 4.9 shows of the antibacterial activities of *A. Afra* plant extract. The antibacterial effect of plant powder can be attributed to a large number of different chemical such as Phenol, Flavonoids, Alkaloid, Saponins and other compounds that serve as a defense against pathogens and herbivores. This chemical play role in membrane disruption caused by lipophilic substance (Lere Keshebo et al., 2016). $SiO_2$ nanoparticles and other materials can be tested for their antibacterial activity using the zone of inhibition assay. In this assay, a filter paper disc or well containing the test chemical is placed on top of an agar plate that has been equally coated with a bacterial culture. If the test substance has antibacterial action, it can prevent bacterial growth in the vicinity after diffusing into the agar. The zone of inhibition refers to the region where bacterial growth is inhibited surrounding the filter paper disc or well.

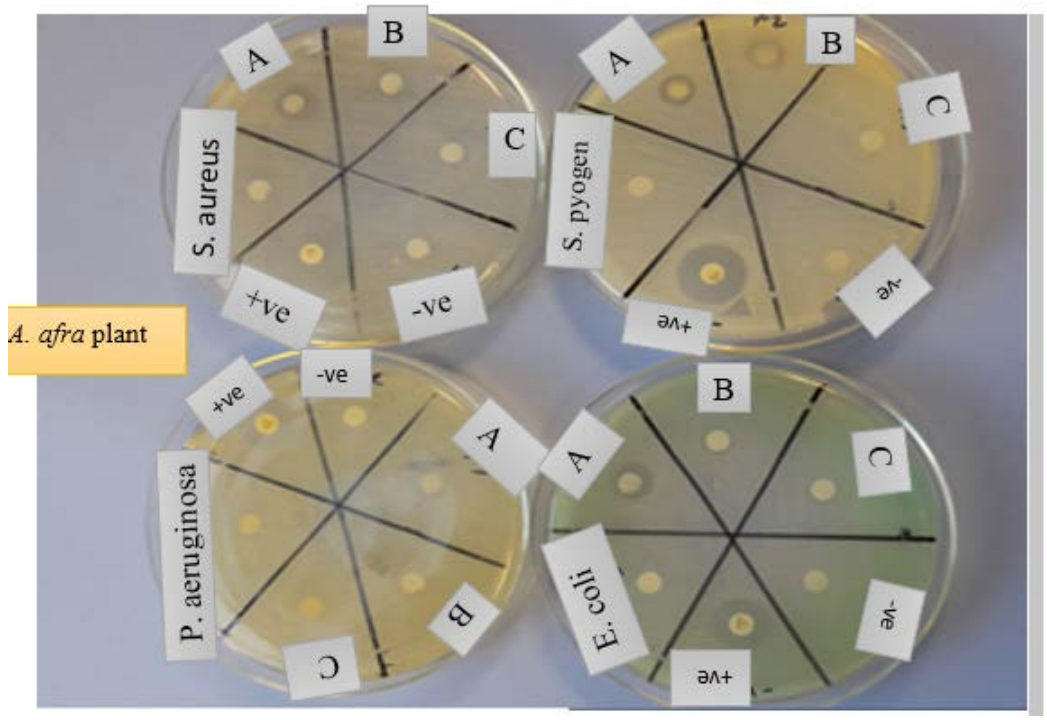


Figure 4.9:Photographs of antibacterial activities of *A.Afra* plant extract A=10mg/mL B=5mg/mL and C=2.5mg/mL

The sizes of the zones of growth inhibition are presented in Table 4.3. $SiO_2$ nanoparticles showed no inhibition zone same result showed by Kadhum, 2017. There is also a photograph shown in Figure 4.10 here their inhibition zones of a maximum of 7.4 ± 0.2 mm and a minimum of 6±0.2 mm in both strains. Due to lack of shape, uniformity and size of $SiO_2$ NPs can also impact their antibacterial activity. With a more uniform shape and size distribution of NPs are generally more effective at killing bacteria than those with a less uniform shape and size distribution. This is because uniform particles can more easily interact with bacterial cells and penetrate their membranes, leading to more effective antimicrobial activity (Selvarajan et al., 2020). Due to its large size, it may reduce the penetration into the bacterial cell wall and the overall contact area.

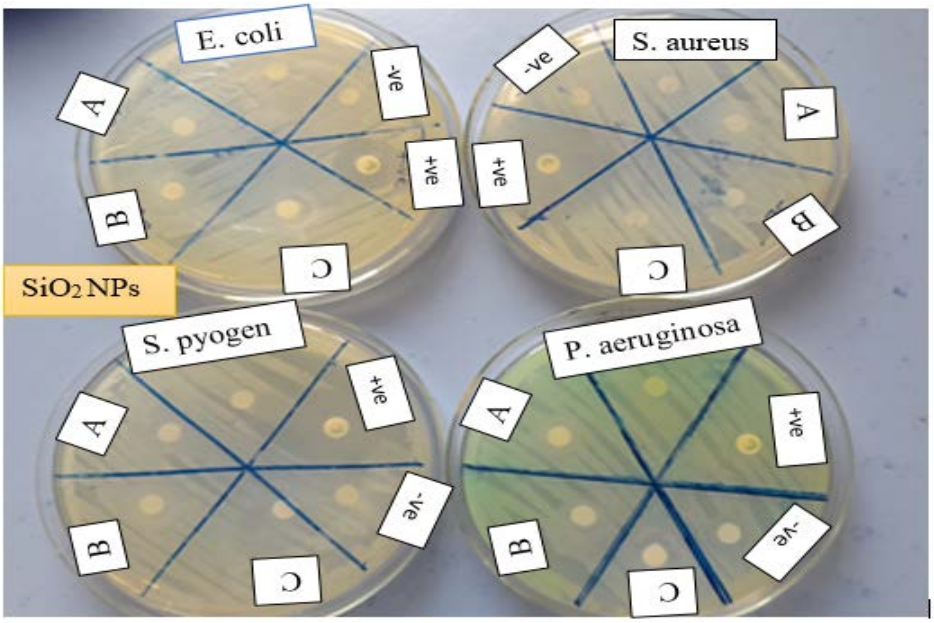


Figure 4.10**:** Photographs of antibacterial activities of $SiO_2$ NPs A=10mg/mL B=5mg/mL and C=2.5mg/mL

$SiO_2$ nanoparticles have relatively low toxicity levels compared to metal-based nanoparticles, such as silver nanoparticles. These metal-based nanoparticles can easily disrupt bacterial cell membranes and produce reactive oxygen species that can damage cellular components, leading to higher antibacterial activities (Assis et al., 2021). Because they do not easily release ions or other reactive species that could harm or kill bacteria, silica ($SiO_2$) nanoparticles are typically regarded as being biocompatible and non-toxic to bacterial cells. $SiO_2$ nanoparticles do not release any ions because of their chemical stability and poor solubility in water and biological fluids. Typically, the surface of $SiO_2$ nanoparticles is extremely stable and inert, which prevents them from easily reacting with water or other molecules in the environment. Furthermore, $SiO_2$ nanoparticles limited solubility minimizes the release of ions into the solution, further lowering their potential toxicity (Raturi et al., 2021).So $SiO_2$ NPs can be used as carriers or delivery for active antibacterial agents such as Ag ions or other antibiotics, to enhance their activity and improve their ability to target bacteria. Additionally, the size of silica nanoparticles can affect their biodistribution and cellular uptake, which can impact their effectiveness as drug carriers (Janjua et al., 2021).The antibacterial activity of the synthesized Ag NPs was investigated against *S. aureus, S. pyogen, E. coli, and P. aerugines.* The viable disc diffusion method was performed to assess the antibacterial properties of Ag NPs at various concentrations of 10, 5, and 2.5 mg/mL. The disc diffusion method

is employed in this technique for several factors. The factor first is affordable, accessible to many laboratories, and reasonably simple. Second, it enables quick screening of various bacterial strains and nanoparticles, allowing researchers to quickly assess a huge number of samples. Thirdly, the method offers a visual representation of the nanoparticles' antibacterial activity, making it simple to compare the outcomes (Y. H. Kim et al., 2008).

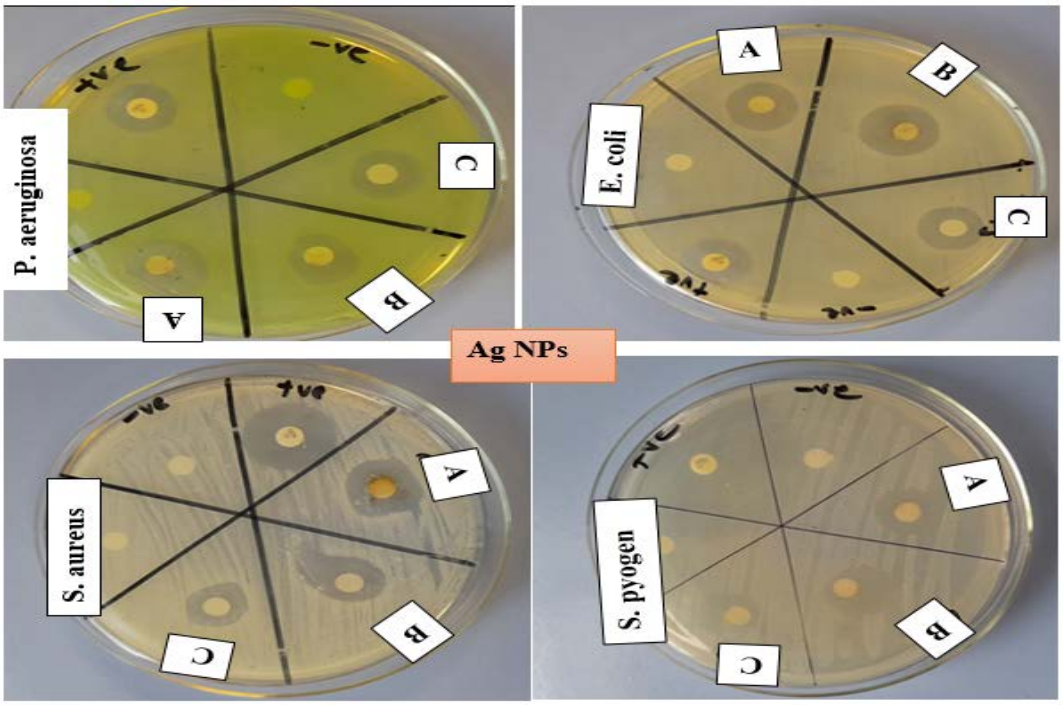


Figure 4.11**:** Photographs of antibacterial activities of Ag NPs A=10mg/mL B=5mg/mL and C=2.5mg/mL

The growth results of strains that were exposed to various concentrations of Ag NPs are shown in Figure 4.11 and Table 4.3. The results show that Ag NPs exhibited significant antibacterial activities against all bacteria, even at the lowest concentration of 2.5 mg/mL. Its inhibition zone was measured between 11±0.2 and 14.5 ± 0.13 The details were described in **(**Table 4.3). A maximum zone of inhibition of 14.5 mm and 14 mm was recorded against *Streptococcus pyogen* and *Staphylococcus aureus* at a concentration of 10 mg/mL. The least zone of inhibition was observed 11mm in *E. coli* and *Pseudomonas aeruginosa* at 2.5 mg/mL. These results show Gram-positive bacteria were more sensitive towards Ag NPs. The result showed that the effect was dose-dependent. Because the result shows that as Ag NPs concentration increased from 2.5 mg/mL to 10 mg/mL, the activity also increased.

Ag NPs' activities toward those bacteria are due to having the ability to penetrate bacterial cell walls, changing the structure of cell membranes and even leading to cell death. The strong antimicrobial action of Ag NPs is related to their nanoscale size and unique properties (Kukushkina et al., 2021). Their efficacy is not only to their nanoscale size but also to their reactivity towards bacteria DNA or amino acids. They can increase the permeability of cell membranes, produce reactive oxygen species, and interrupt the replication of deoxyribonucleic acid by releasing silver ions (Yin et al., 2020) and as a concentration of these NPs increases the Ag ions released to the bacterial cell also increase. Current results also confirm the antibacterial activity of Ag NPs is dose-dependent. This suggests that the inhibition zone increased as the concentration of Ag NPs (Table 4.3). Generally, by the mechanism of $Ag^{+}$ ions released from AgNPs denaturize proteins by forming reactive oxygen species first and then interacting with sulfhydryl groups. lastly, the bacterial damage caused by the adhesion of AgNPs (Urnukhsaikhan et al., 2021).

The main objective of combining these two nanoparticles, Ag NPs and $SiO_2$ NPs, is to develop composites with better antibacterial properties to target both gram-negative and gram-positive bacteria. The results obtained suggest that the composite can be used as an effective antibacterial material in this application. The enhanced antibacterial activity of the composites can be attributed to the chemical and physical properties of the nanoparticles, together with the large surface area of the $SiO_2$ NPs. The antibacterial activity was more pronounced against the gram-positive (*S. aureus, S. pneumonia*) than the gram-negative (*E. coli, P. aeruginosa*) (Table 4.3**)**. Based on the results presented in Figure 4.12, it appears that the Ag/$SiO_2$NCs have antimicrobial activity against both Gram-positive and Gram-negative bacteria. The inhibition zone results show that the highest antimicrobial activity was observed at a concentration of 10mg/mL for all tested bacteria, with a maximum inhibition zone ranging from 14±0.15 to 16±0.12 mm. At lower concentrations of 2.5mg/mL, the inhibition zones were slightly reduced, with the minimum inhibition zones ranging from 13.5±0.13 to 14±0.1 mm.It's interesting to note that the antibacterial activity of the Ag/$SiO_2$NCs was higher than that of earlier research (Qin et al., 2017) indicating that the synthesis process or the characteristics of the nanoparticles themselves may be responsible for the increased activity. It is important to remember that the conditions of the study and the particular bacterial strain being examined can have an impact on the antibacterial activity of the Ag/$SiO_2$NCs.

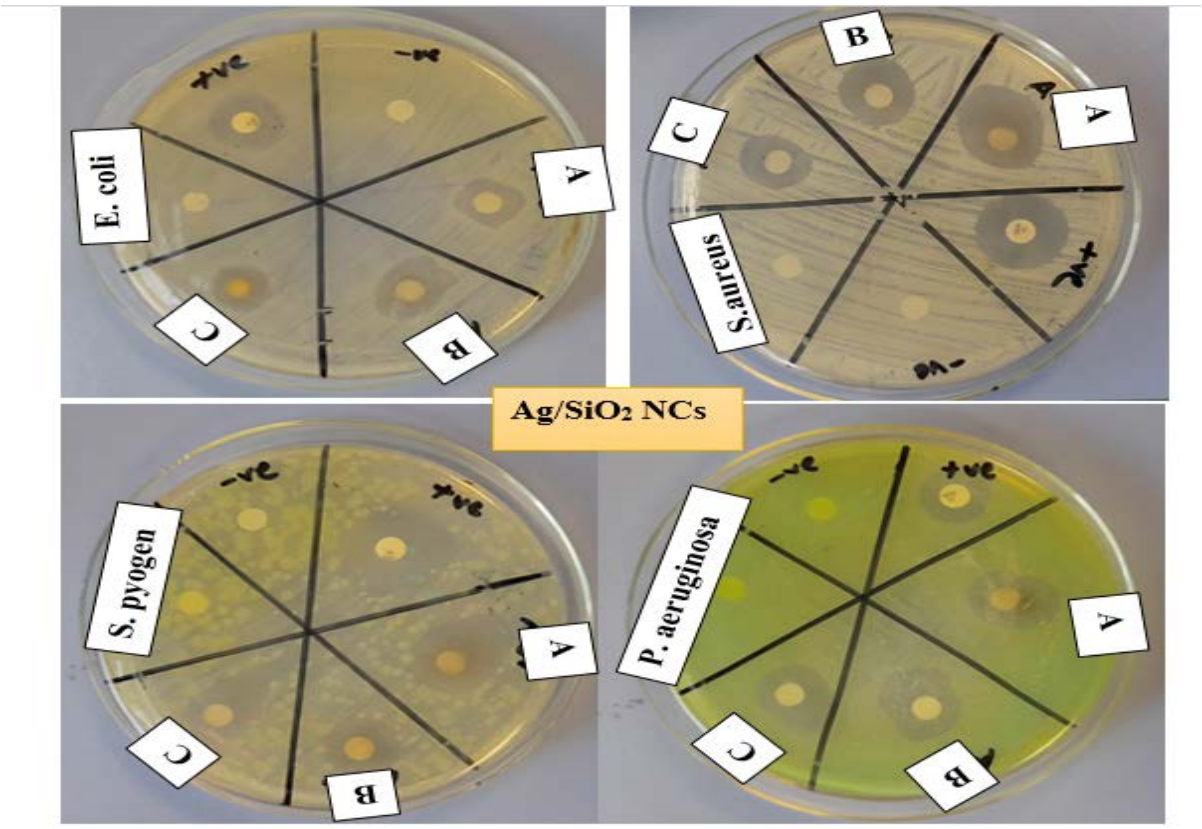


Figure 4.12**:** Photographs of antibacterial activities of $Ag/SiO_2$ NCs at A=10mg/mL B=5mg/mL and C=2.5mg/mL

When a number of Ag NPs come into contact, they bind together to form larger clusters, which is known as aggregation. As a result, there is less surface area accessible to interact with bacterial cells since the surface area to volume ratio of the Ag NPs drops. Ag NPs can produce a coating of proteins, lipids, or other biomolecules on their surface as a result of aggregation, which might further lessen their antibacterial efficacy by preventing their contact with bacterial cells. In the current study, we aim to produce well-dispersed $Ag/SiO_2$ composite nanoparticles by loading Ag NPs of a controlled size onto the surface of $SiO_2$ NCs and to kill the bacteria on target. The result indicated that *Staphylococcus aureus* and *Streptococcus pyogen* (Gram-positive) bacteria have high antibacterial activity when compared to *Pseudomonas aeuruginosa* and *Escherichia coli* (Gram-negative) bacteria. This might be due to *Staphylococcus aureus* and *Streptococcus pyogen* bacteria having a thick peptidoglycan layer whereas *Pseudomonas aeruginous* and *Escherichia coli* bacteria have thinner peptidoglycan but are surrounded by a lipid layer outside. According to *Slavin et al.* small NPs tend to be more toxic than large NPs can be explained by the small NP's relatively larger surface area to volume ratio as compared to larger NPs.

Table 4.3**:** Results of dilution and zone of clearance in mm for synthesized NPs and NCs

| Types of NPs/NCs | Dilution Results, Means of three replications, and Standard error (±SE) of Inhibition zones in mm | | | | | | |
|---|---|---|---|---|---|---|---|
| **No** | Types of NPs/NCs | Types of Organism | 10mg/mL (A) | 5 mg/mL (B) | 2.5mg/mL (C) | Gentamicin (+) | DMSO (-ve) |
| **1** | **$SiO_2$** | *E. coli* ATCC25923 | 6±0.2 | 6±0.2 | 6±0.2 | 24±0 | 6±0 |
| | | *P. aeruginosa* ATCC27853 | 7.4±0.21 | 6±0.2 | 6±0.09 | 22±0 | 6±0 |
| | | *S. aureus* ATCC25923 | 7±0.17 | 7±0.19 | 6±0.19 | 20±0.3 | 6±0 |
| | | *S. Pyogenes* ATCC19615 | 7.1±0.3 | 6±0 | 6±0.1 | 21±0.6 | 6±0 |
| **2** | **Ag** | *E. coli* ATCC25923 | 13±0.2 | 12±0.2 | 11.5±0.2 | 16±0.2 | 6±0 |
| | | *P. aeruginosa* ATCC27853 | 12.3±0.1 | 12.5±0.1 | 11±0.08 | 17±0.05 | 6±0 |
| | | *S. aureus* ATCC25923 | 14±0.2 | 13±0.2 | 13±0.2 | 25±0.2 | 6±0 |
| | | *S. Pyogenes* ATCC19615 | 14.5±0.13 | 13.3±0.1 | 13±0.06 | 22±0 | 6±0 |
| **3** | | E. coli ATCC25923 | 15±0.1 | 14.5±0.1 | 13.5±0.07 | 17±0.24 | 6±0 |
| | | *P. aeruginosa* ATCC27853 | 14±0.15 | 13±0.15 | 13.5±0.13 | 15±0.07 | 6±0 |

| | | | | | | | |
|---|---|---|---|---|---|---|---|
| | **Ag/SiO$_2$** | *S. aureus* ATCC25923 | 16±0.12 | 15±0.12 | 14±0.07 | 22±0.12 | 6±0 |
| | | S. Pyogenes ATCC19615 | 16±0.25 | 14±0.26 | 13.5±0.15 | 25±0.17 | 6±0 |
| **4** | ***A.Afra* Plant leaf extract** | E. coli ATCC25923 | 8±0.3 | 8.7±0.25 | 7.3±0.1 | 22±0.12 | 6±0 |
| | | *P. aeruginosa* ATCC27853 | 8±0.1 | 7.5±0.18 | 7±0.37 | 22±0.3 | 6±0 |
| | | *S. aureus* ATCC25923 | 9±0.33 | 8±0.26 | 7±0.21 | 23±0 | 6±0 |
| | | S. Pyogen ATCC19615 | 7±0.32 | 7±0.32 | 6.88±0.32 | 22±0.21 | 6±0 |

Depending on this Ag/$SiO_2$ NCs high antibacterial activity than Ag NPs.Since bacteria have more opportunities to come into contact with Ag nanoparticles on the surface of $SiO_2$ nanoparticles due to the antibacterial activity's great adsorption capacity, bacteria and some of the dispersed Ag nanoparticles become adsorbed there (*Y. H. Kim et al., 2008*). From this perspective, an ideal degree of Ag nanoparticle loading is advised for the synthesis of Ag produced on the surface of $SiO_2$ nanoparticles for an antibacterial activity to prevent the aggregation of Ag nanoparticles. Generally, silver ions ($Ag^+$) interact with bacterial cell membranes, causing damage to the cell wall and membrane, leading to leakage of intracellular contents and ultimately cell death. The $SiO_2$ matrix also contributes to the antibacterial activity by providing a stable platform for Ag nanoparticles and enhancing their dispersion. Overall, the combination of Ag nanoparticles and $SiO_2$ NPs provides a synergistic effect for antibacterial activity (Allafchian et al., 2017).

### 4.3.1 Minimum Inhibitory Concentration (MIC) and Minimum bactericidal concentration (MBC) of Ag/$SiO_2$ Nanocomposites

The results of the antibacterial effects of Ag/$SiO_2$ nanocomposites against selected bacteria via the MIC and the MBC are summarized in Table 4.4. The bactericidal effect of nanocomposites is dependent on the concentration of nanocomposites and the initial bacterial concentration. In this

study, the initial bacterial concentration was $1\times10^8$ CFU $mL^{-1}$. The MIC value can be determined through a series of dilution tests, where the nanocomposite is tested at different concentrations to determine the minimum concentration required to inhibit bacterial growth. The MBC value for $Ag/SiO_2$ nanocomposites can vary depending on a variety of factors, including the size and distribution of the Ag nanoparticles, the concentration of Ag in the nanocomposite, and the specific bacterial strain being tested. The MBC value can be determined through a series of dilution tests, where the nanocomposite is tested at different concentrations to determine the minimum concentration required to kill the bacteria (Chikezie, 2017; Selvan et al., 2020).As compared to the components of the composite in this study, the $Ag/SiO_2$ nanocomposite showed higher antibacterial activity against both Gram-positive and Gram-negative bacteria, particularly for Gram-positive bacteria. Gram-positive bacteria are more sensitive to this nanocomposite than Gram-negative bacteria, which have an extra lipopolysaccharide-based outer membrane and a thin peptidoglycan layer. This extra membrane indicates that there is also an additional membrane layer known as periplasm, which increases its resistance compared to gram-positive bacteria.

Table 4.4**:** MIC ($\mu gmL^{-1}$) and MBC ($\mu gmL^{-1}$) of $Ag/SiO_2$ nanocomposites

| Bacterial strain | Strain no | MIC ($\mu gmL^{-1}$) | MBC ($\mu gmL^{-1}$) |
|---|---|---|---|
| *S.aureus* | ATCC25923 | 78.124 | 156.134 |
| *S. Pyogenes* | ATCC19615 | 78.113 | 245.23 |
| *E. coli* | ATCC25922 | 156.134 | 321.68 |
| *P. aeruginosa* | ATCC27853 | 157.258 | 327.96 |

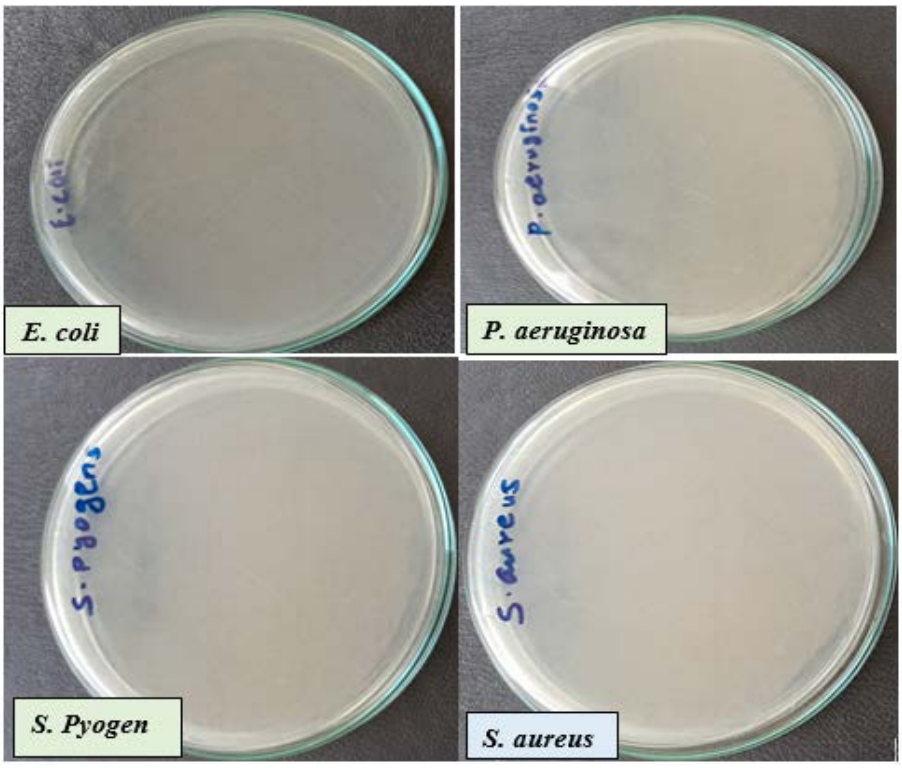


Figure 4.13**:** Photographs of MBC of $Ag/SiO_2$ NCs

The gram positive and gram negative bacteria used in test tube with different amount was taken and compared with blank sample which used as reference point and the absorbance was recorded 1.62 and 1.6 respectively. The MICs observed for $Ag/SiO_2$ NCs were 78.124 and 78.13 $\mu gmL^{-1}$ for *S. aureus* and *S. pyrogen*, respectively. *E. coli* and *P. aeruginosa* strains were found to be 156.134 and 157.258 $gmL^{-1}$, respectively. The MBC for $Ag/SiO_2$ NCs were observed 156.134 and 245.23 $\mu gmL^{-1}$ for gram positive strain, respectively. 321.68 and 327.96 $\mu gmL^{-1}$ were observed for gram negative strain and tested on the bacteria whether it growth or not. The MBC result showed that there is no growth in all bacterial strains (Figure 4.13). Gram-positive bacteria are more sensitive to $Ag/SiO_2$ nanocomposites in MIC and MBC tests, which can be attributed to the thicker peptidoglycan layer in their cell wall. However, the sensitivity of bacteria to $Ag/SiO_2$ nanocomposites can be influenced by other factors, and further research is needed to fully understand the mechanisms underlying these differences. In summary, $Ag/SiO_2$ nanocomposites exhibit strong antimicrobial activity against a variety of bacteria, and their MIC and MBC values can be determined using standard methods. The antimicrobial activity is believed to be due to the release of silver ions from the surface of the nanoparticles, and the silica matrix provides stability

and biocompatibility. These properties make $Ag/SiO_2$ nanocomposites promising candidates for various applications in medicine and industry.

## 4.4. Antifungal Activity Analysis

The antifungal activity of the Ag NPs, $SiO_2$ NPs, $Ag/SiO_2$ NCs, and *A. Afra* plant extract was tested against the fungal strain *Candida albinos* (CA) ATCC9955. *Candida albicans* is a type of yeast that is naturally present in the human body. It is usually found in small amounts in the mouth, digestive tract, and skin. The zone of inhibition (ZOI) was measured at different concentrations of 10 mg/mL, 5 mg/mL, and 2.5 mg/mL for NPs and NCs. The result is shown in Figure 4.14 and Table 4.5. Antifungal activity was shown by an inhibition zone, which was characterized by a clear zone between the wells (containing samples) and a certain distance. The formation of inhibition zones around the wells shows fungal sensitivity to antifungal and antibiotic ingredients (which are used as positive controls).

The positive control used in the well was ketoconazole which functioned as a control of the test solution by comparing the diameter of the inhibition zone formed. DMSO was used as a negative control. In comparison, the antifungal activity of compounds and concentrations of NPs and NCs at 2.5 and 5 mg/mL was weaker than at 10 mg/mL, suggesting that the activity displayed is dose-dependent. As Table 4.5 shows, when the concentration of Ag NPs at 2.5 mg/mL, 5 mg/mL, and 10 mg/mL increases, the zone of inhibition increases, respectively. The increased availability of silver ions at higher concentrations can be the cause of the expansion of the zone of inhibition with increasing AgNPs concentration. Ag NPs produce silver ions when they come into contact with microorganisms, and these ions can interact with the cell membrane and other parts of the fungi to cause cell death. A larger zone of inhibition results from the availability of more silver ions to interact with the bacteria at higher Ag NP concentrations (Siddiqi et al., 2018).

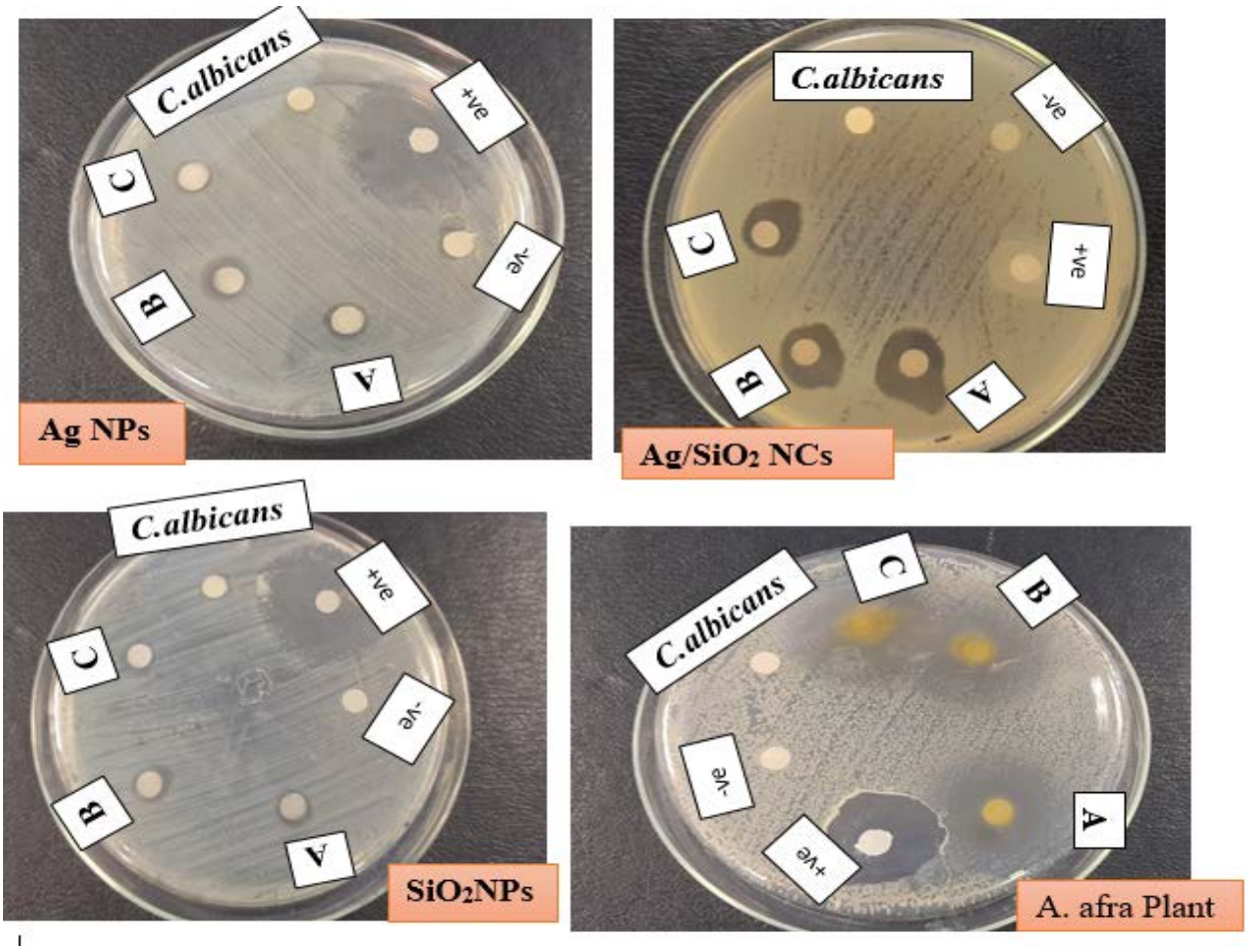


Figure 4.14: Photographs of antifungal activities of Ag NP, $SiO_2$ NPs, Ag/$SiO_2$ NCs, and *A. Afra* Plant at A=10mg/mL B=5mg/mL and C=2.5mg/mL

*Candida albicans* showed strong activity in Ag/$SiO_2$ NCs with a maximum zone of inhibition of 14± 0.2, 13.5 ± 0.2 and 11 ± 0.3 mm at the concentrations of 10, 5, and 2.5 mg/mL, respectively. Figure 4.14 showed Ag NPs with a maximum zone of inhibition of 10 ± 0.3, 8 ± 0.3, and 7.5 ± 0.18 mm at the concentrations of 10, 5, and 2.5 mg/mL, respectively. Also the leave *A. Afra* extract showed good activity with inhibition zone 10±0.11,9±0.3 and 8±0.3mm at concentrations of 10,5 and 2.5mg/mL respectively. $SiO_2$ NPs showed weak activity comparably, with a zone of inhibition of 8± 0.3,7±0.3 and 6.3±0.5 mm at the concentration of 10, 5, and 2.5 mg/mL respectively. This finding is supported by the results of El-Zahed *et al.*, (2022).The result showed Ag/$SiO_2$ NCs show high activity due to unlike the free AgNPs, those immobilized onto the silica surface had a higher release rate of the silver ions and contact-mode interactions with more bacterial cells, enhancing the antibacterial effect of the Ag/$SiO_2$NCs.As shown in Table 4.5 *A.Afra* Plants have better activity in their natural defense mechanisms against fungal infections, which can be devastating for

infection disease. They produce various chemical compounds, also known as secondary metabolites, that exhibit antifungal properties. These compounds help protect plants from harmful fungi and ensure their growth, development, and survival. Some of these compounds include phenolic compounds, alkaloids, saponins, and flavonoids (Baka & El-Zahed, 2022). In comparison, the antifungal activity of $SiO_2$ nanoparticles at concentrations of 2.5 and 5 mg/mL was weaker than at 10 mg/mL, suggesting that the activity displayed is dose-dependent.

Table 4.5: Antifungal activity of Ag NPs, $SiO_2$ NPs, Ag/$SiO_2$ NCs and Artemisia Afra leaf extract

| Types of NPs/NCs | Dilution Results, Means of three replications, and Standard error (±SE) of Inhibition zones in mm | | | | | | |
|---|---|---|---|---|---|---|---|
| No | Types of NPs/NCs | Types of Organism | 10mg/mL (A) | 5 mg/mL (B) | 2.5mg/mL (C) | Ketoconazole (+ve) | DMSO (-ve) |
| 1 | $SiO_2$ | *Candida albicans* ATCC9955 | 8±0.3 | 7±0.3 | 6.3±0.5 | 22±0 | 6 |
| 2 | Ag | | 10±0.3 | 8±0.3 | 7.5±0.18 | 21±0.3 | 6 |
| 3 | Ag/$SiO_2$ | | 14±0.2 | 13±0.25 | 11±0.3 | 20±0.3 | 6 |
| 4 | *A.Afra* Plant | | 10±0.11 | 9±0.3 | 8±0.3 | 22±0 | 6 |

As Table 4.5 shows, when the concentration of $SiO_2$ NPs increases, the zone of inhibition increases. In Table 4.5, Ag NPs showed a better inhibition effect. In most cases, inhibition increased as the concentration of Ag NPs increased. This could be due to the high density at which the solution was able to saturate and cohere to fungal growth and to deactivate plant pathogenic fungi (S. W. Kim et al., 2012). Some reports on the mechanism of the inhibitory action of silver ions on microorganisms have shown that upon treatment with $Ag^+$, DNA loses its ability to replicate. The Ag/$SiO_2$ NCs induced dose-dependent intracellular ROS, which exerted antifungal effects. Ag NPs' production of ROS may have antifungal effects because ROS are known to be harmful to cells, including fungal cells. Beyond a certain point, ROS levels can result in oxidative damage to proteins, lipids, and nucleic acids within cells, which ultimately results in cell death.

Therefore, the observed antifungal effects may have been a result of the dose-dependent rise in intracellular ROS caused by the $Ag/SiO_2$ NCs.

The results of the biosynthesized $Ag/SiO_2$ NCs showed better antifungal activity as compared to the $SiO_2$ and Ag NPs. This might be due to the smaller average crystalline size, the high band gap, and the lower aggregation. $Ag/SiO_2$ NCs have a larger inhibition zone because silver nanoparticles are incorporated into a silica matrix to form $Ag/SiO_2$ nanocomposites. These antifungal properties are maintained, and in some cases, the effectiveness may even be enhanced. This is because the silica matrix can help improve the stability, dispersion, and controlled release of silver nanoparticles (Egger et al., 2009).Generally, when contrast to bacteria, it is showing reduced activity in fungi. This may be related to the tougher cell walls and chitin, which is composed of polysaccharides with a N-acetyl glucosamine and nitrogen group in fungus. As a result, samples cannot move freely between the outside and interior layers of the cell wall (Achamo et al., 2022). $Ag/SiO_2$ nanocomposites have been shown to exhibit effective antifungal properties due to the presence of silver nanoparticles. Silver nanoparticles have been widely recognized as antifungal agents because they can disrupt fungal cell membranes, produce reactive oxygen species (ROS), and interfere with DNA replication, thus inhibiting fungal growth and replication.

# 5. CONCLUSIONS AND RECOMMENDATIONS

## 5.1. Conclusions

In this work successfully reported the use of $Ag/SiO_2$ nanocomposites, which were prepared by green method to investigate the antibacterial and antifungal activity. The crystalline size, functional group, band gap, and morphological structure of the NPs and NCs was confirmed by XRD, FTIR, UV-Vis, and SEM analysis methods. The XRD confirms the crystalline size of $Ag/SiO_2$ NCs was calculated by using Debye Scherrer's formula. FTIR measurements were carried out to identify the possible biomolecules responsible for capping and efficient stabilization of the nanocomposites synthesized by the leaf extract. A band gap of $Ag/SiO_2$ NCs increased than NPs. The SEM image analyses revealed the composite of Ag and $SiO_2$ NPs confirmed spherical shape attached to the pore of $SiO_2$ NPs. $Ag/SiO_2$ have higher antibacterial and antifungal activity than Ag NPs and $SiO_2$ NCs.The antibacterial studies were conducted against the gram-negative species, *E. coli*, *P. aeruginosa,* and gram-positive species, *S. pyogenes, S. aureus, a*nd *Candida albicans* for antifungal activity. Therefore, $Ag/SiO_2$ NCs show higher activity in both Gram-positive and Gram-negative bacteria. In conclusion, green method $Ag/SiO_2$ NCs is low toxicity, environmental compatibility and easily proved to be antibacterial and antifungal.

## 5.2. Recommendations

Based on the present finding of $Ag/SiO_2$ Nanocomposite by using *Artemisia Afra* plant for antibacterial and antifungal activity, the following recommendation is forwarded to benefit those who want to focus on this result of the study under consideration.

- To investigate the shape of particles, more detailed morphology, and surface area of nanocomposite the samples should be characterized by TEM and BET analysis respectively.
- Other synthesis approach to completely remove plant extracts
- The toxicity test of the synthesized NPs and NCs should also be carried out for the drug development process
- The antifungal studies can be extended to other fungal strain

# Research Fund Acknowledgment

This research thesis was funded by Adama Science and Technology University under the grant number of ASTU/SM-R/687/23, Adama, Ethiopia

# 6.Reference


Abduraimova, A., Molkenova, A., Duisembekova, A., Mulikova, T., Kanayeva, D., & Atabaev, T. S. (2021). Cetyltrimethylammonium bromide (Ctab)-loaded sio2–ag mesoporous nanocomposite as an efficient antibacterial agent. *Nanomaterials*, *11*(2), 1–9. https://doi.org/10.3390/nano11020477

Achamo, T., Zereffa, E. A., Murthy, H. C. A., Ramachandran, V. P., & Balachandran, R. (2022). Phyto-mediated synthesis of copper oxide nanoparticles using Artemisia abyssinica leaf extract and its antioxidant, antimicrobial and DNA binding activities. *Green Chemistry Letters and Reviews*, *15*(3), 598–614. https://doi.org/10.1080/17518253.2022.2121620

Ahmed, S., Ahmad, M., Swami, B. L., & Ikram, S. (2016). A review on plants extract mediated synthesis of silver nanoparticles for antimicrobial applications: A green expertise. *Journal of Advanced Research*, *7*(1), 17–28. https://doi.org/10.1016/j.jare.2015.02.007

Akintelu, S. A., & Folorunso, A. S. (2020). A Review on Green Synthesis of Zinc Oxide Nanoparticles Using Plant Extracts and Its Biomedical Applications. *BioNanoScience*, *10*(4), 848–863. https://doi.org/10.1007/s12668-020-00774-6

AL-Jobory, H. S., Hassan, K. M. A., Kareem, Z. H., & Alkaim, A. F. (2019). Green synthesis of silver nanoparticles and its antibacterial activity: A review. *Plant Archives*, *19*(3), 2363–2367.

Allafchian, A. R., Banifatemi, S. S., & Jalali, S. A. H. (2017). Synthesis and Characterization of Ag/SiO2 Nanoparticles Embedded in TPS and TEOS Sol-gel Matrix with Excellent Antibacterial Activity. *Nanoscience &Nanotechnology-Asia*, *8*(1), 33–40. https://doi.org/10.2174/2210681207011704191502O9

Arti. (2020). Introduction to Nanomaterials. *Nanotechnology*, *December 2011*, 1–10. https://doi.org/10.1201/9781003082859-1

Asfaw, N., & Demissew, S. (2015). Essential oil composition of four Artemisia species from Ethiopia. *Bulletin of the Chemical Society of Ethiopia*, *29*(1), 123–128. https://doi.org/10.4314/bcse.v29i1.11

Assis, M., Simoes, L. G. P., Tremiliosi, G. C., Coelho, D., Minozzi, D. T., Santos, R. I., Vilela, D. C. B., Santos, J. R. Do, Ribeiro, L. K., Rosa, I. L. V., Mascaro, L. H., Andrés, J., & Longo,

E. (2021). Sio2-ag composite as a highly virucidal material: A roadmap that rapidly eliminates sars-cov-2. *Nanomaterials*, *11*(3), 1–19. https://doi.org/10.3390/nano11030638

Asst, R., Asst, P., & Xrd, T. (2018). *SYNTHESIS OF SILICA NANOPARTICLES VIA GREEN APPROACH BY USING HOT AQUEOUS EXTRACT OF THUJA ORIENTALIS LEAF AND THEIR EFFECT ON BIOFILM FORMATION*. *50*.

Azimi, R., & Lasemi, Z. (2022). Environmentally friendly synthesis of Ag/SiO2 nanoparticles using Thymus kotschyanus extract and its application as a green catalyst for synthesis of spirooxindoles. *Research on Chemical Intermediates*, *48*(4), 1615–1630. https://doi.org/10.1007/s11164-022-04667-z

Babu, R. H., Yugandhar, P., & Savithramma, N. (2018). *Synthesis , characterization and antimicrobial studies of bio silica nanoparticles prepared from Cynodon dactylon L .: a green*.

Baka, Z. A., & El-Zahed, M. M. (2022). Antifungal activity of silver/silicon dioxide nanocomposite on the response of faba bean plants (Vicia faba L.) infected by Botrytis cinerea. *Bioresources and Bioprocessing*, *9*(1). https://doi.org/10.1186/s40643-022-00591-7

Balaji, D. S., Basavaraja, S., Deshpande, R., Mahesh, D. B., Prabhakar, B. K., & Venkataraman, A. (2009). Extracellular biosynthesis of functionalized silver nanoparticles by strains of Cladosporium cladosporioides fungus. *Colloids and Surfaces B: Biointerfaces*, *68*(1), 88–92. https://doi.org/10.1016/j.colsurfb.2008.09.022

Balakumaran, M. D., Ramachandran, R., Balashanmugam, P., Mukeshkumar, D. J., & Kalaichelvan, P. T. (2016). Mycosynthesis of silver and gold nanoparticles: Optimization, characterization and antimicrobial activity against human pathogens. *Microbiological Research*, *182*, 8–20. https://doi.org/10.1016/j.micres.2015.09.009

Balciunaitiene, A., Viskelis, P., Viskelis, J., Streimikyte, P., Liaudanskas, M., Bartkiene, E., Zavistanaviciute, P., Zokaityte, E., Starkute, V., Ruzauskas, M., & Lele, V. (2021). Green synthesis of silver nanoparticles using extract of Artemisia absinthium l., Humulus lupulus l. and Thymus vulgaris l., physico-chemical characterization, antimicrobial and antioxidant activity. *Processes*, *9*(8). https://doi.org/10.3390/pr9081304

Bano, I., & Deora, G. S. (2019). Preliminary phytochemical screening and GC-MS analysis of methanolic leaf extract of Abutilon pannosum (Forst. F.) Schlect. from Indian Thar desert. *Journal of Pharmacognosy and Phytochemistry*, *8*(1), 894–899. https://www.phytojournal.com/archives/2019.v8.i1.6866/preliminary-phytochemical-screening-and-gc-ms-analysis-of-methanolic-leaf-extract-of-ltemgtabutilon-pannosum-ltemgtforst-f-schlect-from-indian-thar-desert

Baran, M. F. (2019). Synthesis and Antimicrobial Applications of Silver Nanoparticles From artemisia absinthium plant. *Biological and Chemical Research*, *6*, 96–103.

Bélteky, P., Rónavári, A., Igaz, N., Szerencsés, B., Tóth, I. Y., Pfeiffer, I., Kiricsi, M., & Kónya, Z. (2019). Silver nanoparticles: Aggregation behavior in biorelevant conditions and its impact on biological activity. *International Journal of Nanomedicine*, *14*, 667–687. https://doi.org/10.2147/IJN.S185965

Bora, K. S., & Sharma, A. (2010). Phytochemical and Pharmacological potential of Artemisia absinthium Linn. and Artemisia asiatic Nakai: A review. *Journal of Pharmacy Research*, *3*(2), 325–328.

Cantón, E., Espinel-Ingroff, A., & Pemán, J. (2009). Trends in antifungal susceptibility testing using CLSI reference and commercial methods. *Expert Review of Anti-Infective Therapy*, *7*(1), 107–119. https://doi.org/10.1586/14787210.7.1.107

Cha, H. W. A. J. I. N., Kim, Y. H., & Cha, H. G. I. L. (2007). *Ag ( CORE )/ SiO 2 ( SHELL ) NANOPARTICLES*. *14*(4), 693–696.

Chikezie, I. O. (2017). Determination of minimum inhibitory concentration (MIC) and minimum bactericidal concentration (MBC) using a novel dilution tube method. *African Journal of Microbiology Research*, *11*(23), 977–980. https://doi.org/10.5897/ajmr2017.8545

Cotton, G. C., Lagesse, N. R., Parke, L. S., & Meledandri, C. J. (2019). Antibacterial nanoparticles. In *Comprehensive Nanoscience and Nanotechnology* (Vols. 1–5). Elsevier Ltd. https://doi.org/10.1016/B978-0-12-803581-8.10409-6

Demissie, M. G., Sabir, F. K., Edossa, G. D., & Gonfa, B. A. (2020). Synthesis of Zinc Oxide Nanoparticles Using Leaf Extract of Lippia adoensis (Koseret) and Evaluation of Its

Antibacterial Activity. *Journal of Chemistry*, *2020*. https://doi.org/10.1155/2020/7459042

Deng, Z., Chen, M., & Wu, L. (2007). Novel method to fabricate SiO2/Ag composite spheres and their catalytic, surface-enhanced raman scattering properties. *Journal of Physical Chemistry C*, *111*(31), 11692–11698. https://doi.org/10.1021/jp073632h

Desalegn, T., Murthy, H. C. A., & Adimasu, Y. (2021). *Medicinal Plant Syzygium Guineense ( Willd .) DC Leaf Extract Mediated Green*. *8*(1).

Desalegn, T., Ravikumar, C. R., & Murthy, H. C. A. (2021). Eco-friendly synthesis of silver nanostructures using medicinal plant Vernonia amygdalina Del. leaf extract for multifunctional applications. *Applied Nanoscience (Switzerland)*, *11*(2), 535–551. https://doi.org/10.1007/s13204-020-01620-7

Deshmukh, P., Bhatt, J., Peshwe, D., & Pathak, S. (2012). Determination of silica activity index and XRD, SEM and EDS studies of amorphous SiO 2 extracted from rice Husk Ash. *Transactions of the Indian Institute of Metals*, *65*(1), 63–70. https://doi.org/10.1007/s12666-011-0071-z

Dong, Y., Zhu, H., Shen, Y., Zhang, W., & Zhang, L. (2019). Antibacterial activity of silver nanoparticles of different particle size against Vibrio Natriegens. *PLoS ONE*, *14*(9), 1–12. https://doi.org/10.1371/journal.pone.0222322

Drug, D. (2021). *Green Synthesis and Biomedical Applications of ZnO Nanoparticles : Role of PEGylated-ZnO Nanoparticles as*. *231*, 1–19.

Duhan, S., Devi, S., & Srivastava, M. (2010). Characterization of nanocrystalline Ag/SiO2 nanocomposites and synthesis by wet chemical method. *Indian Journal of Pure and Applied Physics*, *48*(4), 271–275.

Egger, S., Lehmann, R. P., Height, M. J., Loessner, M. J., & Schuppler, M. (2009). Antimicrobial properties of a novel silver-silica nanocomposite material. *Applied and Environmental Microbiology*, *75*(9), 2973–2976. https://doi.org/10.1128/AEM.01658-08

El-Zahed, M. M., Abou-Dobara, M. I., El-Sayed, A. K. A., & Baka, Z. A. M. (2022). Ag/SiO2 nanocomposite mediated by Escherichia coli D8 and their antimicrobial potential. *Nova Biotechnologica et Chimica*, *21*(1), 1–11. https://doi.org/10.36547/nbc.1023

Elemike, E. E., Onwudiwe, D. C., Ekennia, A. C., & Jordaan, A. (2018). Synthesis and characterisation of silver nanoparticles using leaf extract of Artemisia afra and their in vitro antimicrobial and antioxidant activities. *IET Nanobiotechnology*, *12*(6), 722–726. https://doi.org/10.1049/iet-nbt.2017.0297

Garg, P., Garg, R., & Praveen Garg, C. (2019). Phytochemical screening and quantitative estimation of total flavonoids of Ocimum sanctum in different solvent extract. *~ 16 ~ The Pharma Innovation Journal*, *8*(2), 16–21. www.thepharmajournal.com

Gonelimali, F. D., Lin, J., Miao, W., Xuan, J., Charles, F., Chen, M., & Hatab, S. R. (2018). Antimicrobial properties and mechanism of action of some plant extracts against food pathogens and spoilage microorganisms. *Frontiers in Microbiology*, *9*(JUL), 1–9. https://doi.org/10.3389/fmicb.2018.01639

Graven, E. H., Dean, S. G., Svoboda, K. P., Mavi, S., & Gundidza, M. G. (1992). Antimicrobial and antioxidative properties of the volatile (essential) oil of Artemisia afra Jacq. *Flavour and Fragrance Journal*, *7*(3), 121–123. https://doi.org/10.1002/ffj.2730070305

Gudimalla, A., Jose, J., Jose, R., & Sabu, V. (2020). Green Synthesis of Silver Nanoparticles Using Nymphae odorata Extract Incorporated Films and Antimicrobial Activity. *Journal of Polymers and the Environment*, *0123456789*. https://doi.org/10.1007/s10924-020-01959-6

Hagos, M., Ramadevi, D., & Kumar, Y. P. (2018). OpenNano Synthesis of silver nanoparticles using aqueous extract of Dolichos lablab for reduction of 4-Nitrophenol , antimicrobial and anticancer activities. *OpenNano*, *3*(March), 28–37. https://doi.org/10.1016/j.onano.2018.04.001

Hardikar, V. V., & Matijević, E. (2000). Coating of nanosize silver particles with silica. *Journal of Colloid and Interface Science*, *221*(1), 133–136. https://doi.org/10.1006/jcis.1999.6579

Hawar, S. N., Al-Shmgani, H. S., Al-Kubaisi, Z. A., Sulaiman, G. M., Dewir, Y. H., & Rikisahedew, J. J. (2022). Green Synthesis of Silver Nanoparticles from Alhagi graecorum Leaf Extract and Evaluation of Their Cytotoxicity and Antifungal Activity. *Journal of Nanomaterials*, *2022*. https://doi.org/10.1155/2022/1058119

Holder, C. F., & Schaak, R. E. (2019). Tutorial on Powder X-ray Diffraction for Characterizing

Nanoscale Materials. *ACS Nano*, *13*(7), 7359–7365. https://doi.org/10.1021/acsnano.9b05157

Huang, T., Li, X., Maier, M., O'Brien-Simpson, N. M., Heath, D. E., & O'Connor, A. J. (2023). Using inorganic nanoparticles to fight fungal infections in the antimicrobial resistant era. *Acta Biomaterialia*, *158*, 56–79. https://doi.org/10.1016/j.actbio.2023.01.019

Jamkhande, P. G., Ghule, N. W., Bamer, A. H., & Kalaskar, M. G. (2019). Metal nanoparticles synthesis: An overview on methods of preparation, advantages and disadvantages, and applications. *Journal of Drug Delivery Science and Technology*, 101174. https://doi.org/10.1016/j.jddst.2019.101174

Jana, S., Ghosh, S. K., Nath, S., Pande, S., Praharaj, S., Panigrahi, S., Basu, S., Endo, T., & Pal, T. (2006). Synthesis of silver nanoshell-coated cationic polystyrene beads: A solid phase catalyst for the reduction of 4-nitrophenol. *Applied Catalysis A: General*, *313*(1–2), 41–48. https://doi.org/10.1016/j.apcata.2006.07.007

Janjua, T. I., Cao, Y., Yu, C., & Popat, A. (2021). Clinical translation of silica nanoparticles. *Nature Reviews Materials*, *6*(12), 1072–1074. https://doi.org/10.1038/s41578-021-00385-x

Jeelani, P. G., Mulay, P., Venkat, R., & Ramalingam, C. (2020). Multifaceted Application of Silica Nanoparticles. A Review. *Silicon*, *12*(6), 1337–1354. https://doi.org/10.1007/s12633-019-00229-y

Jubu, P. R., Yam, F. K., Igba, V. M., & Beh, K. P. (2020). Tauc-plot scale and extrapolation effect on bandgap estimation from UV–vis–NIR data – A case study of β-Ga2O3. *Journal of Solid State Chemistry*, *290*, 121576. https://doi.org/10.1016/j.jssc.2020.121576

Kadhum, S. A. (2017). The effect of two types of nano-particles (ZnO & SiO2) on different types of bacterial growth. *Biomedical and Pharmacology Journal*, *10*(4), 1701–1708. https://doi.org/10.13005/bpj/1282

Kalpana, V. N., & Devi Rajeswari, V. (2018). A Review on Green Synthesis, Biomedical Applications, and Toxicity Studies of ZnO NPs. *Bioinorganic Chemistry and Applications*, *2018*, 1–12. https://doi.org/10.1155/2018/3569758

Karthik, C., Caroline, D. G., Dhanam Priya, M., & Pandi Prabha, S. (2021a). Synthesis,

Characterization of Ag-SiO2 Nanocomposite and Its Application in Food Packaging. *Journal of Inorganic and Organometallic Polymers and Materials*, *31*(6), 2532–2541. https://doi.org/10.1007/s10904-020-01853-7

Karthik, C., Caroline, D. G., Dhanam Priya, M., & Pandi Prabha, S. (2021b). Synthesis, Characterization of Ag-SiO2 Nanocomposite and Its Application in Food Packaging. *Journal of Inorganic and Organometallic Polymers and Materials*, *31*(6), 2532–2541. https://doi.org/10.1007/s10904-020-01853-7

Kayed, K., Issa, M., & Alsoki, E. (2023). The Band Gap of Silver Nanoparticles in Ag/Ag2O Composites Synthesized by Oxygen Plasma Treatment of Silver Thin Films. *Plasmonics*, 711–717. https://doi.org/10.1007/s11468-023-01800-5

Kessler, A., Hedberg, J., & Blomberg, E. (2022). *Reactive Oxygen Species Formed by Metal and Metal Oxide Nanoparticles in Physiological Media — A Review of Reactions of Importance to Nanotoxicity and Proposal for Categorization*.

Khan, F., Shariq, M., Asif, M., Siddiqui, M. A., Malan, P., & Ahmad, F. (2022). *Green Nanotechnology : Plant-Mediated Nanoparticle Synthesis and Application*.

Khan, I., Saeed, K., & Khan, I. (2019). Nanoparticles: Properties, applications and toxicities. *Arabian Journal of Chemistry*, *12*(7), 908–931. https://doi.org/10.1016/j.arabjc.2017.05.011

Khan, M. Z. H., Tareq, F. K., Hossen, M. A., & Roki, M. N. A. M. (2018). *GREEN SYNTHESIS AND CHARACTERIZATION OF SILVER NANOPARTICLES USING CORIANDRUM SATIVUM LEAF EXTRACT*. *13*(1), 158–166.

Khattab, S., El Sherif, F., AlDayel, M., Yap, Y. K., Meligy, A., & Ibrahim, H. I. M. (2022). Silicon dioxide and silver nanoparticles elicit antimicrobial secondary metabolites while enhancing growth and multiplication of Lavandula officinalis in-vitro plantlets. *Plant Cell, Tissue and Organ Culture*, *149*(1–2), 411–421. https://doi.org/10.1007/s11240-021-02224-x

Khedkar, C. V., Daware, K. D., Badgujar, P. S., Kolekar, Y. D., Gosavi, S. W., & Patil, S. I. (2021). Ag–SiO2 nanocomposite for the optical detection of Hg(II) ions and catalytic reduction of methylene blue. *Optical Materials*, *120*(July), 111426. https://doi.org/10.1016/j.optmat.2021.111426

Khezerlou, A., Alizadeh-Sani, M., Azizi-Lalabadi, M., & Ehsani, A. (2018). Nanoparticles and their antimicrobial properties against pathogens including bacteria, fungi, parasites and viruses. In *Microbial Pathogenesis* (Vol. 123). Elsevier Ltd. https://doi.org/10.1016/j.micpath.2018.08.008

Kim, S. W., Jung, J. H., Lamsal, K., Kim, Y. S., Min, J. S., & Lee, Y. S. (2012). Antifungal effects of silver nanoparticles (AgNPs) against various plant pathogenic fungi. *Mycobiology*, *40*(1), 53–58. https://doi.org/10.5941/MYCO.2012.40.1.053

Kim, Y. H., Kim, C. W., Cha, H. G., Jo, B. K., Ahn, G. W., Hong, E. S., & Kang, Y. S. (2008). Preparation of antibacterial silver-containing silica nanocomposite. *Surface Review and Letters*, *15*(1–2), 117–122. https://doi.org/10.1142/s0218625x08011093

Kim, Y. H., Lee, D. K., Cha, H. G., Kim, C. W., & Kang, Y. S. (2007). Synthesis and characterization of antibacterial Ag - SiO2 nanocomposite. *Journal of Physical Chemistry C*, *111*(9), 3629–3635. https://doi.org/10.1021/jp068302w

Kukushkina, E. A., Hossain, S. I., Sportelli, M. C., Ditaranto, N., Picca, R. A., & Cioffi, N. (2021). Ag-based synergistic antimicrobial composites. A critical review. *Nanomaterials*, *11*(7). https://doi.org/10.3390/nano11071687

Kumar, D., Kumar, G., Das, R., & Agrawal, V. (2018). Strong larvicidal potential of silver nanoparticles ( AgNPs ) synthesized using Holarrhena antidysenterica ( L .) Wall . bark extract against malarial vector , Anopheles stephensi Liston Strong larvicidal potential of silver nanoparticles ( AgNPs ) synthe. *Process Safety and Environmental Protection*, *116*(May), 137–148. https://doi.org/10.1016/j.psep.2018.02.001

Lere Keshebo, D., Washe, A. P., & Alemu, F. (2016). Determination of Antimicrobial and Antioxidant Activities of Extracts from Selected Medicinal Plants. *American Scientific Research Journal for Engineering*, *16*(1), 212–222. http://asrjetsjournal.org/

Li, Z., Jia, Z., Ni, T., & Li, S. (2017). Green and facile synthesis of fibrous Ag/cotton composites and their catalytic properties for 4-nitrophenol reduction. *Applied Surface Science*, *426*, 160–168. https://doi.org/10.1016/j.apsusc.2017.07.173

Liu, N. Q., Van der Kooy, F., & Verpoorte, R. (2009). Artemisia afra: A potential flagship for

African medicinal plants? *South African Journal of Botany*, *75*(2), 185–195. https://doi.org/10.1016/j.sajb.2008.11.001

Martini, M. C., Zhang, T., Williams, J. T., Abramovitch, R. B., Weathers, P. J., & Shell, S. S. (2020). Artemisia annua and Artemisia afra extracts exhibit strong bactericidal activity against Mycobacterium tuberculosis. *Journal of Ethnopharmacology*, *262*(July), 113191. https://doi.org/10.1016/j.jep.2020.113191

Mebert, A. M., Baglole, C. J., Desimone, M. F., & Maysinger, D. (2017). Nanoengineered silica : Properties , applications and toxicity. *Food and Chemical Toxicology*. https://doi.org/10.1016/j.fct.2017.05.054

Mohammed, C. H. (2019). Ag-SiO2 nanoparticales prepared by Sol-Gel methods for antibacterial effect. *Iraqi Journal of Physics*, *16*(39), 135–151. https://doi.org/10.30723/ijp.v16i39.112

Mohd Radzuan, N. A., Sulong, A. B., & Sahari, J. (2017). A review of electrical conductivity models for conductive polymer composite. *International Journal of Hydrogen Energy*, *42*(14), 9262–9273. https://doi.org/10.1016/j.ijhydene.2016.03.045

Moreno-Trejo, M. B., & Sánchez-Domínguez, M. (2016). Mesquite gum as a novel reducing and stabilizing agent for modified tollens synthesis of highly concentrated ag nanoparticles. *Materials*, *9*(10). https://doi.org/10.3390/ma9100817

Mrsc, S. P., & Universiy, P. (2015). *NANOCOMPOSITES AND IT ’ S APPLICATION-REVIEW NANOCOMPOSITES AND IT ’ S APPLICATION -REVIEW - Shivani Pandya INTRODUCTION : December*. https://doi.org/10.13140/RG.2.1.2798.9840

Nandanwar, R., Singh, P., & Haque, F. (2015). Synthesis and Characterization of SiO2 Nanoparticles by Sol-Gel Process and Its Degradation of Methylene Blue. *American Chemical Science Journal*, *5*(1), 1–10. https://doi.org/10.9734/acsj/2015/10875

Nayak, P. P. (2021). *Synthesis of SiO 2 -Nanoparticles from Rice Husk Ash and its Comparison with Commercial Amorphous Silica through Material Characterization*. 1209–1214.

Nguyen, H. C., Nguyen, T. T., Dao, T. H., Ngo, Q. B., Pham, H. L., & Nguyen, T. B. N. (2016). Preparation of Ag/SiO2 nanocomposite and assessment of its antifungal effect on soybean plant (a Vietnamese species DT-26). *Advances in Natural Sciences: Nanoscience and*

*Nanotechnology*, *7*(4), 1–7. https://doi.org/10.1088/2043-6262/7/4/045014

Okaiyeto, K., Ojemaye, M. O., Hoppe, H., Mabinya, L. V, & Okoh, A. I. (2019). Phytofabrication of Silver/ Silver Chloride Oedera genistifolia : Characterization and Antibacterial Potential. *Molecules*, *24*, 4382.

Okpala, C. C. (2013). *Nanocomposites – An Overview*. *8*(11), 17–23.

Otari, S. V., Shinde, V. V., Hui, G., Patel, S. K. S., Kalia, V. C., Kim, I. W., & Lee, J. K. (2019). Biomolecule-entrapped SiO2 nanoparticles for ultrafast green synthesis of silver nanoparticle–decorated hybrid nanostructures as effective catalysts. *Ceramics International*, *45*(5), 5876–5882. https://doi.org/10.1016/j.ceramint.2018.12.054

Patil, M. P., & Kim, G. Do. (2017). Eco-friendly approach for nanoparticles synthesis and mechanism behind antibacterial activity of silver and anticancer activity of gold nanoparticles. *Applied Microbiology and Biotechnology*, *101*(1), 79–92. https://doi.org/10.1007/s00253-016-8012-8

Pavani, K. V, Banerjee, A., & Suresh, S. (2013). Phyto-synthesis of Silver Nanoparticles Using Extracts of Ipomoea indica Flowers. *American Journal of Nanomaterials*, *1*(1), 5–8. https://doi.org/10.12691/ajn-1-1-2

Periakaruppan, R., Manju Praveena, S., Priya, C., Ranjitha, P., Gokul Raj, S., & Danaraj, J. (2022). Biosynthesis of Silica Nanoparticles Using the Leaf Extract of Punica granatum and Assessment of Its Antibacterial Activities Against Human Pathogens. *Applied Biochemistry and Biotechnology*, *194*(11), 5594–5605. https://doi.org/10.1007/s12010-022-03994-6

Pillai, A. M., Sivasankarapillai, V. S., Rahdar, A., Joseph, J., Sadeghfar, F., Anuf A, R., Rajesh, K., & Kyzas, G. Z. (2020). Green synthesis and characterization of zinc oxide nanoparticles with antibacterial and antifungal activity. *Journal of Molecular Structure*, *1211*, 128107. https://doi.org/10.1016/j.molstruc.2020.128107

Prabha, S., Durgalakshmi, D., Rajendran, S., & Lichtfouse, E. (2021). Plant-derived silica nanoparticles and composites for biosensors, bioimaging, drug delivery and supercapacitors: a review. *Environmental Chemistry Letters*, *19*(2), 1667–1691. https://doi.org/10.1007/s10311-020-01123-5

Prakash, P., Gnanaprakasam, P., Emmanuel, R., Arokiyaraj, S., & Saravanan, M. (2013). Green synthesis of silver nanoparticles from leaf extract of Mimusops elengi, Linn. for enhanced antibacterial activity against multi drug resistant clinical isolates. *Colloids and Surfaces B: Biointerfaces*, *108*, 255–259. https://doi.org/10.1016/j.colsurfb.2013.03.017

Prasetya, N. B. A., Ngadiwiyana, Ismiyarto, & Sarjono, P. R. (2019). Synthesis and study of antibacterial activity of polyeugenol. *IOP Conference Series: Materials Science and Engineering*, *509*(1). https://doi.org/10.1088/1757-899X/509/1/012101

Qin, R., Li, G., Pan, L., Han, Q., Sun, Y., & He, Q. (2017). *Journal of Nanoscience and Nanotechnology*. *17*(4), 2305–2311. https://doi.org/10.1166/jnn.2017.13042

Raturi, G., Sharma, Y., Rana, V., Thakral, V., Myaka, B., Salvi, P., Singh, M., Dhar, H., & Deshmukh, R. (2021). Exploration of silicate solubilizing bacteria for sustainable agriculture and silicon biogeochemical cycle. *Plant Physiology and Biochemistry*, *166*(March), 827–838. https://doi.org/10.1016/j.plaphy.2021.06.039

Rawat, M. (2016a). a Review on Green Synthesis and Characterization of Silver Nanoparticles and Their Applications: a Green Nanoworld. *World Journal of Pharmacy and Pharmaceutical Sciences*, *5*(7), 730–762. https://doi.org/10.20959/wjpps20167-7227

Rawat, M. (2016b). a Review on Green Synthesis and Characterization of Silver Nanoparticles and Their Applications: a Green Nanoworld. *World Journal of Pharmacy and Pharmaceutical Sciences*, *July*, 730–762. https://doi.org/10.20959/wjpps20167-7227

Rodrigues, M. C., Rolim, W. R., Viana, M. M., Souza, T. R., Gonçalves, F., Tanaka, C. J., Bueno-Silva, B., & Seabra, A. B. (2020). Biogenic synthesis and antimicrobial activity of silica-coated silver nanoparticles for esthetic dental applications. *Journal of Dentistry*, *96*(March), 103327. https://doi.org/10.1016/j.jdent.2020.103327

Salem, S. S., Hammad, E. N., Mohamed, A. A., & El-Dougdoug, W. (2023). A Comprehensive Review of Nanomaterials: Types, Synthesis, Characterization, and Applications. *Biointerface Research in Applied Chemistry*, *13*(1). https://doi.org/10.33263/BRIAC131.041

Saravanan, S. (2020). *Synthesis of SiO2 Nanoparticles by Sol-Gel Method and Their Optical and Synthesis of SiO 2 Nanoparticles by Sol-Gel Method and Their Optical and Structural*

*Properties*. *January*.

Sasivarnam, M., Anbukumaran, A., Dhanasekaran, S., & Abomughaidv, M. M. (2021). *Rapid Green synthesis of Nano SiO2 using Bryophyllum pinnatum leaf and evaluation of physicochemical quality attributes*. 1–20.

Science, M. O. F., The, U., & Guidance, E. (n.d.). *National Institute of Technology , Rourkela*.

Selvan, D. S. A., Shobana, S., Thiruvasagam, P., Murugesan, S., & Rahiman, A. K. (2020). Evaluation of Antimicrobial and Antidiabetic Activities of Ag@SiO2 Core–Shell Nanoparticles Synthesized with Diverse Shell Thicknesses. *Journal of Cluster Science*, *31*(4), 739–749. https://doi.org/10.1007/s10876-019-01682-w

Selvarajan, V., Obuobi, S., Lai, P., & Ee, R. (2020). *Silica Nanoparticles — A Versatile Tool for the Treatment of Bacterial Infections*. *8*(July), 1–16. https://doi.org/10.3389/fchem.2020.00602

Sembiring, S., Riyanto, A., Firdaus, I., Junaidi, & Situmeang, R. (2022). Structure and Properties of Silver-Silica Composite Prepared From Rice Husk Silica and Silver Nitrate. *Ceramics - Silikaty*, *66*(2), 167–177. https://doi.org/10.13168/cs.2022.0011

Shaikh, J. R., & Patil, M. (2020). Qualitative tests for preliminary phytochemical screening: An overview. *International Journal of Chemical Studies*, *8*(2), 603–608. https://doi.org/10.22271/chemi.2020.v8.i2i.8834

Shi, Y., Zhang, X. L., Feng, G., Chen, X., & Lu, Z. H. (2015). Ag-SiO2 nanocomposites with plum-pudding structure as catalyst for hydrogenation of 4-nitrophenol. *Ceramics International*, *41*(10), 14660–14667. https://doi.org/10.1016/j.ceramint.2015.07.188

Shrivas, K., Sahu, S., Patra, G. K., Jaiswal, N. K., & Shankar, R. (2016). Localized surface plasmon resonance of silver nanoparticles for sensitive colorimetric detection of chromium in surface water, industrial waste water and vegetable samples. *Analytical Methods*, *8*(9), 2088–2096. https://doi.org/10.1039/c5ay03120f

Siddiqi, K. S., Husen, A., & Rao, R. A. K. (2018). A review on biosynthesis of silver nanoparticles and their biocidal properties. *Journal of Nanobiotechnology*, *16*(1). https://doi.org/10.1186/s12951-018-0334-5

Singh, J., Dutta, T., Kim, K. H., Rawat, M., Samddar, P., & Kumar, P. (2018). “Green” synthesis of metals and their oxide nanoparticles: Applications for environmental remediation. *Journal of Nanobiotechnology*, *16*(1), 1–24. https://doi.org/10.1186/s12951-018-0408-4

Singh, M., & Singhal, A. (2018). Modeling of shape and size effects for the band gap of semiconductor nanoparticles. *Proceedings - 2nd International Conference on Micro-Electronics and Telecommunication Engineering, ICMETE 2018*, 339–342. https://doi.org/10.1109/ICMETE.2018.00080

*$SiO_2$ Nanocomposites.pdf*. (n.d.).

Slavin, Y. N., Asnis, J., Häfeli, U. O., & Bach, H. (2017). Metal nanoparticles: Understanding the mechanisms behind antibacterial activity. *Journal of Nanobiotechnology*, *15*(1), 1–20. https://doi.org/10.1186/s12951-017-0308-z

Syafiuddin, A., Salmiati, Salim, M. R., Beng Hong Kueh, A., Hadibarata, T., & Nur, H. (2017). A Review of Silver Nanoparticles: Research Trends, Global Consumption, Synthesis, Properties, and Future Challenges. *Journal of the Chinese Chemical Society*, *64*(7), 732–756. https://doi.org/10.1002/jccs.201700067

Taheri, M. (2018). Green synthesis of silver/silica nanocomposite in seconds at room temperature using reducing agents obtained from silicon nanoparticles. *Laser Physics*, *28*(12). https://doi.org/10.1088/1555-6611/aae5a4

Thangamani, N., & Bhuvaneshwari, N. (2022). Synthesis, characterization of Ag nanoparticles using the green approach towards degradation of environmental pollutant. *Journal of Materials Science: Materials in Electronics*, *33*(12), 9155–9162. https://doi.org/10.1007/s10854-021-07188-4

The, I., In, P., & By, S. (2021). *Zinc Oxide Nanoparticles : Different synthesis approaches and applications*. *January*.

Thomas, S., Nair, S. K., Jamal, E. M. A., Al-Harthi, S. H., Varma, M. R., & Anantharaman, M. R. (2008). Size-dependent surface plasmon resonance in silver silica nanocomposites. *Nanotechnology*, *19*(7). https://doi.org/10.1088/0957-4484/19/7/075710

Toit, A., & Kooy, F. Van Der. (2019). Artemisia afra, a controversial herbal remedy or a treasure

trove of new drugs? *Journal of Ethnopharmacology*, 112127. https://doi.org/10.1016/j.jep.2019.112127

Tri, P., Le, T. V. K., & Tran, V. Q. (2021). *Improved Synthesis of Ag / SiO 2 Colloidal Nanocomposites and Their Antibacterial Activity*. *March*, 0–8. https://doi.org/10.1166/jnn.2021.19021

Tutaj, K., Szlazak, R., Szalapata, K., Starzyk, J., Luchowski, R., Grudzinski, W., Osinska-Jaroszuk, M., Jarosz-Wilkolazka, A., Szuster-Ciesielska, A., & Gruszecki, W. I. (2016). Amphotericin B-silver hybrid nanoparticles: Synthesis, properties and antifungal activity. *Nanomedicine: Nanotechnology, Biology, and Medicine*, *12*(4), 1095–1103. https://doi.org/10.1016/j.nano.2015.12.378

Urnukhsaikhan, E., Bold, B. E., Gunbileg, A., & Sukhbaatar, N. (2021). Antibacterial activity and characteristics of silver nanoparticles biosynthesized from Carduus crispus. *Scientific Reports*, 1–12. https://doi.org/10.1038/s41598-021-00520-2

V. Patil, G., K. Dass, S., & Chandra, R. (2011). Artemisia afra and Modern Diseases. *Journal of Pharmacogenomics & Pharmacoproteomics*, *02*(03). https://doi.org/10.4172/2153-0645.1000105

Yaseen, M., Ahmad, M., Wani, T. A., Ahmad, M., Gani, B. A., & Qureshi, R. (2017). Phytochemical screening and antioxidant activity of extracts of the leaf and stem of Achillea millefolium. *International Journal of Advanced Science and Research*, *2*(6), 55–59.

Yin, I. X., Zhang, J., Zhao, I. S., Mei, M. L., Li, Q., & Chu, C. H. (2020). The antibacterial mechanism of silver nanoparticles and its application in dentistry. *International Journal of Nanomedicine*, *15*, 2555–2562. https://doi.org/10.2147/IJN.S246764

Zaki, A. G., Hasanien, Y. A., & Sayyad, G. S. El. (2022). Novel fabrication of - SiO 2 / Ag nanocomposite by gamma irradiated Fusarium oxysporum to combat Ralstonia solanacearum. *AMB Express*. https://doi.org/10.1186/s13568-022-01372-3

Zhang, X.-F., Liu, Z.-G., Shen, W., & Gurunathan, S. (2016). Silver Nanoparticles: Synthesis, Characterization, Properties, Applications, and Therapeutic Approaches. *International Journal of Molecular Sciences*, *17*(9), 1534. https://doi.org/10.3390/ijms17091534

# APPENDIX

**Appendix 1.** Phytochemical test for plant extract

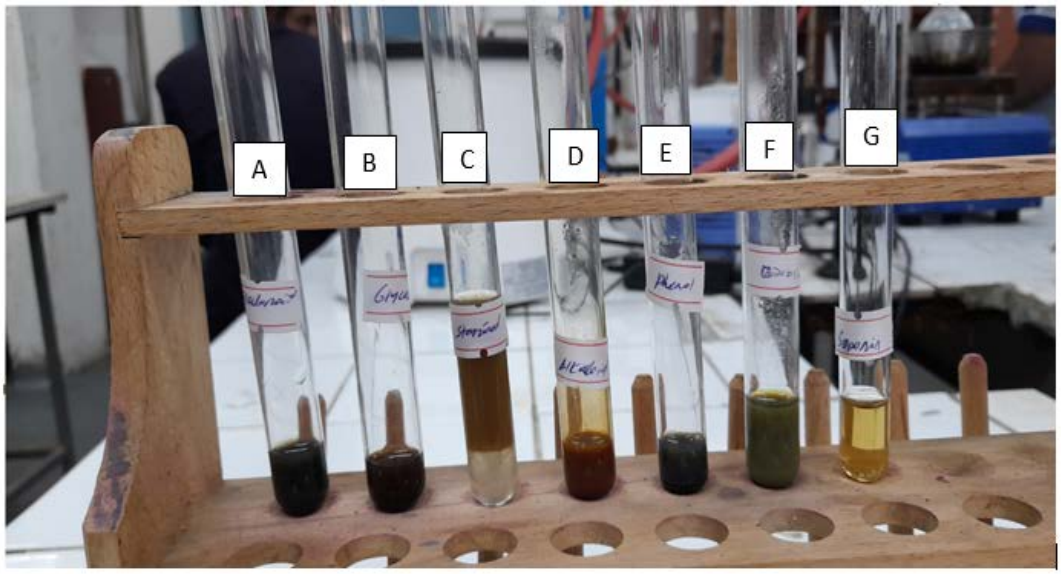


Figure A1**:** Phytochemical test colors are observed when the extract is tested for A). Flavonoid B). Glycosides, C). Steroid D). Alkaloid E) Phenol F) Reducing sugar G). Saponins

**Appendix 2.** Color change during Synthesis of NPs and NCs

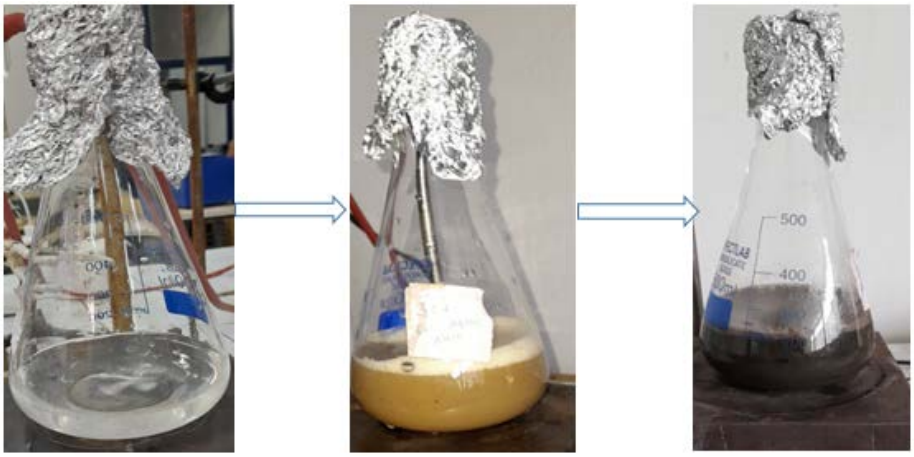


Figure A2: Color change observed during Synthesis of Ag Nanoparticle

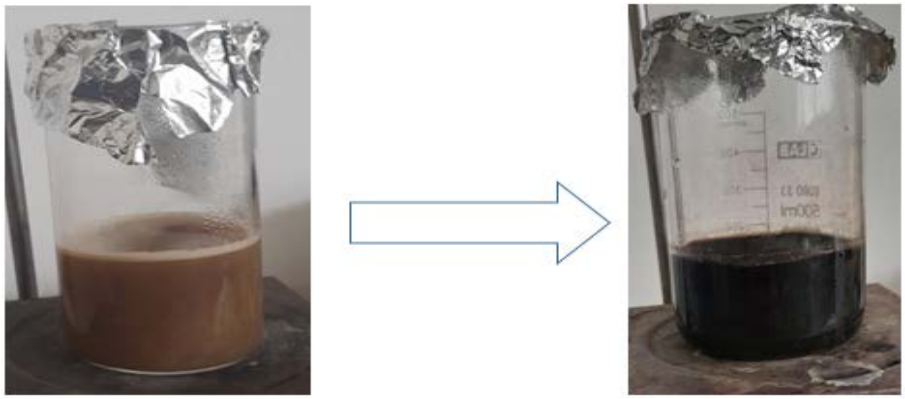

Figure A3*:* Color change observed during Synthesis $Ag/SiO_2$ Nanocomposite

**Appendix 3**. Diameter of Zone of inhibition for Antibacterial and antifungal activity

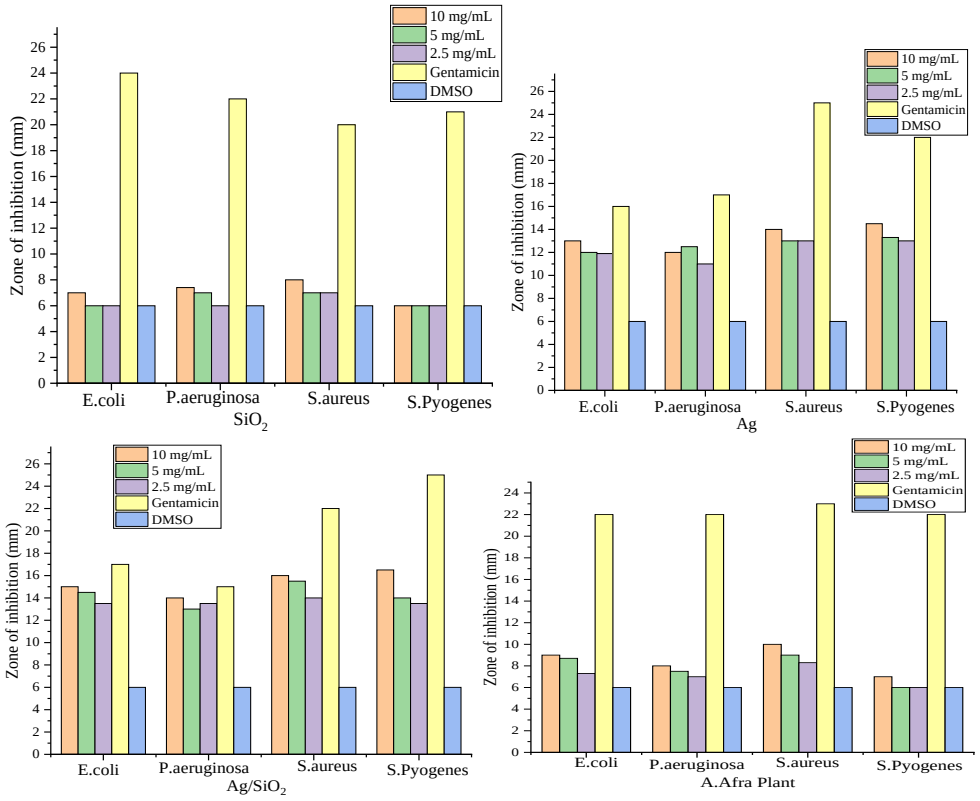


Figure A4**:** Diameter of Zone of inhibition of synthesized NPs and NCs at different concentrations against E. coli, P. aeruginosa, S. aureus, and S. Pyogenes bacterial strain

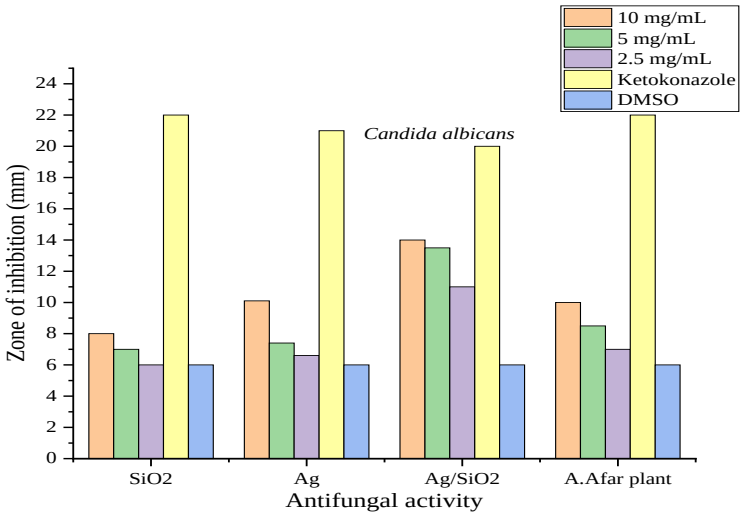


Figure A5**:** Diameter of Zone of inhibition of synthesized NPs and NCs at different concentration against *Candida albicans*

**Appendix 4**: MIC and MBC test for antibacterial activity

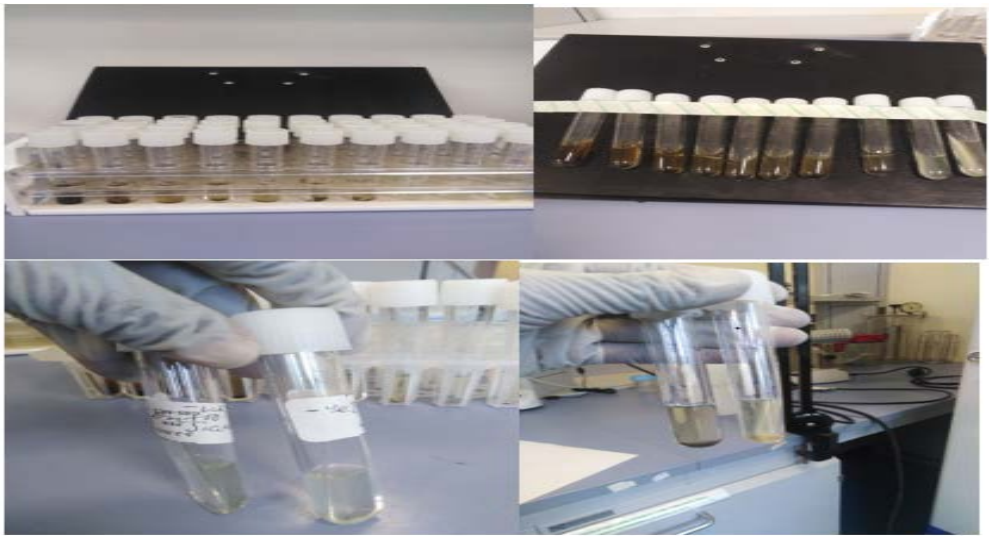

Figure A6: MIC and MBC test

**Appendix 5**. Summary of NPs and NCs for antibacterial and antifungal activity data

Table A1: Summary of SiO2 NPs antibacterial activity data

| | | | | $SiO_2$ | | | |
|---|---|---|---|---|---|---|---|
| | Con | Trial 1 | Trial 2 | Trial 3 | Mean | STDEV | SE |
| | 10 | 6 | 7 | 6 | 6.333333 | 0.57735 | 0.229416 |
| E.coli | 5 | 6 | 7 | 6 | 6.333333 | 0.57735 | 0.229416 |
| | 2.5 | 6 | 6 | 7 | 6.333333 | 0.57735 | 0.229416 |
| | Gent +ve | 24 | 24 | 24 | 24 | 0 | 0 |
| | DMSO | 6 | 6 | 6 | 6 | 0 | 0 |
| P.aeruginosa | 10 | 7 | 7 | 8.3 | 7.433333 | 0.750555 | 0.27529 |
| | 5 | 7.3 | 6 | 6 | 6.433333 | 0.750555 | 0.295913 |
| | 2.5 | 6 | 6.4 | 6 | 6.133333 | 0.23094 | 0.09325 |
| | Gent +ve | 22 | 22 | 22 | 22 | 0 | 0 |
| | DMSO | 6 | 6 | 6 | 6 | 0 | 0 |
| S.aureus | 10 | 7 | 6.55 | 7.5 | 7.016667 | 0.475219 | 0.179403 |
| | 5 | 7 | 6.55 | 7.59 | 7.046667 | 0.521568 | 0.19648 |
| | 2.5 | 7 | 6.4 | 6 | 6.466667 | 0.503322 | 0.197927 |
| | Gent +ve | 20 | 20.4 | 23 | 21.13333 | 1.628906 | 0.354333 |
| | DMSO | 6 | 6 | 6 | 6 | 0 | 0 |
| S.pyogen | 10 | 7.5 | 6 | 7.8 | 7.1 | 0.964365 | 0.36192 |
| | 5 | 6 | 6 | 6 | 6 | 0 | 0 |
| | 2.5 | 6 | 6 | 6.7 | 6.233333 | 0.404145 | 0.161874 |
| | Gent +ve | 21 | 21 | 23 | 21.66667 | 1.154701 | 0.248069 |
| | DMSO | 6 | 6 | 6 | 6 | 0 | 0 |

Note:STDVE-Standard Deviation SE-Standard Error

Table A2: Summary of Ag NPs antibacterial activity data

| Ag | | | | | | | |
|---|---|---|---|---|---|---|---|
| | Con | Trial 1 | Trial 2 | Trial 3 | Mean | STDEV | SE |
| | 10 | 13 | 14 | 12.2 | 13.06667 | 0.90185 | 0.249489 |
| E.coli | 5 | 12 | 11 | 13 | 12 | 1 | 0.288675 |
| | 2.5 | 11 | 11.3 | 12.3 | 11.53333 | 0.680686 | 0.200433 |
| | Gent +ve | 16 | 17 | 16 | 16.33333 | 0.57735 | 0.142857 |
| | DMSO | 6 | 6 | 6 | 6 | 0 | 0 |
| P.aeruginosa | 10 | 12 | 12 | 13 | 12.33333 | 0.57735 | 0.164399 |
| | 5 | 12.5 | 13 | 12 | 12.5 | 0.5 | 0.141421 |
| | 2.5 | 11 | 11.5 | 11 | 11.16667 | 0.288675 | 0.086387 |

| | | | | | | | |
|---|---|---|---|---|---|---|---|
| | Gent +ve | 17 | 17 | 17.4 | 17.13333 | 0.23094 | 0.055793 |
| | DMSO | 6 | 6 | 6 | 6 | 0 | 0 |
| S.aureus | 10 | 14 | 15 | 13 | 14 | 1 | 0.267261 |
| | 5 | 13 | 14 | 12 | 13 | 1 | 0.27735 |
| | 2.5 | 13 | 14 | 12 | 13 | 1 | 0.27735 |
| | Gent +ve | 24 | 25 | 26 | 25 | 1 | 0.2 |
| | DMSO | 6 | 6 | 6 | 6 | 0 | 0 |
| S.pyogen | 10 | 14 | 14.5 | 15 | 14.5 | 0.5 | 0.131306 |
| | 5 | 13 | 14 | 13 | 13.33333 | 0.57735 | 0.158114 |
| | 2.5 | 13 | 13.4 | 13 | 13.13333 | 0.23094 | 0.063725 |
| | Gent +ve | 22 | 22 | 22 | 22 | 0 | 0 |
| | DMSO | 6 | 6 | 6 | 6 | 0 | 0 |

Table A3: Summary of $Ag/SiO_2$ NC antibacterial activity data

| | | | | $Ag/SiO_2$ | | | |
|---|---|---|---|---|---|---|---|
| | Con | Trial 1 | Trial 2 | Trial 3 | Mean | STDEV | SE |
| | 10 | 14.5 | 15.5 | 15 | 15 | 0.5 | 0.129099 |
| E.coli | 5 | 14 | 15 | 14.5 | 14.5 | 0.5 | 0.131306 |
| | 2.5 | 13.5 | 14 | 13.5 | 13.66667 | 0.288675 | 0.078087 |
| | Gent +ve | 17 | 16 | 18 | 17 | 1 | 0.242536 |
| | DMSO | 6 | 6 | 6 | 6 | 0 | 0 |
| P.aeruginosa | 10 | 14 | 15 | 14 | 14.33333 | 0.57735 | 0.152499 |
| | 5 | 13 | 14 | 13 | 13.33333 | 0.57735 | 0.158114 |
| | 2.5 | 13 | 13.5 | 14 | 13.5 | 0.5 | 0.136083 |
| | Gent +ve | 15 | 15.5 | 15 | 15.16667 | 0.288675 | 0.074125 |
| | DMSO | 6 | 6 | 6 | 6 | 0 | 0 |
| S.aureus | 10 | 16.5 | 15.5 | 16 | 16 | 0.5 | 0.125 |
| | 5 | 15 | 14.5 | 15.5 | 15 | 0.5 | 0.129099 |
| | 2.5 | 14 | 14.5 | 14 | 14.16667 | 0.288675 | 0.076696 |
| | Gent +ve | 22 | 22 | 23 | 22.33333 | 0.57735 | 0.122169 |
| | DMSO | 6 | 6 | 6 | 6 | 0 | 0 |
| S.pyogen | 10 | 17 | 15 | 16 | 16 | 1 | 0.25 |
| | 5 | 14 | 15 | 13 | 14 | 1 | 0.267261 |
| | 2.5 | 13 | 14 | 14 | 13.66667 | 0.57735 | 0.156174 |
| | Gent +ve | 25.5 | 25.5 | 24 | 25 | 0.866025 | 0.173205 |

| | | | | | | | |
|---|---|---|---|---|---|---|---|
| | DMSO | 6 | 6 | 6 | 6 | 0 | 0 |

Table A4: Summary of *A.Afra* plant antibacterial activity data

| | | | | *A.Afra* | | | |
|---|---|---|---|---|---|---|---|
| | Con | Trial 1 | Trial 2 | Trial 3 | Mean | STDEV | SE |
| | 10 | 9 | 7 | 8 | 8 | 1 | 0.353553 |
| E.coli | 5 | 8.5 | 8 | 9.5 | 8.666667 | 0.763763 | 0.259437 |
| | 2.5 | 7 | 7.5 | 7.5 | 7.333333 | 0.288675 | 0.1066 |
| | Gent +ve | 22 | 23 | 23 | 22.66667 | 0.57735 | 0.121268 |
| | DMSO | 6 | 6 | 6 | 6 | 0 | 0 |
| P.aeruginosa | 10 | 8 | 8.5 | 8 | 8.166667 | 0.288675 | 0.101015 |
| | 5 | 7 | 7.5 | 8 | 7.5 | 0.5 | 0.182574 |
| | 2.5 | 7 | 8 | 6 | 7 | 1 | 0.377964 |
| | Gent +ve | 22 | 22.5 | 22 | 22.16667 | 0.288675 | 0.061314 |
| | DMSO | 6 | 6 | 6 | 6 | 0 | 0 |
| S.aureus | 10 | 9 | 10 | 8 | 9 | 1 | 0.333333 |
| | 5 | 9 | 7.5 | 8 | 8.166667 | 0.763763 | 0.267261 |
| | 2.5 | 7 | 8 | 7 | 7.333333 | 0.57735 | 0.213201 |
| | Gent +ve | 23 | 23 | 23 | 23 | 0 | 0 |
| | DMSO | 6 | 6 | 6 | 6 | 0 | 0 |
| S.pyogen | 10 | 7.5 | 6 | 7.5 | 7 | 0.866025 | 0.327327 |
| | 5 | 7.5 | 7.5 | 6 | 7 | 0.866025 | 0.327327 |
| | 2.5 | 7.5 | 6 | 7 | 6.833333 | 0.763763 | 0.292174 |
| | Gent +ve | 21 | 22 | 23 | 22 | 1 | 0.213201 |
| | DMSO | 6 | 6 | 6 | 6 | 0 | 0 |

Table A5:Summary of Antifungal activity data

| | | | *Candida albicans* | | | | |
|---|---|---|---|---|---|---|---|
| | conc | Trial 1 | Trial 2 | Trial 2 | Mean | STDEV | SE |
| | 10 | 7.5 | 9 | 7.5 | 8 | 0.866025 | 0.306186 |
| | 5 | 7 | 8 | 6 | 7 | 1 | 0.377964 |
| | 2.5 | 6 | 7 | 6 | 6.333333 | 0.57735 | 0.229416 |
| | Keto +ve | 22 | 22 | 22 | 22 | 0 | 0 |
| $SiO_2$ | DMSO | 6 | 6 | 6 | 6 | 0 | 0 |
| | 10 | 10 | 11 | 9 | 10 | 1 | 0.316228 |
| | 5 | 9 | 7 | 8 | 8 | 1 | 0.353553 |
| Ag | 2.5 | 8 | 7 | 7.5 | 7.5 | 0.5 | 0.182574 |

| | | | | | | | |
|---|---|---|---|---|---|---|---|
| | Keto +ve | 22 | 21 | 22 | 21.66667 | 0.57735 | 0.124035 |
| | DMSO | 6 | 6 | 6 | 6 | 0 | 0 |
| | 10 | 14 | 13 | 15 | 14 | 1 | 0.267261 |
| | 5 | 13 | 12 | 14 | 13 | 1 | 0.27735 |
| | 2.5 | 12 | 10 | 11 | 11 | 1 | 0.301511 |
| | Keto +ve | 20.5 | 20 | 20 | 20.16667 | 0.288675 | 0.064282 |
| | DMSO | 6 | 6 | 6 | 6 | 0 | 0 |
| $Ag/SiO_2$ | 10 | 11 | 10 | 9 | 10 | 1 | 0.316228 |
| | 5 | 9 | 8 | 10 | 9 | 1 | 0.333333 |
| | 2.5 | 8 | 9 | 7 | 8 | 1 | 0.353553 |
| | Keto +ve | 22 | 22 | 22 | 22 | 0 | 0 |
| *A.Afra* | DMSO | 6 | 6 | 6 | 6 | 0 | 0 |